Summer 2013

Topics in Electromagnetic, Acoustic, and Potential Scattering Theory

Umaporn Nuntaplook
Old Dominion University

TOPICS IN ELECTROMAGNETIC, ACOUSTIC, AND POTENTIAL SCATTERING THEORY

by

Umaporn Nuntaplook
B.S. 2004, Mahidol University, Thailand
M.S. 2008, Old Dominion University

A Dissertation Submitted to the Faculty of
Old Dominion University in Partial Fulfillment of the
Requirements for the Degree of

DOCTOR OF PHILOSOPHY

COMPUTATIONAL AND APPLIED MATHEMATICS

OLD DOMINION UNIVERSITY
August 2013

Approved by:

John Adam (Director)

John Tweed (Member)

Linda Vahala (Member)

Tony Slaba (Member)

ABSTRACT

TOPICS IN ELECTROMAGNETIC, ACOUSTIC, AND POTENTIAL SCATTERING THEORY

Umaporn Nuntaplook
Old Dominion University, 2013
Director: Dr. John Adam

With recent renewed interest in the classical topics of both acoustic and electromagnetic aspects for nano-technology, transformation optics, fiber optics, metamaterials with negative refractive indices, cloaking and invisibility, the topic of time-independent scattering theory in quantum mechanics is becoming a useful field to re-examine in the above contexts. One of the key areas of electromagnetic theory — scattering of plane electromagnetic waves — is based on the properties of the refractive indices in the various media. It transpires that the refractive index of a medium and the potential in quantum scattering theory are intimately related. In many cases, understanding such scattering in radially symmetric media is sufficient to gain insight into scattering in more complex media. Meeting the challenge of variable refractive indices and possibly complicated boundary conditions therefore requires accurate and efficient numerical methods, and where possible, analytic solutions to the radial equations from the governing scalar and vector wave equations (in acoustics and electromagnetic theory, respectively). Until relatively recently, researchers assumed a constant refractive index throughout the medium of interest. However, the most interesting and increasingly useful cases are those with non-constant refractive index profiles. In the majority of this dissertation the focus is on media with piecewise constant refractive indices in radially symmetric media. The method discussed is based on the solution of Maxwell's equations for scattering of plane electromagnetic waves from a dielectric (or "transparent") sphere in terms of the related Helmholtz equation. The main body of the dissertation (Chapters 2 and 3) is concerned with scattering from (i) a uniform spherical inhomogeneity embedded in an external medium with different properties, and (ii) a piecewise-uniform central inhomogeneity in the external medium. The latter results contain a natural generalization of the former (previously known) results. The link with time-independent quantum mechanical scattering, via morphology-dependent resonances (MDRs), is discussed in Chapter 2. This requires a generalization of the classical problem for

scattering of a plane wave from a uniform spherically-symmetric inhomogeneity (in which the velocity of propagation is a function only of the radial coordinate r, i.e., $c = c(r)$) to a piecewise-uniform inhomogeneity. In Chapter 3 the Jost-function formulation of potential scattering theory is used to solve the radial differential equation for scattering which can be converted into an integral equation corresponding via the Jost boundary conditions. The first two iterations for the zero angular momentum case $l = 0$ are provided for both two-layer and three-layer models. It is found that the iterative technique is most useful for long wavelengths and sufficiently small ratios of interior and exterior wavenumbers. Exact solutions are also provided for these cases. In Chapter 4 the time-independent quantum mechanical 'connection' is exploited further by generalizing previous work on a spherical well potential to the case where a delta 'function' potential is appended to the exterior of the well (for $l \neq 0$). This corresponds to an idealization of the former approach to the case of a 'coated sphere'. The poles of the associated 'S-matrix' are important in this regard, since they correspond directly with the morphology-dependent resonances discussed in Chapter 2. These poles (for the $l = 0$ case, to compare with Nussenzveig's analysis) are tracked in the complex wavenumber plane as the strength of the delta function potential changes. Finally, a set of 4 Appendices is provided to clarify some of the connections between (i) the scattering of acoustic/electromagnetic waves from a penetrable/dielectric sphere and (ii) time-independent potential scattering theory in quantum mechanics. This, it is hoped, will be the subject of future work.

This thesis is dedicated to my father, Lan Nuntaplook, my mother, Fongnual Nuntaplook, and my sister, Pakaporn Singjanusong for their love!

ACKNOWLEDGMENTS

I would like to give special acknowledgement and express the deepest appreciation to my advisor Dr. John Adam for his valuable guidance, support and constant attention throughout my graduate studies. Without his guidance and persistent help this dissertation would not have been possible. I also would like to extend my sincere appreciation to my committee members, Dr. John Tweed, Dr. Linda Vahala, Dr. Noam Zeev, and Dr. Tony Slaba, for their help and support. In addition, I would like to thank Dr. Hideaki Kaneko, Dr. Boriboon Novaprateep, and Dr. Yongwimon Lenbury, who introduced me to Old Dominion University, for their support and advice. Special thanks to Department of Mathematics and Statistics of Old Dominion University and to full scholarship from the Commission on Higher Education Congress: University Staff Development Consortium of Thailand, (2006 - 2012) for giving me the great opportunities to study in the USA.

I would like to thank my family for their love, support and encouragement. I would like to give very special thanks to my mom and my husband Sarun for always supporting me in my good and bad times and helping me persevere. I also would like to thank my best friends, little Drew, adorable Amanda, P′ Tookta, and Colonel for all their help and support and also bringing the wonderful and fun memories to my life. Many thanks to P′ Banana for helping me with Latex. Finally, I would like to thank all my friends, both in Thailand and in the United States for all their help, support and encouragement.

TABLE OF CONTENTS

LIST OF TABLES

LIST OF FIGURES

CHAPTER 1

INTRODUCTION

The following quote from a paper by Adam and Laven [6] (although written from a ray-theoretic approach) explains in part why the scattering of electromagnetic plane waves from spheres is such an important and topical subject:

"This paper uses geometrical optics to analyze the scattering of light by inhomogeneous spheres in which the refractive index is a function of the radius only. The results may be of value in the field of rainbow refractometry and thermometry, which are optical techniques used to measure the refractive index (and hence the temperature) of transparent particles (including fuel droplets), and the cross-sectional shape of dielectric cylinders. Such techniques can be used to determine very small spatial and time-varying changes in refractive index, and are valuable for analysis of the combustion of liquid hydrocarbons, the injection of sprays in high-pressure environments, as well as the spraying drying techniques employed in the food, agricultural and pharmaceutical industries. Gradients of refractive index can be caused when droplets undergo simultaneous heating and evaporation in a combustion chamber, and will be primarily radial if internal convection can be neglected compared with thermal conduction. Similar refractometry studies have been carried out to determine the refractive indices and radii of unclad optical fibers."

Furthermore, the following quotation from Lock [18] illustrates how several complementary mathematical approaches in theoretical optics can bring a richer understanding of any particular optical effect (in this case, the rainbow):

"The theory of the rainbow has been formulated at many levels of sophistication. In the geometrical-optics theory of Descartes, a rainbow occurs when the angle of the light rays emerging from a water droplet after a number of internal reflections reaches an extremum. In Airy's wave-optics theory, the distortion of the wave front of the incident light produced by the internal reflections describes the production of the supernumerary bows and predicts a shift of a few tenths of a degree in the angular position of the rainbow from its geometrical-optics location. In Mie theory, the rainbow appears as a strong enhancement in the electric field scattered by the water droplet. Although the Mie electric field is the exact solution to the light-scattering

problem, it takes the form of an infinite series of partial wave contributions that is slowly convergent and whose terms have a mathematically complicated form. In the complex angular momentum theory, the sum over partial waves is replaced by an integral, and the rainbow appears as a confluence of saddle-point contributions in the portion of the integral that describes light rays that have undergone a single internal reflection within the water droplet."

The use of classical electromagnetic theory to describe the scattering of plane electromagnetic waves by a sphere with a constant refractive index is commonly known as the *Mie solution*. This is also referred to as Mie scattering (or less accurately, Mie theory), named for Gustav Mie (1869 – 1957) who was interested in the scattering of such waves from colloidal metal solutions, and published his results in 1908. The historical development of the topic is well discussed by Kerker [3]. The theory of electromagnetic (in particular, light) scattering from a radially inhomogeneous sphere has been developed by many authors (again, see references in Kerker [3]). To this extent, the problem has been understood for many years. However, recent developments in optics and nanotechnology (see Leonhardt and Philbin [4], and references therein) have renewed interest in these classical solutions.

A central feature of the research presented here is the intriguing formal connection between the acoustic and electromagnetic scattering problems on one hand, and time-independent potential scattering theory on the other. Specifically, a potential 'well' can be associated with a finite domain D where the refractive index everywhere exceeds one, i.e. $n(\mathbf{r}) > 1$, $\mathbf{r} \in D$. In most of this study, 3-layer piecewise constant refractive indices are chosen to represent non-uniform media, and they have corresponding potential well/barrier combinations, some of whose scattering properties can be determined using methods of potential scattering theory. In so doing, previous results for uniform scattering inhomogeneities have been extended and generalized both analytically and numerically. The reasons for this analysis are as follows. Many approximately spherically symmetric scatterers in optical media (phytoplankton, animal cells, aerosols, optical fibers, plasmas, combustion mixtures, ice/rain mixtures, planetary atmospheres, and even in seismology though the waves are elastic in nature) have non-constant refractive indices, and these are generally not continuous functions. Furthermore, as shown in Adam and Laven [6], for the sub-class of differentiable refractive indices $n(r)$, $r = |\mathbf{r}|$, different optical features arise if the gradient of $n(r)$ is positive or negative in some sub-interval of the drop

radius. Since analytic solutions for these cases are few and far between (see Adam [33] and references therein), a three-layer model consisting of two concentric spheres and the exterior domain can be used to mimic the broad features of these differentiable cases. In fact, in view of the above examples, they may be more realistic than these mathematically idealized cases!

In Chapter 2, the study of morphology-dependent resonances (MDRs) and electromagnetic scattering by a uniform sphere, based on the important paper by Johnson [7], is discussed and extended to accommodate a two-layer piecewise-uniform sphere (when embedded in the external medium this becomes a three-layer model). Appendix B analyses certain features of a differentiable refractive index profile (submitted to Applied Mathematics Letters). Also in Chapter 2, a simple model with a well-barrier potential is developed for the case of the angular momentum 'quantum number' $l = 0$. The idea behind this is to have a 'template' with four adjustable parameters (the well depth, barrier height and well/barrier widths) to mimic the $l \neq 0$ cases, for which the so-called "centrifugal barrier" can temporarily trap wave energy associated with MDRs. Chapter 3 adopts the same approach for what was originally studied as a problem in acoustics [12]. The vector problem in electromagnetic theory can be reduced to two (in general non-identical) scalar problems in this geometry (one for each polarization) and these can be treated in the same way as the acoustic problem, but as before, the theory is extended to accommodate piecewise-uniform media. Chapter 4 addresses the case of a 'coated' sphere. Such spheres are used, for example, in nanotechnology and in connection with 'optical tweezer' technology (see Chapter 4). Furthermore, a coated sphere may be a more appropriate model for certain biological cells than a homogeneous sphere. The seminal paper of Nussenzveig [15] is extended by taking the spherical potential well used in that paper, and adding (formally) a delta-function potential to the surface of the well to represent a thin molecular coating on the surface of, for example, a nanosphere. The MDRs discussed in Chapter 2 can be identified mathematically with the poles of the so-called S-matrix of a given potential (see Appendix C). The S-matrix is derived for the $l = 0$ case for this new 'well + delta' potential, and the poles are tracked in the complex wavenumber plane as the strength of the delta function decreases and increases away from zero.

CHAPTER 2

THE SCATTERING OF ELECTROMAGNETIC WAVES IN RADIALLY INHOMOGENEOUS SPHERES: MORPHOLOGY-DEPENDENT RESONANCES (MDRs)

2.1 INTRODUCTION

To study the scattering of electromagnetic waves in radially symmetric media it is necessary to examine the refractive index profile which is the key concept to describe a scattering potential. In general, variable refractive indices and complicated boundary conditions require accurate and efficient methods to solve the system of equations, especially for multilayered problems. One method discussed in this study is based on the Maxwell's equations and the Helmholtz equation for scattering of plane electromagnetic waves from a dielectric sphere using Mie Theory. The scattering electromagnetic energy in a dielectric sphere shows a series of sharp peaks as a function of the size parameter from the cross section. The peaks represent the scattering resonances where the electromagnetic energy is temporally trapped inside the particle near the surface of the sphere in a dielectric potential well. These resonances are referred to as morphology-dependent resonances (MDRs). When the electromagnetic wave propagates around the inside surface of the sphere, it is trapped by almost total internal reflection and finally returns to its starting point in phase. There is an important connection here with potential scattering theory. The refractive index corresponds to a potential well $V(r)$ in the time-independent Schrödinger-type equation. The electromagnetic energy enters and leaves the well by tunneling through a centrifugal barrier that forms the outer boundary of the potential.

2.1.1 ELECTROMAGNETIC EIGENMODES OF SPHERES

"When a beam of electromagnetic radiation is incident on a small dielectric particle of high symmetry, such as a sphere or a circular cylinder, a morphology-dependent

resonance (MDR) is excited in one of the partial waves in the partial-wave expansion of the incident beam at certain combinations of the wavelength of the radiation and the particles radius and refractive index. According to van de Hulsts localization principle, the resonant partial wave corresponds to an incident light ray whose impact parameter with respect to the center of the particle is somewhat larger than the particles radius, and therefore the ray would classically pass the particle without striking it. The fact that MDRs are excited by rays that miss the particle is paradoxical in ray optics, but it is easily understood in wave optics. A portion of the partial wave evanescently tunnels through the centrifugal barrier surrounding the particle and is transmitted to the particles interior. Once inside, the partial wave is trapped in the particles radial interior potential well and successively reflects back and forth within it. At resonance, approximately an integer number of half-wavelengths of the partial wave fit within the radial potential well, and the successive internal reflections are in phase with one another. As a result, a large energy density builds up inside the particle just beneath its surface, and at each internal reflection a certain percentage of the interior field tunnels back out through the centrifugal barrier and is detected in the far zone as a resonant amplification of the scattered light" [1].

"Optical resonances of dielectric spheres, so-called Mie resonances or morphology-dependent resonances, have attracted considerable scientific interest in recent years. The strong resonant field enhancement within and near the surface of the sphere allows the observation of several nonlinear optical phenomena. Resonance spectroscopy has proved to be a highly accurate tool in aerosol research" [5].

"Mie theory provides the rigorous treatment of the interaction of a plane wave with a dielectric sphere. In Mie theory all involved fields are expanded in spherical multipole waves (eigenmodes); in resonance one eigenmode of the sphere is strongly excited. Each multipole wave is characterized by its state of polarization (TE or TM) and two integers, which enter in Mie theory as separation constants. These integers are the mode number $l = 1, 2, ...$, which is connected to the total angular momentum of the mode by $|L| = [l(l+1)]^{1/2}\hbar \approx (l + 1/2)\hbar$, and the azimuthal mode number $m \leq l$, which is a measure for the z component of the angular momentum, $L_z = m\hbar$. Modes that have the same mode number l but differ in m are degenerate; i.e., they occur at the same size parameter $x = k_0 a = (2\pi/\lambda_0)a$ (a is the sphere's radius, k_0 is the wave number, and λ_0 is the wavelength of the illuminating radiation). If a sphere is illuminated by a plane wave, only modes with $m = 1$ are excited. Each

multiple exhibits an infinite number of resonances as a function of the sphere's size parameter" [5].

Though we do not need to discuss them in detail, Figures 1 and 2 are redrawn from [5] to illustrate the basic idea of Mie resonances, variously represented by geometric optics ("rays") and wave theory.

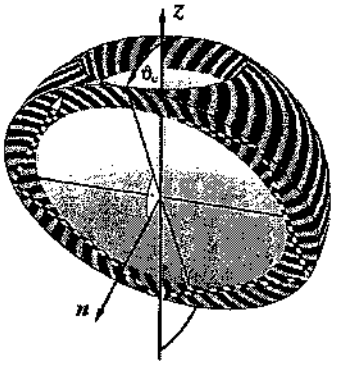

FIG. 1: An illustration of Mie resonances using geometrical optics (redrawn from Ref. [5]).

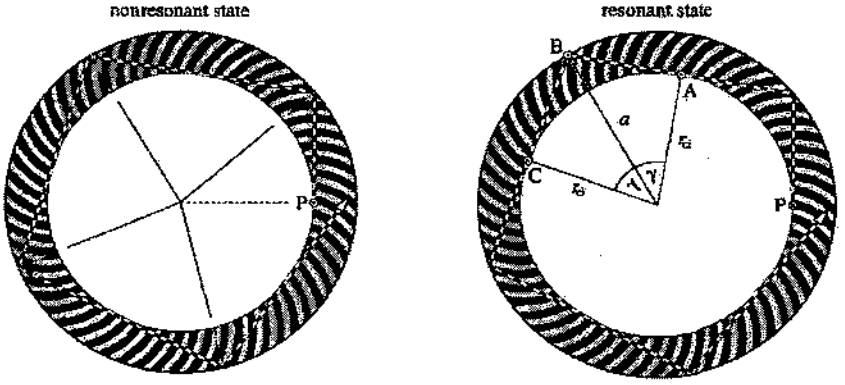

FIG. 2: An illustration of Mie resonances using geometrical optics. Path of a ray within its orbit. In the left part, the size of the cavity is such that consecutive congruences of the same kind are not in phase; this represents a nonresonant case. In the right part, the cavity size is such that consecutive congruences are in phase; this state represents a resonance (redrawn from Ref. [5]).

2.2 SCATTERING THEORY FOR TWO-LAYER MODEL

The most common technique to solve problems of light scattering from a radially inhomogeneous particle is based on solving the second-order, linear differential equations for the radial Debye potential [13]. Several authors have developed the theory of light scattering by a radially inhomogeneous sphere. This section begins with the basic equations for electromagnetic scattering from spherically symmetric particles as shown in Figure 3. The radius of the particle is defined as a, the center is at the origin of the coordinate system, and the refractive index is defined as $n(r)$ which may be a function of the radial coordinate r, and can be a complex number. For the external region outside the sphere, $r > a$, the refractive index, $n(r) = 1$. The wave number is $k = 2\pi/\lambda$, where λ is the wavelength outside the sphere. Assume that the particle is nonmagnetic. Therefore, the electric field for this problem must satisfy the appropriate scattering conditions and also the following vector Helmholtz equation, which is good for the condition assumed here that the magnetic permeability is constant. The complex time-dependence of the electric field is assumed to be harmonic, i.e., $\propto e^{-i\omega t}$.

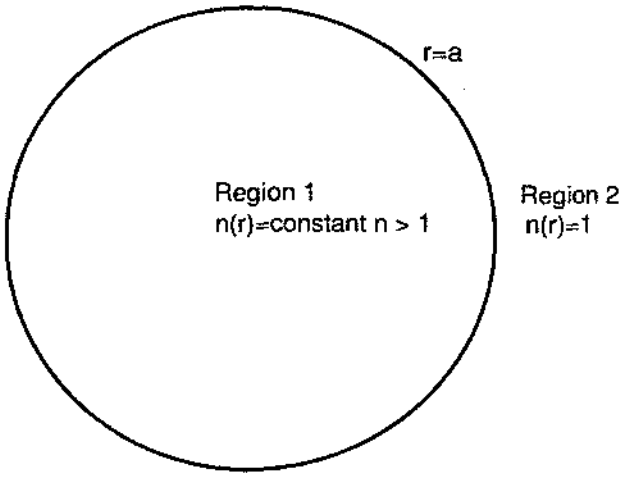

FIG. 3: A constant refractive index associated with a spherical dielectric particle.

Consider the following vector Helmholtz equation:

$$\nabla \times \nabla \times \mathbf{E} - k^2 n^2(r)\mathbf{E} = 0. \tag{1}$$

It can be verified that the following vector wave functions are solutions of (1):

$$\mathbf{M}(r,\theta,\phi) = \nabla \times [\Psi(r,\theta,\phi)\mathbf{r}], \tag{2a}$$

$$\mathbf{N}(r,\theta,\phi) = \frac{1}{kn^2(r)}\nabla \times \nabla \times [\Phi(r,\theta,\phi)\mathbf{r}], \tag{2b}$$

where r, θ, and ϕ are spherical coordinates, $\mathbf{r}$ is the radius vector, and Ψ and Φ are scalar functions that satisfy the differential equations [11]

$$\nabla^2\Psi + k^2 n^2(r)\Psi = 0, \tag{3a}$$

$$\nabla^2\Phi - \frac{1}{n^2(r)}\frac{dn^2(r)}{dr}\frac{\partial\Phi}{\partial r} + k^2 n^2(r)\Phi = 0. \tag{3b}$$

By applying the method of separation of variables to these equations in spherical coordinates, we generate the following equations:

$$\Psi_{l,\,n}(r,\theta,\phi) = \frac{1}{kr}S_l(r)P_l{}^n(cos\theta)\exp(in\phi), \tag{4a}$$

$$\Phi_{l,\,n}(r,\theta,\phi) = \frac{1}{kr}T_l(r)P_l{}^n(cos\theta)\exp(in\phi), \tag{4b}$$

where $P_l{}^n(\cos\theta)$ is the associated Legendre polynomial. The functions $S_l(r)$ and $T_l(r)$ are the radial Debye potentials, which satisfy the following second-order differential equations:

$$\frac{d^2S_l(r)}{dr^2} + [k^2n^2(r) - \frac{l(l+1)}{r^2}]S_l(r) = 0, \tag{5a}$$

$$\frac{d^2T_l(r)}{dr^2} - \frac{2}{n(r)}\frac{dn(r)}{dr} + [k^2n^2(r) - \frac{l(l+1)}{r^2}]T_l(r) = 0. \tag{5b}$$

In regions where the refractive index is a constant value n, the two differential equations (5a) and (5b) have the same form. Substituting the functions (4a) and (4b) into (2a) and (2b), respectively, provides the set of vector wave functions $\mathbf{M}_{l,n}$ and $\mathbf{N}_{l,n}$ that are solutions to (1). The $\mathbf{M}$ fields are called transverse electric (TE) modes, and

the N fields are transverse magnetic (TM) modes. Therefore, $S_l(r)$ are associated with TE fields, and the $T_l(r)$ are associated with TM fields.

In the internal region for a constant refractive index n, $0 \leq r \leq a$:

$$S_l(r) = T_l(r) = \psi_l(nkr) \tag{6}$$

where $\psi_l(nkr)$ is the Riccati-Bessel funtion (see definition below) and the boundary conditions are $S_l(0) = 0$ and $T_l(0) = 0$, which guarantee that the electric fields and magnetic fields are finite at the origin.

In the region outside the particle, the general solutions to (5a) and (5b) are linear combinations of the Riccati-Bessel functions. The electric field in this region consists of the incident wave and an outgoing scattered wave. The Riccati-Bessel functions are defined as:

$$\psi_l(x) = x j_l(x), \tag{7a}$$

$$\chi_l(x) = x y_l(x), \tag{7b}$$

where $j_l(x)$ and $y_l(x)$ are spherical Bessel function of the first and second kinds, respectively.

In the external region: $r > a$

$$S_l(r) = B_l[\chi_l(kr) + \beta_l \psi_l(kr)], \tag{8a}$$

$$T_l(r) = A_l[\chi_l(kr) + \alpha_l \psi_l(kr)], \tag{8b}$$

where $n(r) = 1$, α_l, β_l, A_l, and B_l are constants.

We use the log-derivative formalism for the connection of the internal and external solution where the refractive index is discontinuous, such as at the surface of the sphere and at the boundaries between the layers of multi-layer sphere case (as in Section 2.4). The modified log-derivative functions of $S_l(r)$ and $T_l(r)$ are defined as

$$U_l(r) = \frac{1}{k}\left[\frac{S_l'(r)}{S_l(r)}\right], \tag{9a}$$

$$V_l(r) = \frac{1}{kn^2(r)}\left[\frac{T_l'(r)}{T_l(r)}\right], \tag{9b}$$

where a prime denotes the derivative with respect to the argument of the function. Both of these functions are continuous at all points.

We first consider the continuity at the surface $r = a$ by matching the internal solution from (6) with the external solution from (8a) and (8b) to obtain

$$\psi_l(nka) = B_l[\chi_l(ka) + \beta_l\psi_l(ka)], \tag{10a}$$

$$\psi_l(nka) = A_l[\chi_l(ka) + \alpha_l\psi_l(ka)]. \tag{10b}$$

Hence,

$$B_l = \frac{\psi_l(nka)}{\chi_l(ka) + \beta_l\psi_l(ka)}, \tag{11a}$$

$$A_l = \frac{\psi_l(nka)}{\chi_l(ka) + \alpha_l\psi_l n(ka)}. \tag{11b}$$

For $\beta_l = 0$ and $\alpha_l = 0$ at $r = a$, we have

$$A_l = B_l = \frac{\psi_l(nka)}{\chi_l(ka)}. \tag{12}$$

Now we substitute the external solutions defined by (8a) and (8b) into the modified logarithmic derivatives given by (9a) and (9b) and evaluate them at the surface of the sphere $r = a$. The standard approach in the literature is to use the continuity of the functions $U_l(r)$ and $V_l(r)$ across the boundary to solve for α_l and β_l. The results are

$$\beta_l = -\frac{\psi_l(nx)\chi_l'(x) - n\psi_l'(nx)\chi_l(x)}{\psi_l(nx)\psi_l'(x) - n\psi_l'(nx)\psi_l(x)}, \tag{13a}$$

and

$$\alpha_l = -\frac{\psi_l'(nx)\chi_l(x) - n\psi_l(nx)\chi_l'(x)}{\psi_l'(nx)\psi_l(x) - n\psi_l(nx)\psi_l'(x)}, \tag{13b}$$

where $x = ka$ is the size parameter.

As shown in [7], the coefficients α_l and β_l are related to the a_l and b_l coefficients of Mie theory by the formulas

$$b_l = \frac{1}{1 - i\beta_l}, \tag{14a}$$

$$a_l = \frac{1}{1 - i\alpha_l}. \tag{14b}$$

The a_l and b_l coefficients defined here are the same as the coefficients defined by Bohren and Huffman [8] and are the complex conjugate of the coefficients defined by van de Hulst [9] and by Kerker [3].

2.3 RESONANCE THEORY

2.3.1 QUANTUM-MECHANICAL ANALOGY

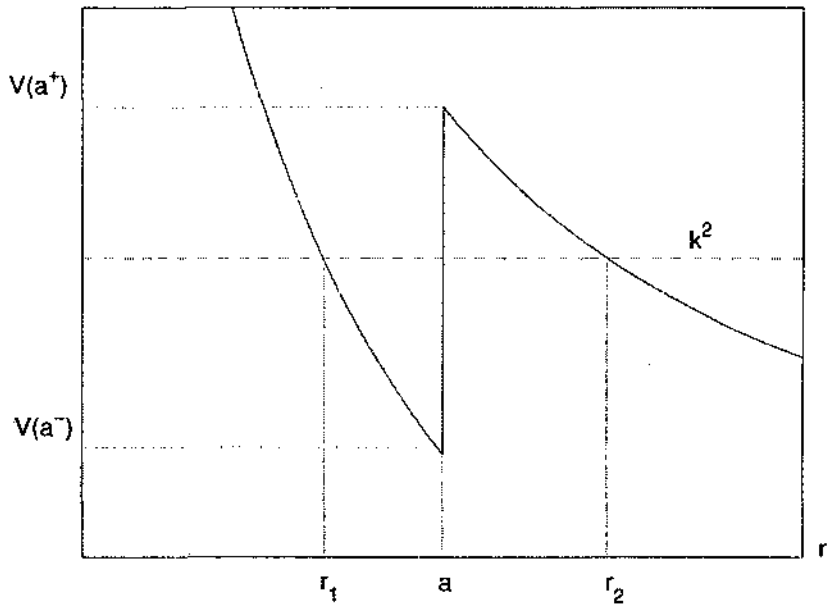

FIG. 4: Effective potential associated with a spherical dielectric particle.

To simplify the second-order differential equations (5a) and (5b), we write the Schrödinger equation in units such that $\hbar^2/2\mu = 1$, where $h = 2\pi\hbar$ is Planck's constant and μ is the reduced mass. The radial Schrödinger equation then has the form

$$-\frac{d^2\psi(r)}{dr^2} + [V(r) + \frac{l(l+1)}{r^2}]\psi(r) = E\psi(r), \tag{15}$$

where $V(r)$ is the potential energy function and E is the total energy. Equation (5a) and the Schrödinger equation will be identical if we define the potential to be

$$V(r) = k^2[1 - n^2(r)] \tag{16}$$

and

$$E = k^2. \tag{17}$$

The total potential (or effective potential) is the sum of the potential function $V(r)$ and the centrifugal potential, which is given by

$$V_l(r) = k^2[1 - n^2(r)] + \frac{l(l+1)}{r^2}. \tag{18}$$

We consider first, as an introduction to the methodology, the special case of a spherical particle with a constant refractive index n. The potential in this case is given by

$$V_l(r) = \begin{cases} k^2(1-n^2) + l(l+1)/r^2, & r \leq a \\ l(l+1)/r^2, & r > a \end{cases} \tag{19}$$

where the values of n^2 and k^2 will define whether this potential is attractive or repulsive. We are interested in the case of a dielectric particle with $n > 1$ and with $k > 0$. For the specific example as presented in Ref. [7], consider the potential function $V_{40}(r)$ for a particle of radius a, the refractive index $n = 1.47$, and wave number $k = 33/a$. For convenience, the unit of length and the particle radius are chosen to be equal. Therefore, $a = 1$ and $k = 33$. As another example, we apply this technique to the case that $n = 4/3$ and $k = 33$. The potential function $V_{40}(r)$ for this case is shown in Figure 4. The well in the region $r_1 < r < a$ for a given k is surrounded by the two classically 'forbidden' regions $0 \leq r < r_1$ and $a < r < r_2$. The points r_1 and r_2 are called the classical turning points. These points can be found by evaluating the local wave number $p_l(r)$, which is defined by $p_l^2(r) = E - V_l(r)$. Therefore, this can be written in the form

$$p_l^2(r) = k^2n^2(r) - \frac{l(l+1)}{r^2}. \tag{20}$$

In the quantum-mechanical problem, the particle can tunnel through the classically forbidden region $a < r < r_2$ into the classically allowed potential well. For specific

values of the energy level, the particles will become temporally trapped in the well, oscillating back and forth many times and finally tunneling back through the classical forbidden region to the outside world. These phenomena are called quasi-bound states or resonances. The resonance described here can be called a shape resonance because the resonance behavior arises from the shape of the potential, i.e., the well and the barrier. Moreover, if the shape resonance has the barrier formed by the centrifugal potential, it is called an orbiting resonance. This resonance corresponds to the usual interpretation of MDRs in terms of light rays propagating around the inside surface of the sphere.

2.3.2 MDR'S INTERPRETED AS SHAPE RESONANCES

We have noted that the electromagnetic scattering problem has a direct connection to the quantum-mechanical problem. Electromagnetic energy can tunnel through the classically forbidden region and become temporarily trapped in resonance states. In the following discussion, we assume that the refractive index is a real quantity (though this is not strictly necessary).

In Figure 4 the shape of the potential well depends on the energy k^2. However, in the quantum-mechanical problem the potential is independent of the energy. This diagram shows the case when the energy k^2 lies between the top, $V(a^+)$, and bottom, $V(a^-)$, of the well. From (19) we see that when k increases, the bottom of the potential well will drop. The energy level k^2 will finally coincide with the top of the well. In quantum mechanics, only certain levels of energy will satisfy the boundary conditions and are allowed in a potential well. The problem of shape resonances is similar in this regard.

The boundary conditions at $r = 0$ are given by $S_l(0) = T_l(0) = 0$. These conditions are necessary to make sure that all scattering solutions are finite at the origin. The solutions for the internal region $0 \leq r \leq a$ are given by (6). The solution for the external region $r > a$ is given by (8a) and (8b). These functions are a linear combination of the Riccati-Bessel functions $\psi_l(kr)$ and $\chi_l(kr)$. In the classically forbidden region, $a < r < r_2$, these two functions have opposite behaviors. When the function $\psi_l(kr)$ has exponential-like increase rapidly in this region, the function $\chi_l(kr)$ has exponential-like decrease. At $r = r_2$ these functions stop their exponential-like behavior and begin an oscillatory behavior in the outside region $r > r_2$.

To find a resonance, we need the condition that the wave function has an exponential-like decay in the barrier region, so it will tend to zero as the barrier is extended to $r \to \infty$. The quasi-bound state will become a real bound state. Therefore, only the (exponential-like) decreasing function $\chi_l(kr)$ is allowed in the barrier region. This implies that the coefficient that multiplies the (exponential-like) increasing function $\psi_l(kr)$ in the wave function defined by (8a) and (8b) must be zero; i.e., $\beta_l = 0$ ($\alpha_l = 0$) at the location of a TE (TM) resonance, respectively. These conditions that are used to determine a shape resonance and to find the location of a MDR are the same.

By substituting $\beta_l = 0$ and $\alpha_l = 0$ in to (13a) and (13b) gives the equations that can be used to determine the locations of TE and TM resonances, respectively:

$$\psi_l(nx)\chi_l'(x) = n\psi_l'(nx)\chi_l(x), \tag{21a}$$

$$\psi_l'(nx)\chi_l(x) = n\psi_l(nx)\chi_l'(x). \tag{21b}$$

These equations have infinitely many discrete values of the size parameter x_0. However, only the finite number of values of x_0 that are in the range between the bottom and top of the potential well are considered to be resonant states. There are no solutions below the bottom of the well. The solutions above the top of the well are not classified as resonances because they are too wide to have the properties discussed above.

In Figure 4, the bottom and the top of the potential well (for the case considered by Johnson, namely $n = 1.47$ and $l = 40$) are 27.5 and 40.5, respectively. This potential has three TE and three TM resonances between 27.5 and 40.5. The TE resonances are located at 31.0589, 34.6112, and 37.6531. The TM resonances are located at 31.5192, 34.9960, and 37.9080. For the case $n = 4/3$ and $l = 40$, the bottom and the top of the potential well are 30.365 and 40.5, respectively. This potential has two TE and two TM resonances. The TE resonances are located at 34.0668 and 37.8985, and the TM resonances are located at 34.4763 and 38.1450.

In Figures 5 and 6, the wave functions for the three TE and TM resonances for the case $n = 1.47$ and $l = 40$ are shown, respectively. They are the Debye potential functions $S_{40}(r)$ and $T_{40}(r)$, obtained by solving (5a) and (5b). At the proper level, they are shown superimposed upon the potential function $V_{40}(r)$. The wave functions show bound state within the region of potential well. The lowest-level wave function

has a single peak, the next level has two peaks (positive and negative), and the third level has three peaks. Electromagnetic energy is temporarily trapped in the potential well. It can enter and leave the potential well by tunneling through the outer centrifugal barrier. The deeper well has a larger barrier than the upper levels.

In Figures 7 and 8, the wave functions for the three TE and TM resonances for the case $n = 4/3$ and $l = 40$ are shown, respectively. They are the Debye potential functions $S_{40}(r)$ and $T_{40}(r)$, obtained by solving (5a) and (5b). At the same proper level in the case $n = 1.47$ and $l = 40$, they are shown superimposed upon the potential function $V_{40}(r)$. The wave functions have only two resonances inside the region of potential well for this case. The lowest-level wave function has a single peak, and the next level has two peaks (positive and negative).

Figure 9 shows the change pattern that the wave function transverses the TE, $l = 40$, located at $x_0 = 34.6112$. The top picture shows the wave function for the case $x > 34.6112$, which is above the resonance. The wave function $S_{40}(r)$ shows an exponential-like increase in the tunneling region. The amplitude of the wave function outside the particle $r > r_2$ is much larger than the amplitude inside the particle. The center picture shows the case $x = 34.6112$, which is the case that the wave function has an exponential-like decrease in the tunneling region. The amplitude of the wave function inside the particle is much larger than the amplitude outside because the field strength increases rapidly in the layer just outside the surface, $a < r < r_2$, and then continues to a maximum inside the particle near the surface (both inside and outside). This is sufficient to define a resonance. The bottom picture shows the case $x < 34.6112$, which is below the resonance. The wave function has an increase exponential-like manner in the tunneling region. Thus, the amplitude inside a particle is smaller than the amplitude outside. This case is very similar to the case $x > 34.6112$ (top picture) except that the exponential-like growth in the tunneling region is in the negative direction (i.e. opposite to the top picture).

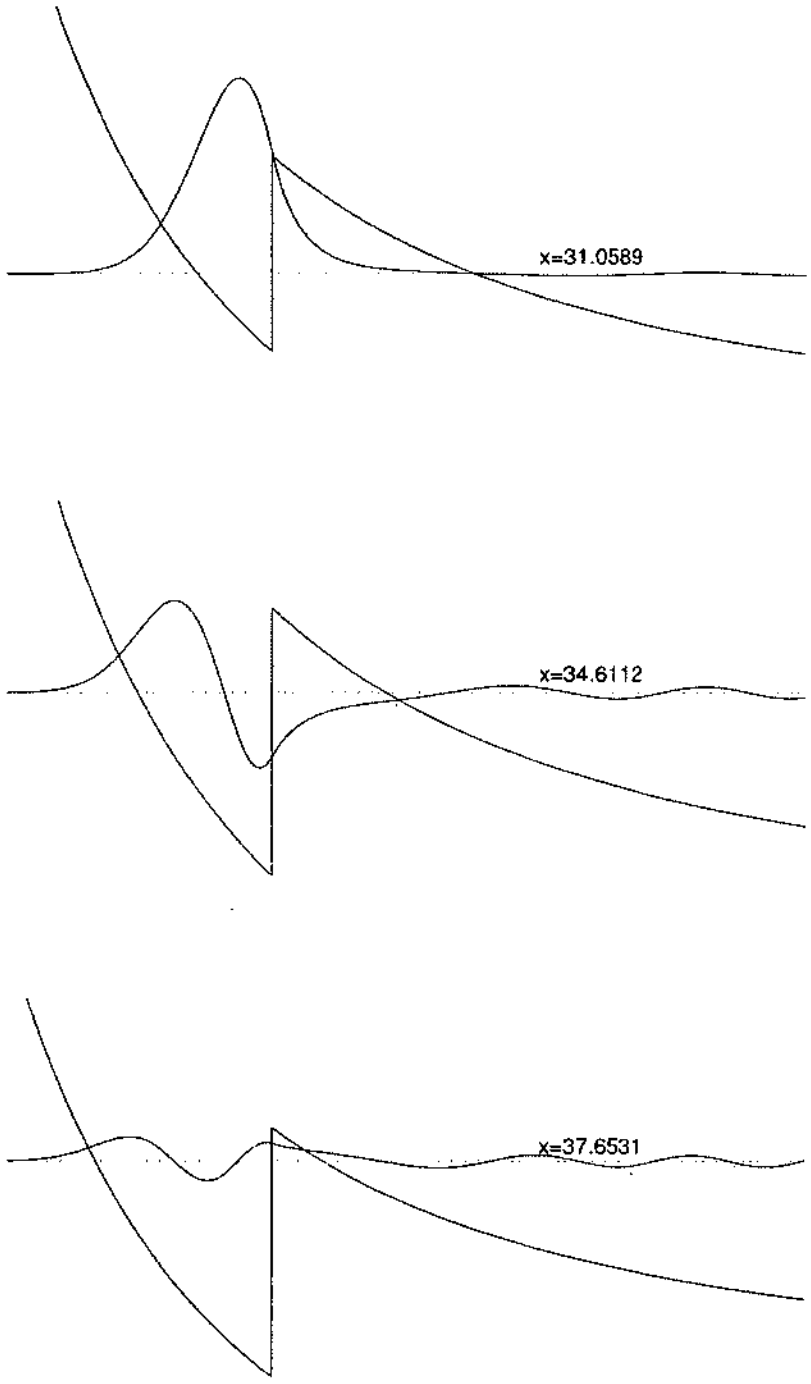

FIG. 5: Radial wave functions for the three TE, $n = 1.47$, $l = 40$ resonances.

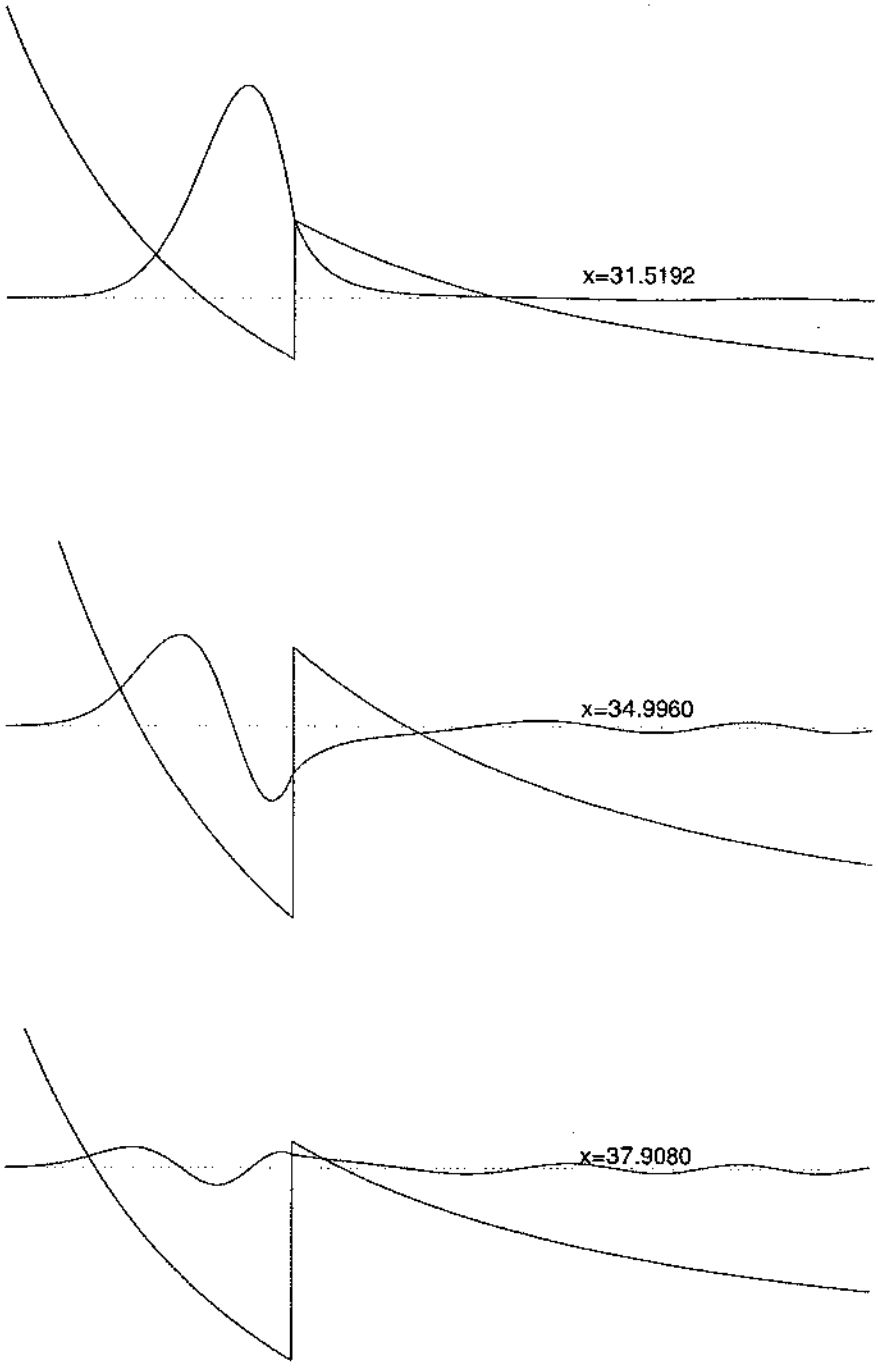

FIG. 6: Radial wave functions for the three TM, $n = 1.47$, $l = 40$ resonances.

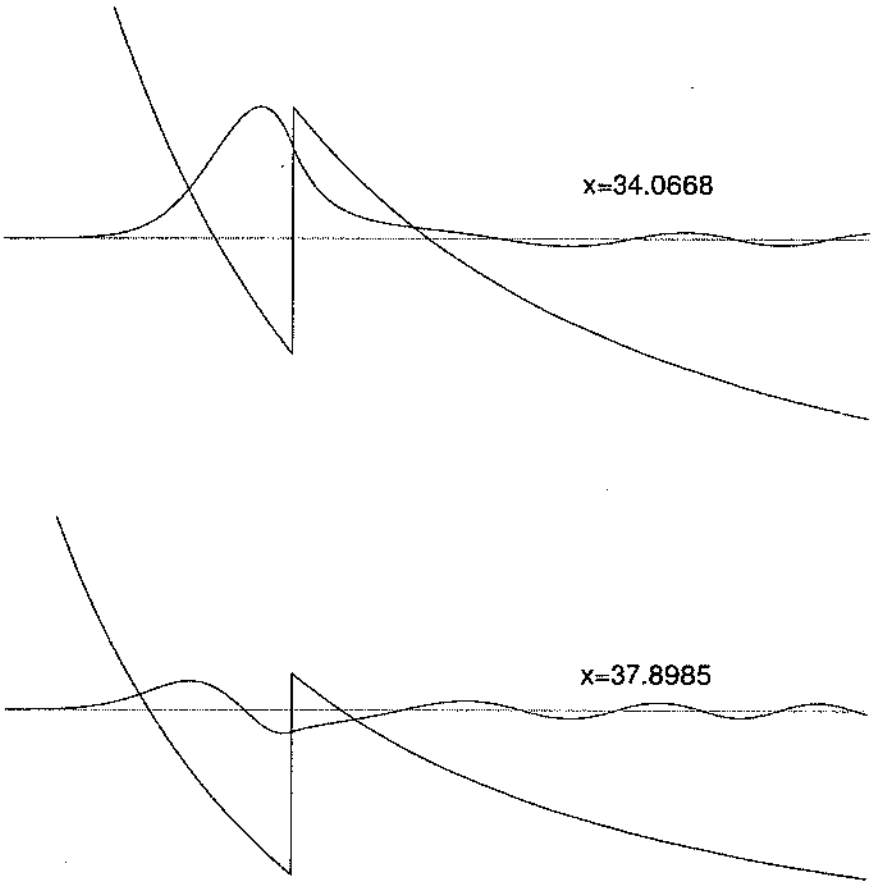

FIG. 7: Radial wave functions for the three TE, $n = 4/3$, $l = 40$ resonances.

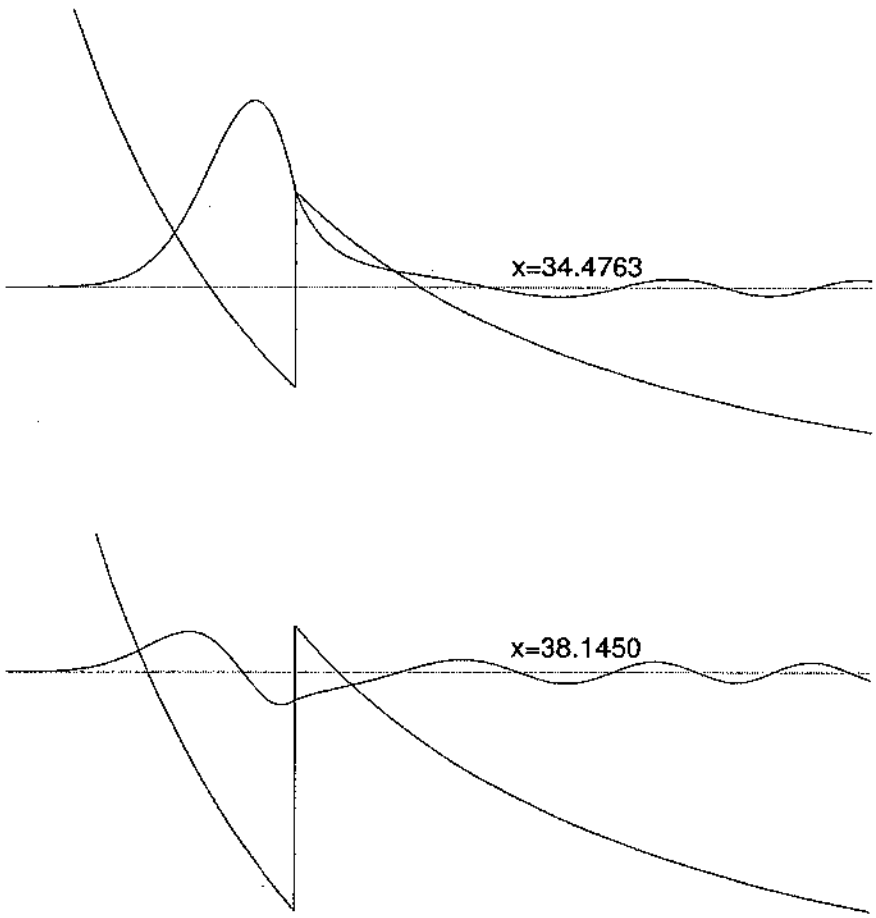

FIG. 8: Radial wave functions for the three TM, $n = 4/3$, $l = 40$ resonances.

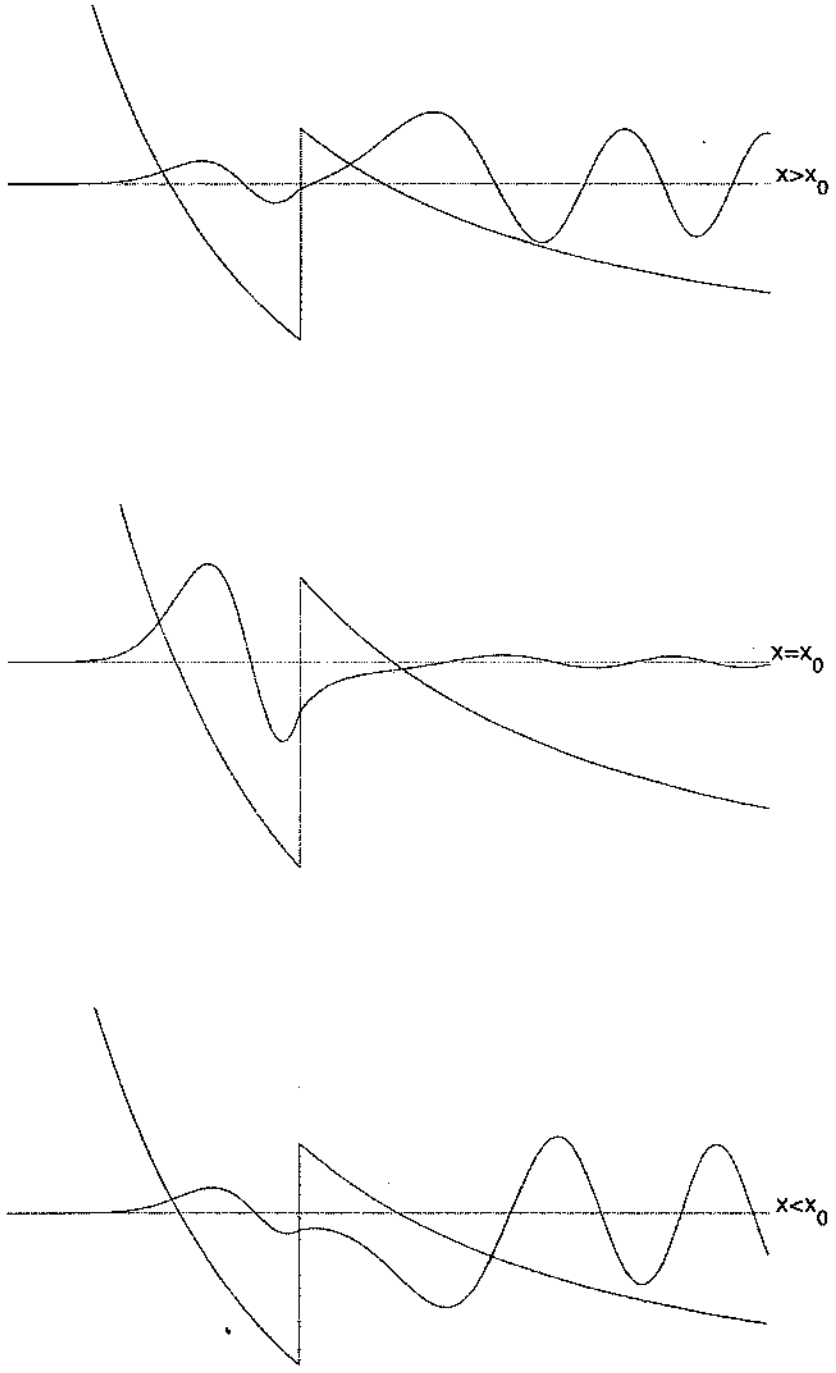

FIG. 9: Behavior of the TE wave function in the vicinity of a resonance: behavior for a size parameter value slightly above resonance (top); on resonance (middle); below resonance(bottom).

2.4 SCATTERING THEORY FOR THREE-LAYER MODEL

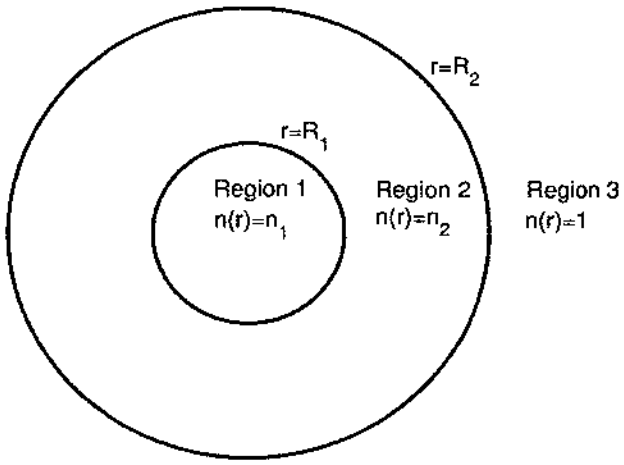

FIG. 10: A piecewise constant refractive index associated with a multi-layer spherical dielectric particle.

We again consider the functions $S_l(r)$ and $T_l(r)$ are the radial Debye potentials, which satisfy the following second-order differential equations (5a) and (5b) (reproduced here for convenience):

$$\frac{d^2S_l(r)}{dr^2} + [k^2n^2(r) - \frac{l(l+1)}{r^2}]S_l(r) = 0,$$

$$\frac{d^2T_l(r)}{dr^2} - \frac{2}{n(r)}\frac{dn(r)}{dr} + [k^2n^2(r) - \frac{l(l+1)}{r^2}]T_l(r) = 0.$$

In the three-layer case, we consider a piecewise constant refractive index associated with a multi-layer spherical dielectric particle as shown in Figure 10. In regions where the indices of refraction have the constant value n_1 and n_2, the two differential equations (5a) and (5b) have the same form in each region, and the linearly independent solutions are again Riccati-Bessel functions,

$$\psi_l(nkr) = nkrj_l(nkr), \tag{22a}$$

$$\chi_l(nkr) = nkry_l(nkr), \tag{22b}$$

where $j_l(nkr)$ and $y_l(nkr)$ are spherical Bessel functions of the first and second kinds, respectively.

Since we need the conditions where the resonances of TE and TM modes of the 3-layer case can be found, the solutions of the differential equations (5a) and (5b) in the various regions are considered in Sections 2.4.1 and 2.4.2.

2.4.1 TE MODE

For the TE mode of the three-layer model

$$\begin{aligned} &\textit{Region } 1\ (0 < r < R_1): && S_{1l}(r) = \psi_l(n_1 kr), \\ &\textit{Region } 2\ (R_1 < r < R_2): && S_{2l}(r) = A_l[\chi_l(n_2 kr) + \alpha_l \psi_l(n_2 kr)], \\ &\textit{Region } 3\ (r > R_2): && S_{3l}(r) = B_l[\chi_l(kr) + \beta_l \psi_l(kr)]. \end{aligned} \tag{23}$$

Matching solutions at $r = R_1$ and $r = R_2$ by using the log-derivative formalism in (9a) and (9b) for the continuity of the solution where the refractive index is discontinuous in each region, we obtain

$$A_l = \frac{\psi_l(n_1 kR_1)}{\chi_l(n_2 kR_1) + \alpha_l(n_2 kR_1)}, \tag{24a}$$

$$B_l = \frac{A_l[\chi_l(n_2 kR_2) + \alpha_l \psi_l(n_2 kR_2)]}{\chi_l(kR_2) + \beta_l \psi_l(kR_2)}, \tag{24b}$$

where

$$\alpha_l = -\frac{n_2 \psi_l(n_1 kR_1)\chi_l'(n_2 kR_1) - n_1 \psi_l'(n_1 kR_1)\chi_l(n_2 kR_1)}{n_2 \psi_l(n_1 kR_1)\psi_l'(n_2 kR_1) - n_1 \psi_l'(n_1 kR_1)\psi_l(n_2 kR_1)}, \tag{25a}$$

$$\beta_l = -\frac{\chi_l'(kR_2)[\chi_l(n_2 kR_2) + \alpha_l \psi_l(n_2 kR_2)] - n_2 \chi_l(kR_2)[\chi_l'(n_2 kR_2) + \alpha_l \psi_l'(n_2 kR_2)]}{\psi_l'(kR_2)[\chi_l(n_2 kR_2) + \alpha_l \psi_l(n_2 kR_2)] - n_2 \psi_l(kR_2)[\chi_l'(n_2 kR_2) + \alpha_l \psi_l'(n_2 kR_2)]}. \tag{25b}$$

2.4.2 TM MODE

For the TM mode

$$\begin{aligned} &\textit{Region } 1\ (0 < r < R_1): && T_{1l}(r) = \psi_l(n_1 kr), \\ &\textit{Region } 2\ (R_1 < r < R_2): && T_{2l}(r) = \bar{A}_l[\chi_l(n_2 kr) + \bar{\alpha}_l \psi_l(n_2 kr)], \\ &\textit{Region } 3\ (r > R_2): && T_{3l}(r) = \bar{B}_l[\chi_l(kr) + \bar{\beta}_l \psi_l(kr)]. \end{aligned} \tag{26}$$

Similar to TE mode, we use (9a) and (9b) for the continuity of the solution where the refractive index is discontinuous in each region at the boundaries $r = R_1$ and $r = R_2$, we obtain

$$\bar{A}_l = \frac{\psi_l(n_1 k R_1)}{\chi_l(n_2 k R_1) + \bar{\alpha}_l(n_2 k R_1)}, \tag{27a}$$

$$\bar{B}_l = \frac{\bar{A}_l[\chi_l(n_2 k R_2) + \bar{\alpha}_l \psi_l(n_2 k R_2)]}{\chi_l(k R_2) + \bar{\beta}_l \psi_l(k R_2)}, \tag{27b}$$

where

$$\bar{\alpha}_l = -\frac{n_2 \psi_l'(n_1 k R_1)\chi_l(n_2 k R_1) - n_1 \psi_l(n_1 k R_1)\chi_l'(n_2 k R_1)}{n_2 \psi_l'(n_1 k R_1)\psi_l(n_2 k R_1) - n_1 \psi_l(n_1 k R_1)\psi_l'(n_2 k R_1)}, \tag{28a}$$

$$\bar{\beta}_l = -\frac{n_2 \chi_l'(k R_2)[\chi_l(n_2 k R_2) + \bar{\alpha}_l \psi_l(n_2 k R_2)] - \chi_l(k R_2)[\chi_l'(n_2 k R_2) + \bar{\alpha}_l \psi_l'(n_2 k R_2)]}{n_2 \psi_l'(k R_2)[\chi_l(n_2 k R_2) + \bar{\alpha}_l \psi_l(n_2 k R_2)] - \psi_l(k R_2)[\chi_l'(n_2 k R_2) + \bar{\alpha}_l \psi_l'(n_2 k R_2)]}. \tag{28b}$$

2.5 SCATTERING THEORY FOR THREE-LAYER MODEL

2.5.1 QUANTUM-MECHANICAL ANALOGY

We begin with considering (15) in Section 2.3.1. The potential in the three-layer case is given by

$$V_l(r) = \begin{cases} k^2(1 - n_1^2) + l(l+1)/r^2, & 0 \le r \le R_1, \\ k^2(1 - n_2^2) + l(l+1)/r^2, & R_1 \le r \le R_2, \\ l(l+1)/r^2, & r > R_2, \end{cases} \tag{29}$$

which corresponds to the refractive index in Figure 10 as shown:

$$n(r) = \begin{cases} n_1, & 0 \le r \le R_1, \\ n_2, & R_1 \le r \le R_2, \\ 1, & r > R_2. \end{cases} \tag{30}$$

The values of n_1^2, n_2^2, and k^2 define the characteristic of the potential, i.e. whether it is attractive or repulsive. In this paper, we focus on a dielectric particle with $n_1 > 1$,

$n_2 > 1$, and $k > 0$. By using similar technique as shown in Ref. [7], we consider the potential function $V_l(r)$ for a particle of multi-layer sphere with radius R_1 and R_2 corresponding with the refractive index n_1 and n_2, and the size parameters $x = kR_1$ and $y = kR_2$, respectively. The specific examples are presented in Section 2.5.2. For convenience, the unit of length and the particle radius are chosen to be equal.

We now separate the refractive index profile into two cases. The potential profiles corresponding to both cases of refractive index are also provided:

Case 1: Increasing refractive index profile (see Figure 11)

$$n(r) = \begin{cases} n_1, & 0 \le r \le R_1, \\ n_2 \ (> n_1), & R_1 \le r \le R_2, \\ 1, & r > R_2. \end{cases} \tag{31}$$

Case 2: Decreasing refractive index profile (see Figure 12)

$$n(r) = \begin{cases} n_1, & 0 \le r \le R_1, \\ n_2 \ (< n_1), & R_1 \le r \le R_2, \\ 1, & r > R_2. \end{cases} \tag{32}$$

In the next section, we have the results for two specific examples. The first example (see Figures 15 and 16) shows the potential function $V_{40}(r)$ and the wave function $S_{40}(r)$ for a particle of radius $R_1 = 0.7$ and $R_2 = 1$, refractive index $n_1 = 1.2$ and $n_2 = 1.5$ (increasing refractive index profile as shown in Figure 11), wavenumbers $k = x_0/R_1 = y_0/R_2$. The potential function $V_{40}(r)$ for this case is shown in Figure 13. The other example (see Figures 17 and 18) shows the potential function $V_{40}(r)$ for a particle of radius $R_1 = 0.7$ and $R_2 = 1$, refractive index $n_1 = 1.52$ and $n_2 = 1.25$ (decreasing refractive index profile as shown in Figure 12), wavenumbers $k = x_0/R_1 = y_0/R_2$. The potential function in this case is shown in Figure 14.

For specific values of the energy level, the particles will become temporally trapped in the well, oscillating back and forth many times and tunneling back through the classical forbidden region to the outside world eventually. This is where we found the shape resonances of the three-layer model.

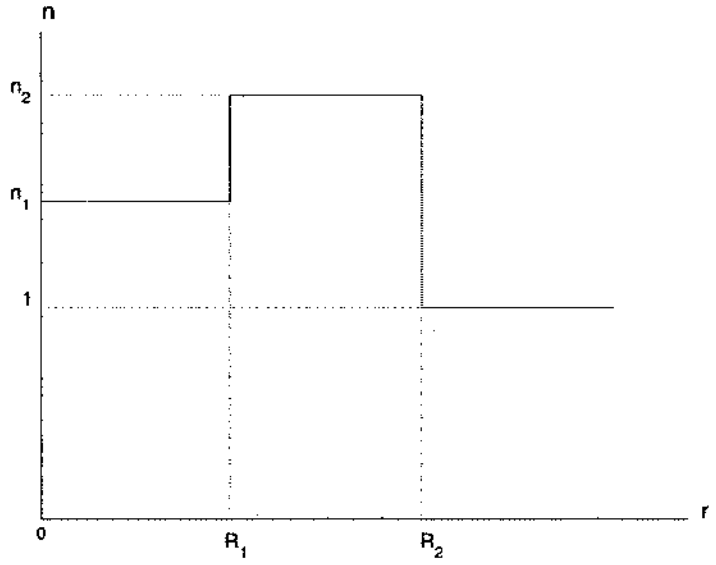

FIG. 11: Case 1: Refractive index profile for $n_1 < n_2$.

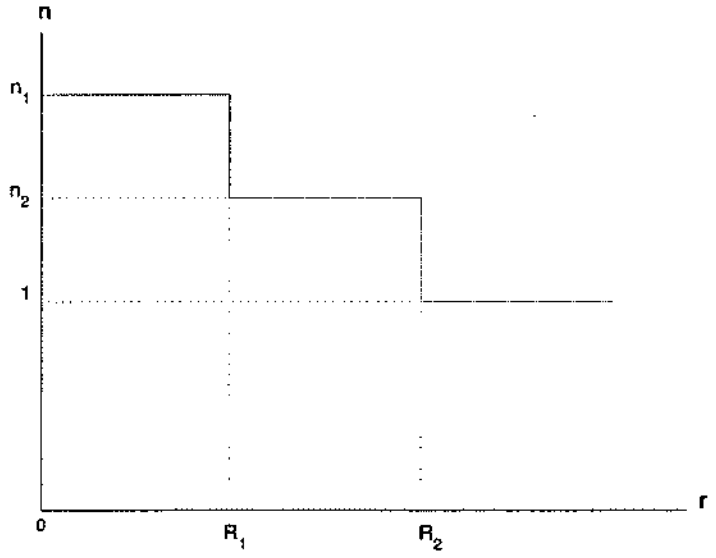

FIG. 12: Case 2: Refractive index profile for $n_1 > n_2$.

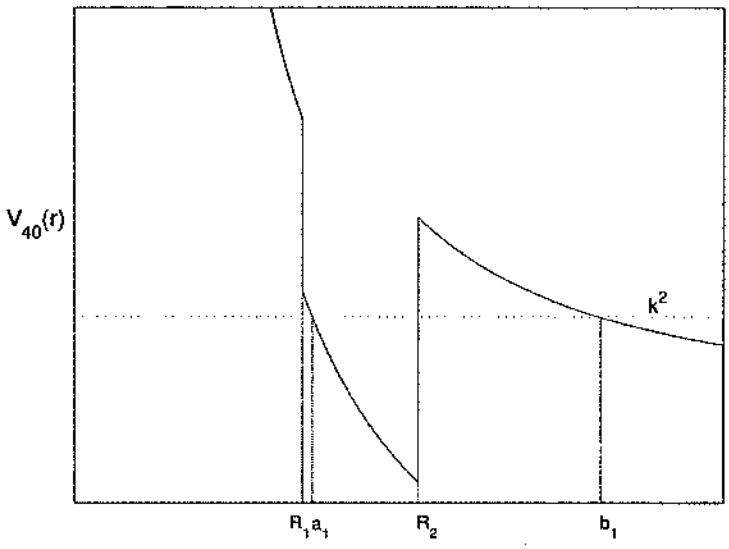

FIG. 13: Case 1: $V(r)$ potential for $n_1 < n_2$.

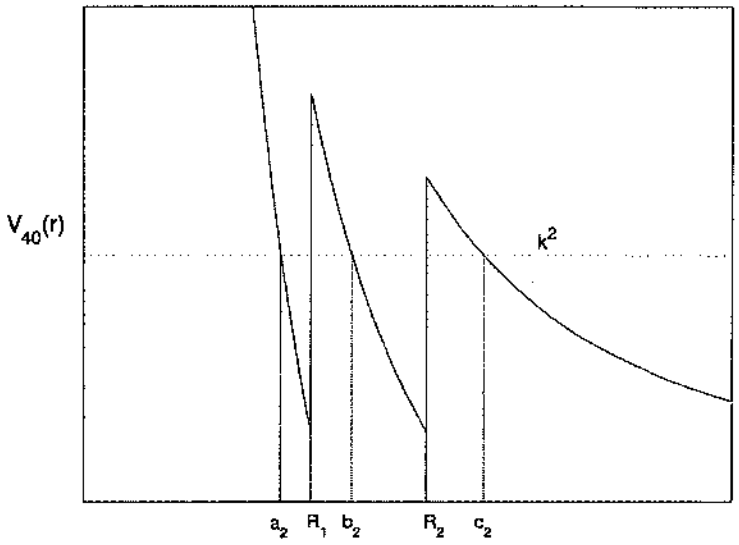

FIG. 14: Case 2: $V(r)$ potential for $n_1 > n_2$.

2.5.2 MDR'S INTERPRETED AS SHAPE RESONANCES

In Figures 13 and 14, the potential well depends on the energy k^2 and the refractive index in each region. The diagram shows the case when the energy k^2 lies between the top and the bottom of the well. From (29) we can see that the shape of the well depends on the values of refractive indices n_1 and n_2 in each region. When $n_1 < n_2$ (see Figure 11), we have a single well (see Figure 13); however, when $n_1 > n_2$ (see Figure 12) we have double wells (see Figure 14).

Similar to the two-layer model, the boundary conditions at $r = 0$ are given by $S_{1l}(0) = T_{1l}(0) = 0$ to guarantee that all scattering solutions are finite at the origin. The solutions in each region are given by (23). These functions are the linear combination of the Riccati-Bessel functions $\psi_l(n_2kr)$ and $\chi_l(n_2kr)$ in Region 2 and $\psi_l(kr)$ and $\chi_l(kr)$ in Region 3.

For the case that $n_1 < n_2$, when n_2 is much larger than n_1, the well will be deeper and wider. The most striking feature of this case is the presence of the potential function $V_{40}(r)$ (for increasing refractive index) is the presence of a potential well in the region $a_1 < r < R_2$. This is a classically allowed region. The well is surrounded by the two classically forbidden regions $0 \leq r < a_1$ and $R_2 < r < b_1$. The points a_1 and b_1 are called the classical turning points. In the equivalent quantum-mechanical problem a particle can tunnel through the classically forbidden region $R_2 < r < b_1$, into the classically allowed potential well.

For the case that $n_1 > n_2$, the most interesting feature of this case is the presence of the potential wells in the regions $a_2 < r < R_1$ and $b_2 < r < R_2$. These are the classically allowed regions. They are surrounded by the three classically forbidden regions $0 \leq r < a_1$, $R_1 < r < b_2$, and $R_2 < r < c_2$. The points a_2, b_2, and c_2 are the classical turning points for this case.

In the forbidden regions $r > b_1$ in Figure 13 and $r > c_2$ in Figure 14, the two functions $\psi_l(kr)$ and $\chi_l(kr)$ have opposite behaviors. When the function $\psi_l(kr)$ has exponential-like behavior increasing rapidly in this region, the function $\chi_l(kr)$ has exponential-like decreasing behavior.

To find the resonance, we need the condition that the wave function has an exponential-like decay in the barrier region to ensure that it goes to zero as the barrier radius $r \to \infty$. Therefore, we need only the exponential-like decreasing function $\chi_l(kr)$ in the barrier region. This implies that the coefficient that multiplies the exponential-like increasing function $\psi_l(kr)$ in the wave function as defined in

Region 3 must be zero, i.e. $\alpha_l = 0$ and $\beta_l = 0$ ($\bar{\alpha}_l = 0$ and $\bar{\beta}_l = 0$) at the location of a TE (TM) resonance, respectively.

By substituting $\alpha_l = 0$ and $\beta_l = 0$, $\bar{\alpha}_l = 0$ and $\bar{\beta}_l = 0$ into (25a), (25b), (28a) and (28b), we have the equations that can be used to determine the locations of TE and TM resonances, respectively:

TE:

$$n_2\psi_l(n_1kR_1)\chi_l'(n_2kR_1) = n_1\psi_l'(n_1kR_1)\chi_l(n_2kR_1), \tag{33a}$$

$$\chi_l'(kR_2)[\chi_l(n_2kR_2) + \alpha_l\psi_l(n_2kR_2)] = n_2\chi_l(kR_2)[\chi_l'(n_2kR_2) + \alpha_l\psi_l'(n_2kR_2)]. \tag{33b}$$

TM:

$$n_2\psi_l'(n_1kR_1)\chi_l(n_2kR_1) = n_1\psi_l(n_1kR_1)\chi_l'(n_2kR_1), \tag{34a}$$

$$n_2\chi_l'(kR_2)[\chi_l(n_2kR_2) + \bar{\alpha}_l\psi_l(n_2kR_2)] = \chi_l(kR_2)[\chi_l'(n_2kR_2) + \bar{\alpha}_l\psi_l'(n_2kR_2)]. \tag{34b}$$

These equations have infinitely many discrete values of the size parameters x_0 and y_0. However, only the finite number of values of x_0 and y_0 that are in the range between the top and the bottom of the potential well are considered to be resonant states. Similar to the two-layer model, there are no solutions below the bottom of the well and above the top of the well.

Figure 15 shows the potential function $V_{40}(r)$ and the wave function $S_{40}(r)$ for $n_1 = 1.2$, $n_2 = 1.5$, and $l = 40$. This potential supports three TE resonances for specific value x_0. They are located at $x_0 = 30.3828$ with $y_0 = 28.2439$ (top), $y_0 = 32.2993$ (middle), $y_0 = 35.4808$ (bottom).

Figure 16 shows the potential function $V_{40}(r)$ and the wave function $S_{40}(r)$ for $n_1 = 1.2$, $n_2 = 1.5$, and $l = 40$. The TE resonances for this example are located at $x_0 = 40.5499$ with $y_0 = 35.4808$ (top), and $y_0 = 38.3548$ (bottom).

Figure 17 shows the potential function $V_{40}(r)$ and the wave function $S_{40}(r)$ for $n_1 = 1.52$, $n_2 = 1.25$, and $l = 40$. The two locations for TE resonances are located at $x_0 = 29.5815$ with $y_0 = 38.2448$ (top), and $y_0 = 38.2448$ (bottom).

Figure 18 shows the potential function $V_{40}(r)$ and the wave function $S_{40}(r)$ for $n_1 = 1.52$, $n_2 = 1.25$, and $l = 40$. The two locations for TE resonances are located at $x_0 = 33.4975$ with $y_0 = 38.2446$.

Figures 19 and 20 show the change pattern that the wave function experiences as the system transverses the TE for both cases of $n_1 < n_2$ and $n_1 > n_2$ with $l = 40$, respectively. In the first case, the TE resonance is located at $x_0 = 30.3828$ and $y_0 = 32.2993$. The top panel shows the case $x = x_0$ and $y = 32.0993 < y_0$ which is below the resonance. The middle panel shows the wave function for case $x = x_0$ and $y = y_0$, which is the resonance case. The bottom panel shows the wave function for the case $x = x_0$ and $y = 32.9993 > y_0$ which is above the resonance. In the second case, the TE resonance is located at $x_0 = 33.4975$ and $y_0 = 38.2446$. The top panel shows the case $x = x_0$ and $y = 37.2446 < y_0$ which is below the resonance. The middle panel shows the wave function for case $x = x_0$ and $y = y_0$, which is the resonance case. The bottom panel shows the wave function for the case $x = x_0$ and $y = 38.9446 > y_0$ which is above the resonance.

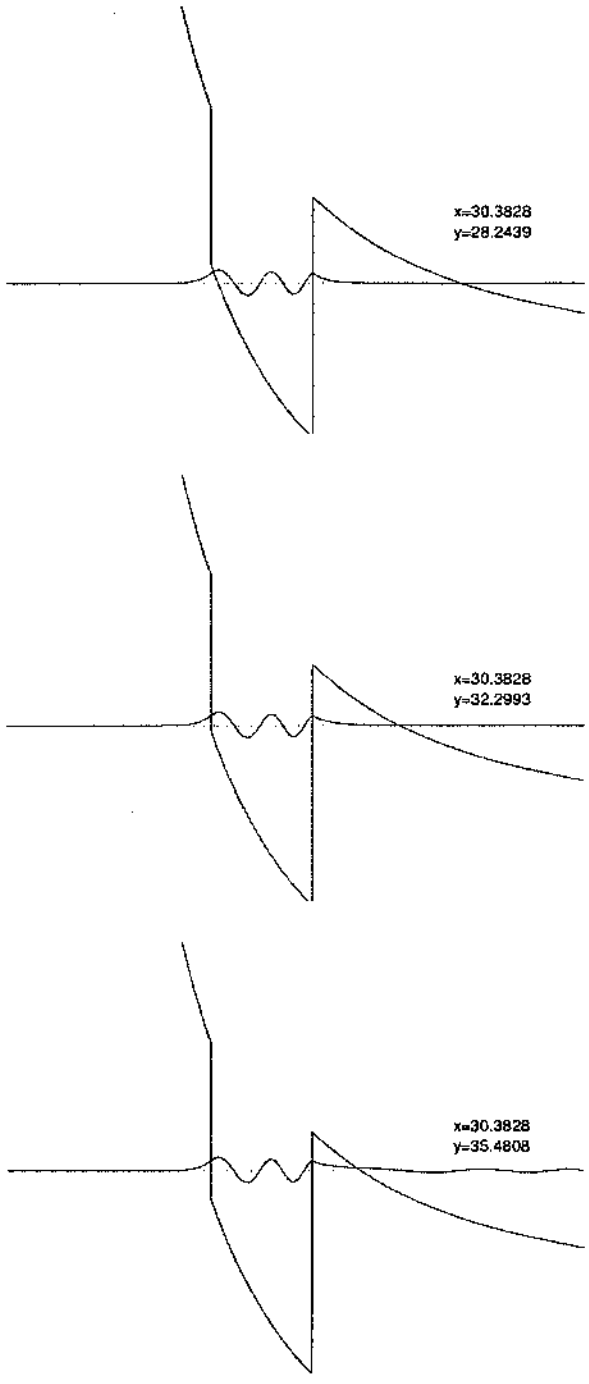

FIG. 15: Radial wave functions for the three TE, $n_1 = 1.2$, $n_2 = 1.5$, $l = 40$ resonances with $x = 30.3828, y = 28.2439$ (top); $x = 30.3828, y = 32.2993$ (middle); $x = 30.3828, y = 35.4808$ (bottom) corresponding to the refractive index profile in Case1.

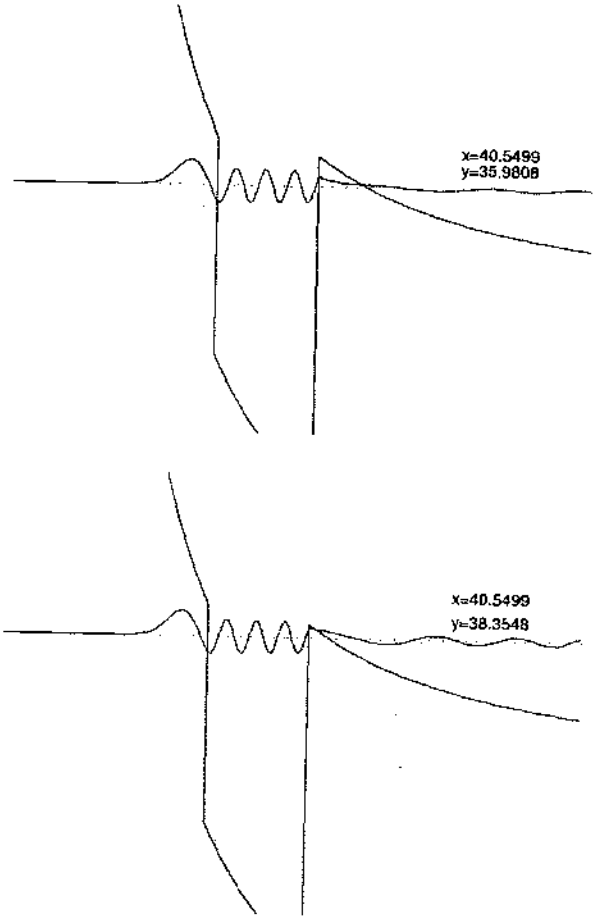

FIG. 16: Radial wave functions for the three TE, $n_1 = 1.2$, $n_2 = 1.5$, $l = 40$ resonances with $x = 40.5499, y = 35.4808$ (top); $x = 40.5499, y = 38.3548$ (bottom) corresponding to the refractive index profile in Case1.

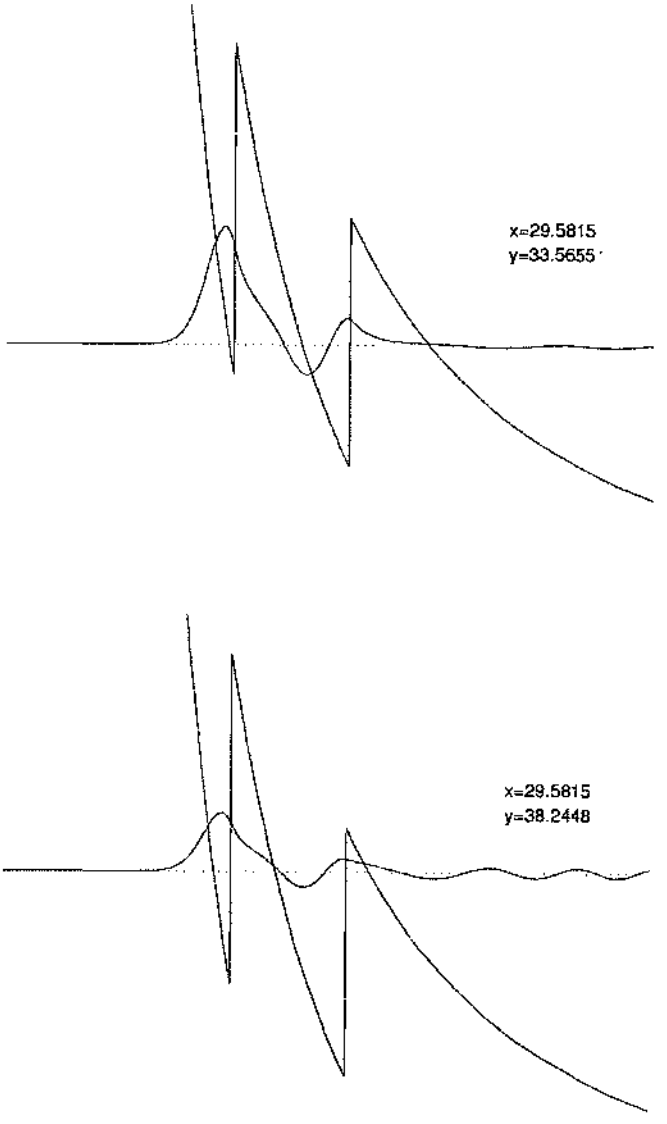

FIG. 17: Radial wave functions for the three TE, $n_1 = 1.52$, $n_2 = 1.25$, $l = 40$ resonances with $x = 29.5815, y = 33.5655$ (top); $x = 29.5815, y = 38.2448$ (bottom), corresponding to the refractive index profile in Case2.

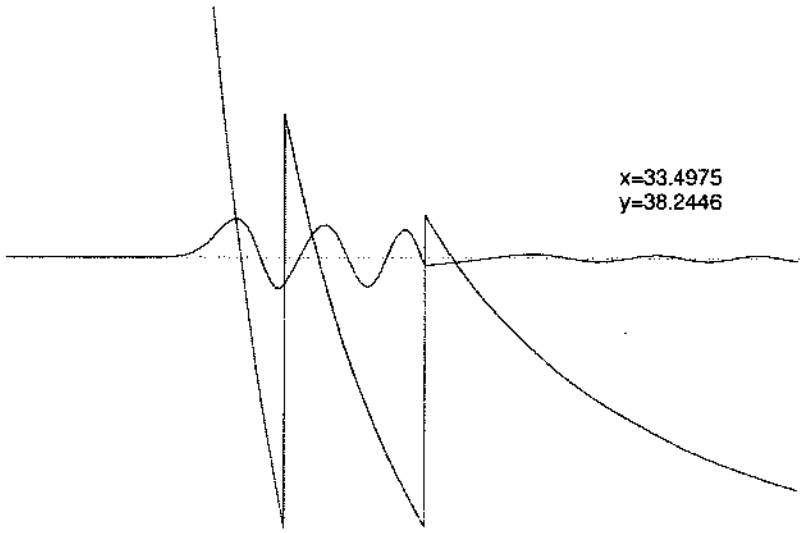

FIG. 18: Radial wave functions for the three TE, $n_1 = 1.52$, $n_2 = 1.25$, $l = 40$ resonances with $x = 33.4975, y = 38.2446$ (corresponding to the refractive index profile in Case2.

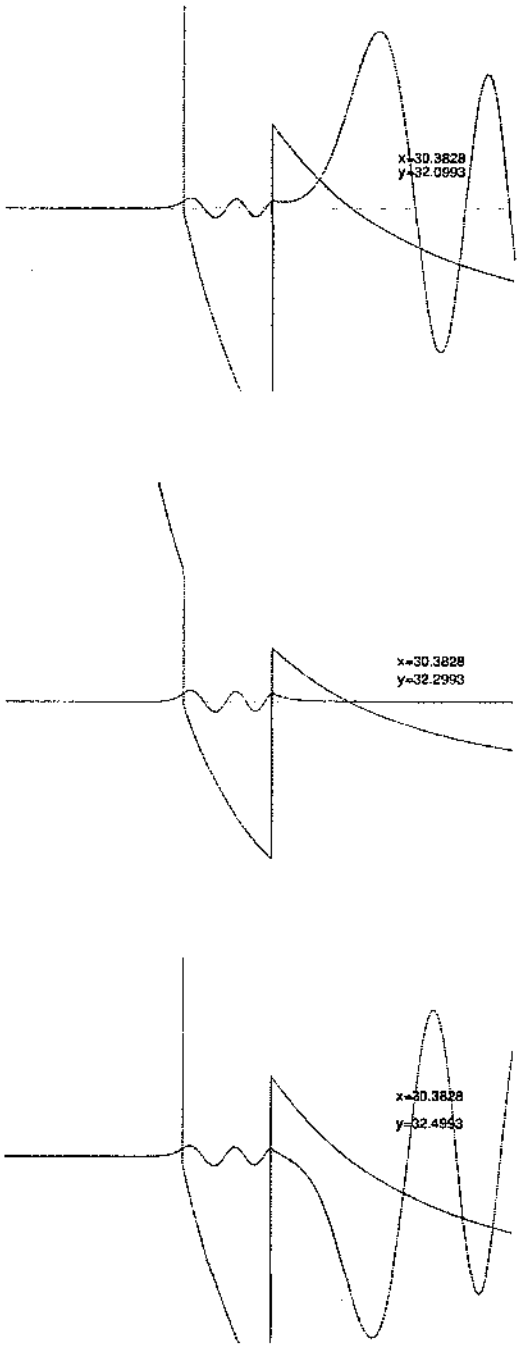

FIG. 19: Behavior of the TE wave function in the vicinity of a resonance for the case $n_1 < n_2$: behavior for a size parameter value slightly below resonance (top); on resonance (middle); above resonance (bottom).

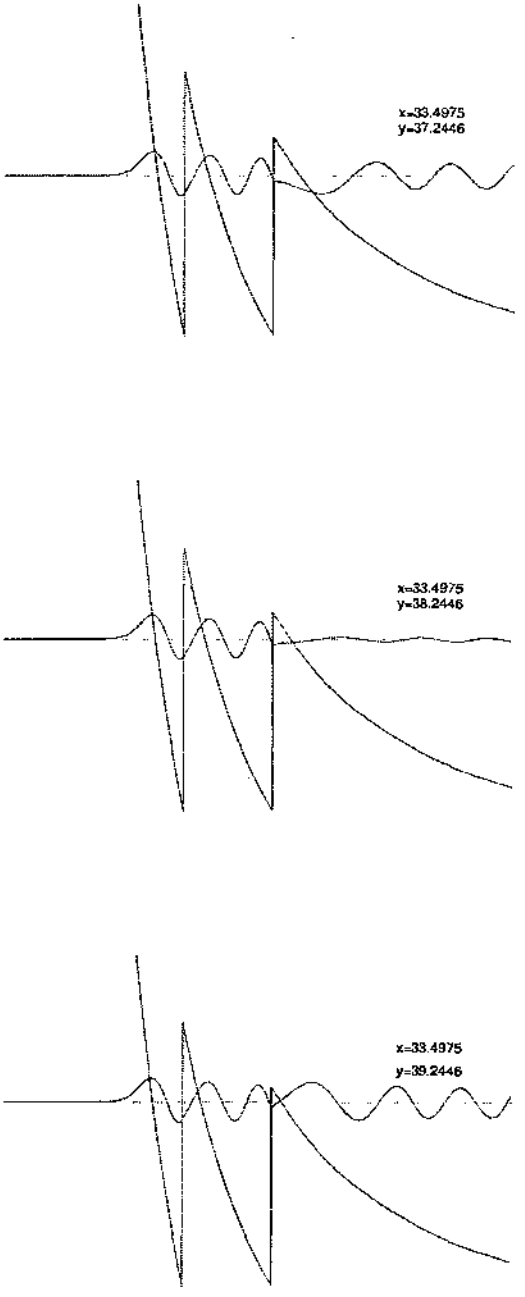

FIG. 20: Behavior of the TE wave function in the vicinity of a resonance for the case $n_1 > n_2$: behavior for a size parameter value slightly below resonance (top); on resonance (middle); above resonance (bottom).

2.6 A DIGRESSION ON RESONANCES USING THE $l = 0$ CASE

Usually in the case of the square well, the time delay is never very large in potential scattering terms. Therefore, to delay the particle for a long time we need a barrier to protect the escape of the particle. We consider the case of the square well with a barrier as shown in Figure 21.

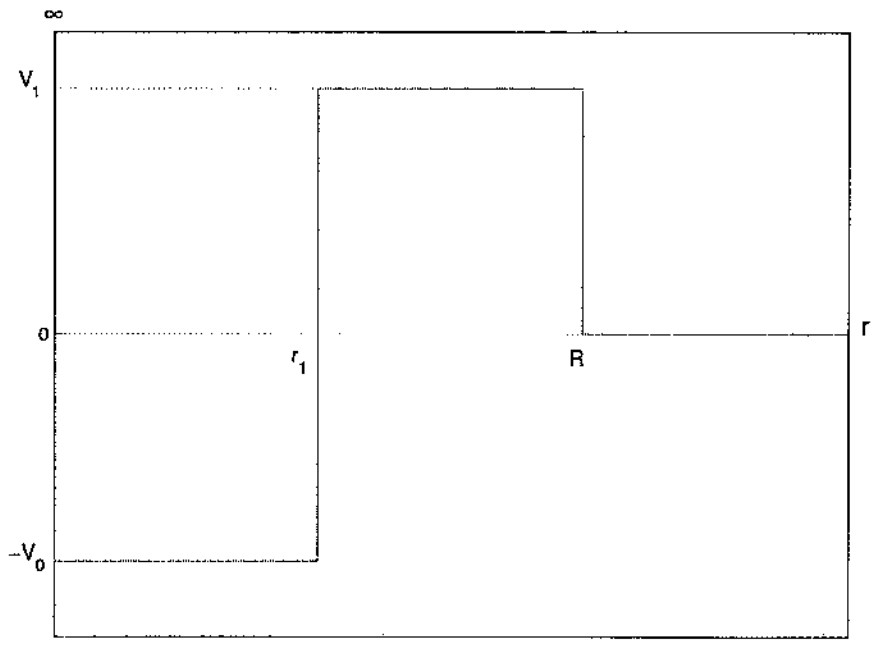

FIG. 21: The one-dimensional potential function of (36), consisting of a rectangular well of depth V_0 and arbitrary width r, and a rectangular barrier of height V_1 and width $R - r_1$.

We generalize a paper in Ref. [10] by considering the one-dimensional potential of Figure 21 which consists of an attractive rectangular well and a repulsive rectangular barrier. The primary reason for this is to derive an $l = 0$ "template" that can be used to "mimic" the $l > 0$ potential wells (see Figure 4). By choosing r_1, R, V_0 and V_1 appropriately we can obtain an approximate representation of $V_l(r)$ in (19).

The stationary Schrödinger wave equation is given by

$$\frac{d^2\psi(r)}{dr^2} + (E - V(r))\psi(r) = 0, \tag{35}$$

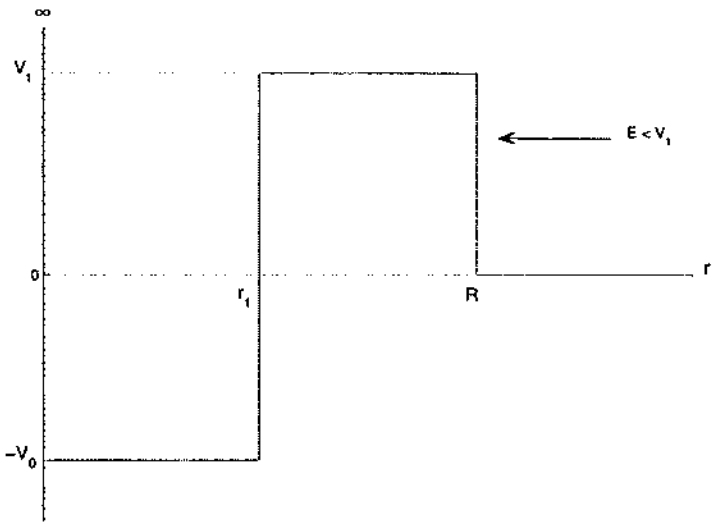

FIG. 22: The one-dimensional potential function of (36), consisting of a rectangular well of depth V_0 and arbitrary width r, and a rectangular barrier of height $V_1 > E$ and width $R - r_1$. The energy level is below the top of the barrier.

where the potential function is defined as (see Figure 21)

$$\begin{aligned} &\textit{Region } 1\ (0 < r < r_1): && V(r) = -V_0 < 0, \\ &\textit{Region } 2\ (r_1 < r < R): && V(r) = V_1 > 0, \\ &\textit{Region } 3\ (r > R): && V(r) = 0. \end{aligned} \tag{36}$$

To find the solution of the Schrödinger wave equation that describes the motion of a 'particle' in the potential and the stationary state of energy $k^2 = E$, we first consider the case that $0 < k^2 < V_1$ for energies below the top of the barrier (see Figure 22). We note that in these units the wave number $k = E^{1/2}$, and all time dependence is suppressed. Then the radial wave function $\psi(r)$ in each region is given as:

In Region 1, we have that

$$\frac{d^2\psi(r)}{dr^2} + (E + V_0)\psi(r) = 0, \tag{37}$$

where $E = k^2$, so let $\bar{k}^2 = E + V_0 = k^2 + V_0$, which yields

$$\psi(kr) = A\sin(\bar{k}r), \tag{38}$$

with the boundary condition $\psi(0) = 0$.

In Region 2, we have that

$$\frac{d^2\psi(r)}{dr^2} + (E - V_1)\psi(r) = 0, \tag{39}$$

where $E = k^2$, so let $\kappa^2 = V_1 - k^2$, which yields

$$\psi(kr) = B(\sinh(\kappa r) + \gamma\cosh(\kappa r)), \tag{40}$$

with two conditions of continuity of the logarithmic derivative of (36) at $r = r_1$ and $r = R$.

In Region 3, we have that

$$\frac{d^2\psi(r)}{dr^2} + E\psi(r) = 0. \tag{41}$$

We normalize the wavefunction to unity, with phase shift δ_0, and we have

$$\psi(kr) = \sin(kr + \delta_0). \tag{42}$$

By using all the boundary conditions, we obtain

$$\gamma = \frac{\frac{\kappa}{\bar{k}}\tan(\bar{k}r_1) - \tanh(\kappa r_1)}{1 - \frac{\kappa}{\bar{k}}\tan(\bar{k}r_1)\tanh(\kappa r_1)}, \tag{43}$$

$$\delta_0 = -kR + \arctan\left\{\frac{k}{\kappa}\frac{\gamma + \tanh(\kappa R)}{1 + \gamma\tanh(\kappa R)}\right\}. \tag{44}$$

Rearranging δ_0 yields

$$\delta_0 = -kR + \arctan\left\{\frac{kR}{\kappa R}\frac{\frac{\kappa r_1}{\bar{k}r_1}\tan(\bar{k}r_1) + \tanh(\kappa(R - r_1))}{[1 + \frac{\kappa r_1}{\bar{k}r_1}\tan(\bar{k}r_1)\tanh(\kappa(R - r_1))]}\right\}, \tag{45}$$

$$B = \frac{\sin(kR + \delta_0)}{\sinh(\kappa R) + \gamma\cosh(\kappa R)}, \tag{46}$$

$$A = \frac{B(\sinh(\kappa r_1) + \gamma\cosh(\kappa r_1))}{\sin(\bar{k}r_1)}. \tag{47}$$

Since $\lim_{\kappa\to 0^+}\gamma = 0$, (45) becomes $\delta_0 = -kR + \arctan(\infty) = -kR + \frac{\pi}{2}$.

We next consider the case that $k^2 > V_1$ for energies above the top of the barrier (see Figure 23). Then the radial wave function $\psi(r)$ in each region is given as:

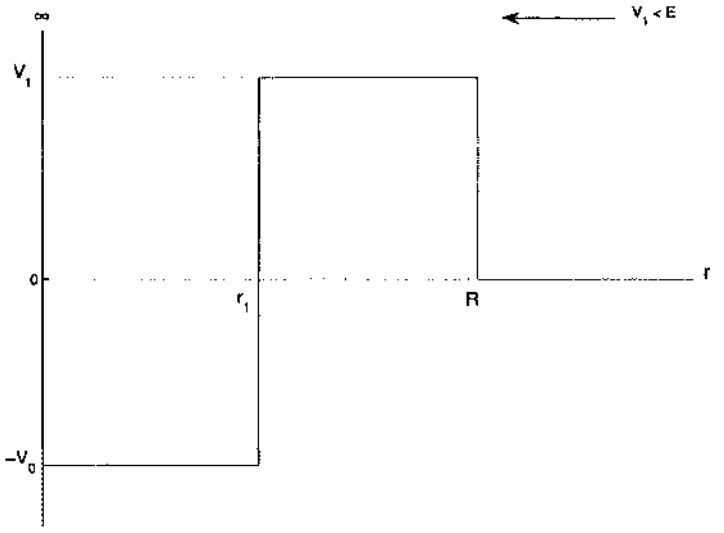

FIG. 23: The one-dimensional potential function of (36), consisting of a rectangular well of depth V_0 and arbitrary width r, and a rectangular barrier of height $V_1 < E$ and width $R - r_1$. The energy level is above the top of the barrier.

In Region 1, we have that

$$\frac{d^2\psi(r)}{dr^2} + (E + V_0)\psi(r) = 0, \tag{48}$$

where $\tilde{k}^2 = E + V_0 = k^2 + V_0$, which yields

$$\psi(kr) = \tilde{A}\sin(\tilde{k}r), \tag{49}$$

with the boundary condition $\psi(0) = 0$.

In Region 2, we have that

$$\frac{d^2\psi(r)}{dr^2} + (E - V_1)\psi(r) = 0, \tag{50}$$

where $\tilde{\kappa}^2 = E - V_1 = k^2 - V_1$, which yields

$$\psi(kr) = B(i\sin(\tilde{\kappa}r) + i\tilde{\gamma}\cos(\tilde{\kappa}r)), \tag{51}$$

with two conditions of continuity of the logarithmic derivative at $r = r_1$ and $r = R$.

In Region 3, we have that

$$\frac{d^2\psi(r)}{dr^2} + E\psi(r) = 0. \tag{52}$$

We normalize the wavefunction to unity, with phase shift δ_0, and we have

$$\psi(kr) = \sin(kr + \delta_0). \tag{53}$$

By using all the boundary conditions, we obtain

$$\tilde{\gamma} = \frac{\frac{\bar{\kappa}}{\bar{k}}\tan(\bar{k}r_1) - \tan(\tilde{\kappa}r_1)}{1 + \frac{\bar{\kappa}}{\bar{k}}\tan(\bar{k}r_1)\tan(\tilde{\kappa}r_1)}, \tag{54}$$

$$\delta_0 = -kR + \arctan\left\{\frac{k}{\tilde{\kappa}}\frac{\tilde{\gamma} + \tan(\tilde{\kappa}R)}{1 - \tilde{\gamma}\tan(\tilde{\kappa}R)}\right\}. \tag{55}$$

Rearranging δ_0 yields

$$\delta_0 = -kR + \arctan\left\{\frac{kR}{\tilde{\kappa}R}\frac{\frac{\bar{\kappa}r_1}{kr_1}\tan(\bar{k}r_1) + \tan(\tilde{\kappa}(R - r_1))}{[1 - \frac{\bar{\kappa}r_1}{kr_1}\tan(\bar{k}r_1)\tan(\tilde{\kappa}(R - r_1))]}\right\}, \tag{56}$$

$$B = \frac{\sin(kR + \delta_0)}{i\sin(\tilde{\kappa}R) + \tilde{\gamma}\cosh(\tilde{\kappa}R)}, \tag{57}$$

$$A = \frac{Bi(\sin(\tilde{\kappa}r_1) + \tilde{\gamma}\cosh(\tilde{\kappa}r_1))}{\sin(\bar{k}r_1)}. \tag{58}$$

By the parameterization method, we first consider the case that $\kappa^2 > 0$. Let $x = kR$, $r_1 = \alpha R$, where $0 < \alpha < 1$. Therefore, $\bar{k} = \sqrt{k^2 + V_0}$ implies that

$$\bar{k}R = \sqrt{k^2R^2 + V_0R^2} = \sqrt{x^2 + \rho_0},$$

where $\rho_0 = V_0R^2$; $\kappa = \sqrt{V_1 - k^2}$ $(k^2 \leq V_1)$ yields

$$\kappa R = \sqrt{V_1R^2 - k^2R^2} = \sqrt{\rho_1 - x^2},$$

where $\rho_1 = V_1R^2$. Also,

$$\begin{aligned}\kappa(R - r_1) &= \sqrt{\rho_1 - x^2} - \alpha\kappa R \\ &= \sqrt{\rho_1 - x^2} - \alpha\sqrt{\rho_1 - x^2} \\ &= (1 - \alpha)\sqrt{\rho_1 - x^2}.\end{aligned}$$

Note that

$$\kappa r_1 = \alpha\kappa R = \alpha\sqrt{\rho_1 - x^2},$$

$$\bar{k}r_1 = \bar{k}R \cdot \frac{r_1}{R} = \alpha\sqrt{\rho_0 + x^2}.$$

$$1 - \alpha = 1 - \frac{r_1}{R} = \frac{R - r_1}{R}.$$

Therefore, (45) becomes

$$\delta_0 = -x + \arctan\left\{\frac{x}{\sqrt{\rho_1 - x^2}} \cdot \frac{[\sqrt{\frac{\rho_1 - x^2}{\rho_0 + x^2}}\tan(\alpha\sqrt{\rho_0 + x^2}) + \tanh((1-\alpha)\sqrt{\rho_1 - x^2})]}{1 + \sqrt{\frac{\rho_1 - x^2}{\rho_0 + x^2}}\tan(\alpha\sqrt{\rho_0 + x^2})\tanh((1-\alpha)\sqrt{\rho_1 - x^2})}\right\}. \tag{59}$$

Similarly, for the case that $\kappa^2 < 0$ or $\kappa^2 = -\tilde{\kappa}^2$, (56) becomes

$$\delta_0 = -x + \arctan\left\{\frac{x}{\sqrt{x^2 - \rho_1}} \cdot \frac{[\sqrt{\frac{x^2 - \rho_1}{x^2 + \rho_0}}\tan(\alpha\sqrt{\rho_0 + x^2}) + \tan((1-\alpha)\sqrt{x^2 - \rho_1})]}{1 - \sqrt{\frac{x^2 - \rho_1}{x^2 + \rho_0}}\tan(\alpha\sqrt{\rho_0 + x^2})\tan((1-\alpha)\sqrt{x^2 - \rho_1})}\right\}. \tag{60}$$

Note that

$$\tilde{\kappa}R = \sqrt{k^2R^2 - V_1R^2} = \sqrt{x^2 - \rho_1},$$
$$\tilde{\kappa}r_1 = \alpha\sqrt{x^2 - \rho_1},$$

and

$$\tilde{\kappa}(R - r_1) = \tilde{\kappa}R(1 - \alpha) = (1 - \alpha)\sqrt{x^2 - \rho_1}.$$

In addition, by using Grandy's wavepacket approach [16], the wave function outside the potential (see (53)) has a very important modification, namely the phase shift $\delta_0(k)$, which plays the crucial roles in constructing a time-dependent scattered wavepacket:

$$\psi(x,t) = \int_0^x g(k)e^{i(kx - \omega t + \delta_0)}dk. \tag{61}$$

The positive spectral function $g(k)$ is taken to have a peak at $k = k_0$, corresponding to a group velocity v_0. This peak is determined by requirement of stationary phase at $k = k_0$, or

$$\frac{d}{dk}[kx - \omega t + \delta_0(k)]_{k=k_0} = 0, \tag{62}$$

provides

$$[x - \frac{d\omega}{dk}t + \frac{d\delta_0(k)}{dk}]_{k=k_0} = 0, \tag{63}$$

or, at $k = k_0$, with $v_g = \frac{d\omega(k)}{dk}$, we obtain

$$x = v_g(k)[t - \frac{1}{v_g(k)}\frac{d\delta_0}{dk}]_{k=k_0} = v_g(k_0)(t - T(k_0)). \tag{64}$$

We can write $T = \frac{1}{v_g}\frac{d\delta_0}{dk}$ in terms of the well/barrier width, R (or just the well, r_1) as (at $k = k_0$),

$$T = \frac{1}{r_1}\frac{d\delta_0}{dk}\frac{R}{v_g}. \tag{65}$$

So T is just the "specific time delay" suffered by a wavepacket in units of the transit time for a "free particle" to cross the distance R.

2.6.1 RESONANCES

In Figure 24, we have plotted the relevant physical parameters for scattering for the case $E > V_1$. By using the parameters from the parameterization method, we let $\alpha = 0.5$, $V_0 = 4$, and $V_1 = 20.$. The most significant feature of this figure is the resonance that occurs at $kR \simeq 1.8$. At this energy, the results show that the following four characteristics are necessary to apply in order to define a resonance appropriately.

(i) The phase shift suddenly increases by approximately π and passes through $-\pi/2$. We can distinguish the features of the phase shift plot as resonances. For example, if the phase shift undergoes a large increase, then the resonance interpretation will be very useful. But if the phase shift is gradually increasing and not by very much, then the resonance will vary broadly and merge into the background and this cannot be used in the resonance concept.

(ii) The scattering strength, measured by $\sin^2\delta_0$, has a sharp maximum and reaches $\sin^2\delta_0 = 1$; If the scattering strength goes through its maximum value (i.e., $\sin^2\delta_0 = 1$), then δ must pass through $\pi/2$. However, such a maximum is not a resonance unless δ is increasing with energy. Therefore, this condition is not sufficient for the existence of a resonance. For example, the peak at $kR = 1$ in Figure 24 does not correspond to a resonance because the time delay ($\propto d\delta_0/dk$) is negative and there is no resonant state. However, a very narrow peak at $kR \simeq 1.8$ in $\sin^2\delta_0$ is a sufficient condition for a resonance. This very narrow peak has the large value of $|d\delta_0/dk|$, and it is known that $|d\delta_0/dk|$ is large if $d\delta_0/dk > 0$.

(iii) The amplitude of the wave in the interior region (the well) has a sharp maximum; it means that at the resonance, the amplitude of oscillation of the system is large.

(iv) The specific time delay $r_1^{-1} d\delta_0/dk$ has a sharp maximum.

Figures 25 through 28 show more examples when the height of the barrier is changed. We have shown four more case with the parameters: $\alpha = 0.5$, $V_0 = 4$, and $V_1 = 15$; $\alpha = 0.5$, $V_0 = 4$, and $V_1 = 4$; $\alpha = 0.5$, $V_0 = 1$, and $V_1 = 20$; and $\alpha = 0.5$, $V_0 = 1$, and $V_1 = 15$.

Figure 29 shows the comparison of δ_0, $|A|$, $\sin^2 \delta_0$, and $r_1^{-1} d\delta_0/dk$ when the height of the barrier is decreased. The resonance becomes broader and tends to disappear. Moreover, we still have the same conclusion if we fix the value of V_1 and increase the value of V_0.

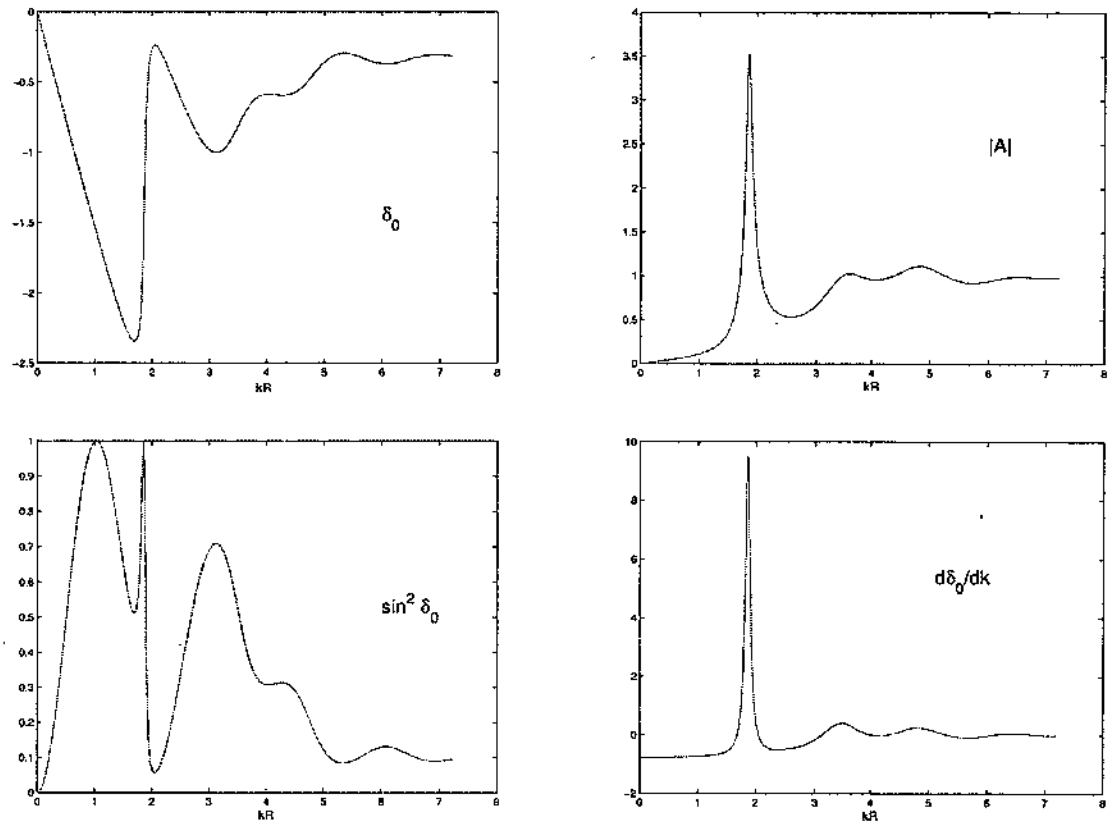

FIG. 24: Scattering from the one-dimensional potential of Figure 21 with $V_0 = 4$ and $V_1 = 20$. The resonance at $kR \simeq 1.8$ is reflected in the behavior of the phase shift δ_0, the scattering strength $\sin^2 \delta_0$, the interior wave amplitude $|A|$, and the specific time delay $d\delta_0/dk$.

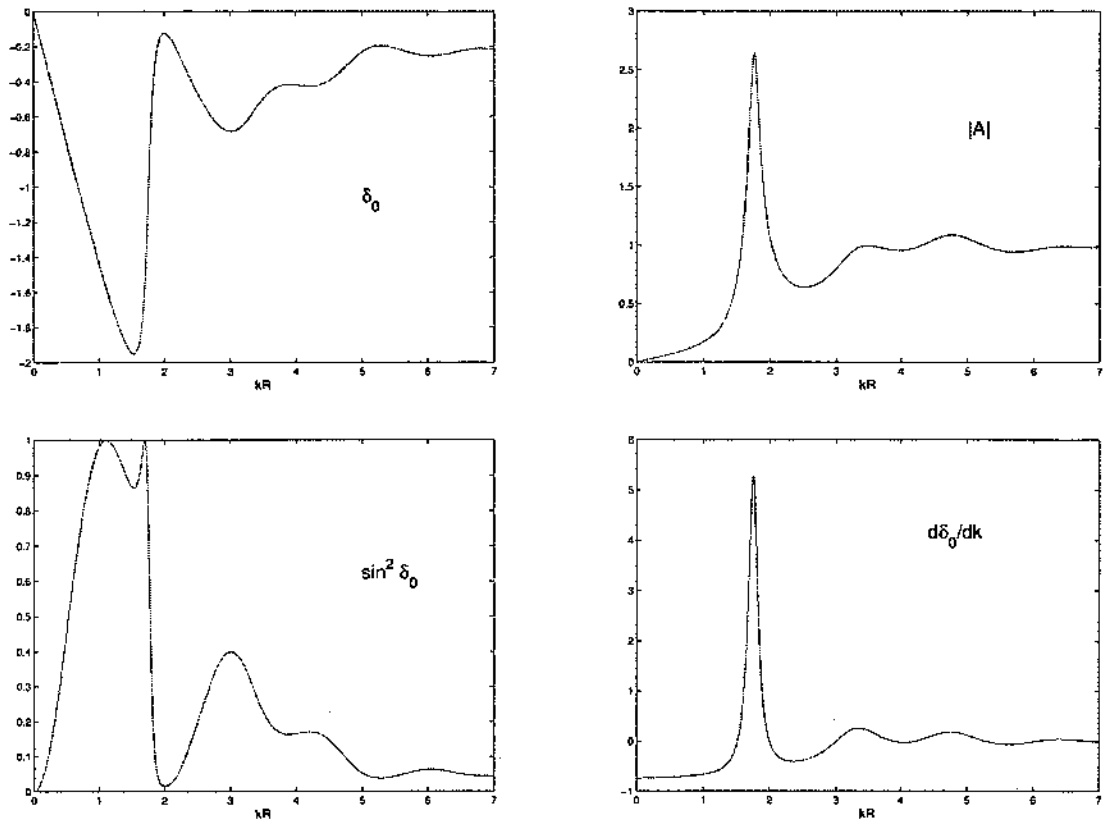

FIG. 25: Scattering from the one-dimensional potential of Figure 21 with $V_0 = 4$ and $V_1 = 15$. The resonance at $kR \simeq 1.8$ is reflected in the behavior of the phase shift δ_0, the scattering strength $\sin^2 \delta_0$, the interior wave amplitude $|A|$, and the specific time delay $d\delta_0/dk$.

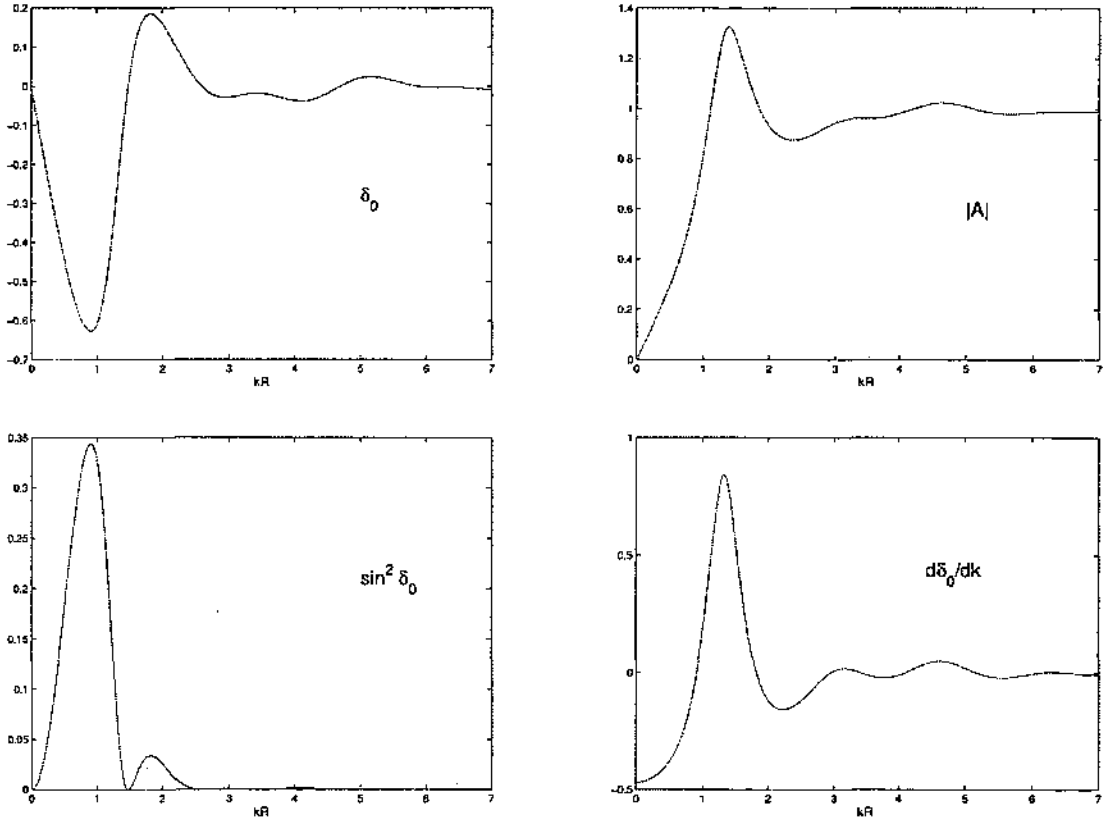

FIG. 26: Scattering from the one-dimensional potential of Figure 21 with $V_0 = 4$ and $V_1 = 4$. The resonance at $kR \simeq 1.8$ is reflected in the behavior of the phase shift δ_0, the scattering strength $\sin^2 \delta_0$, the interior wave amplitude $|A|$, and the specific time delay $d\delta_0/dk$.

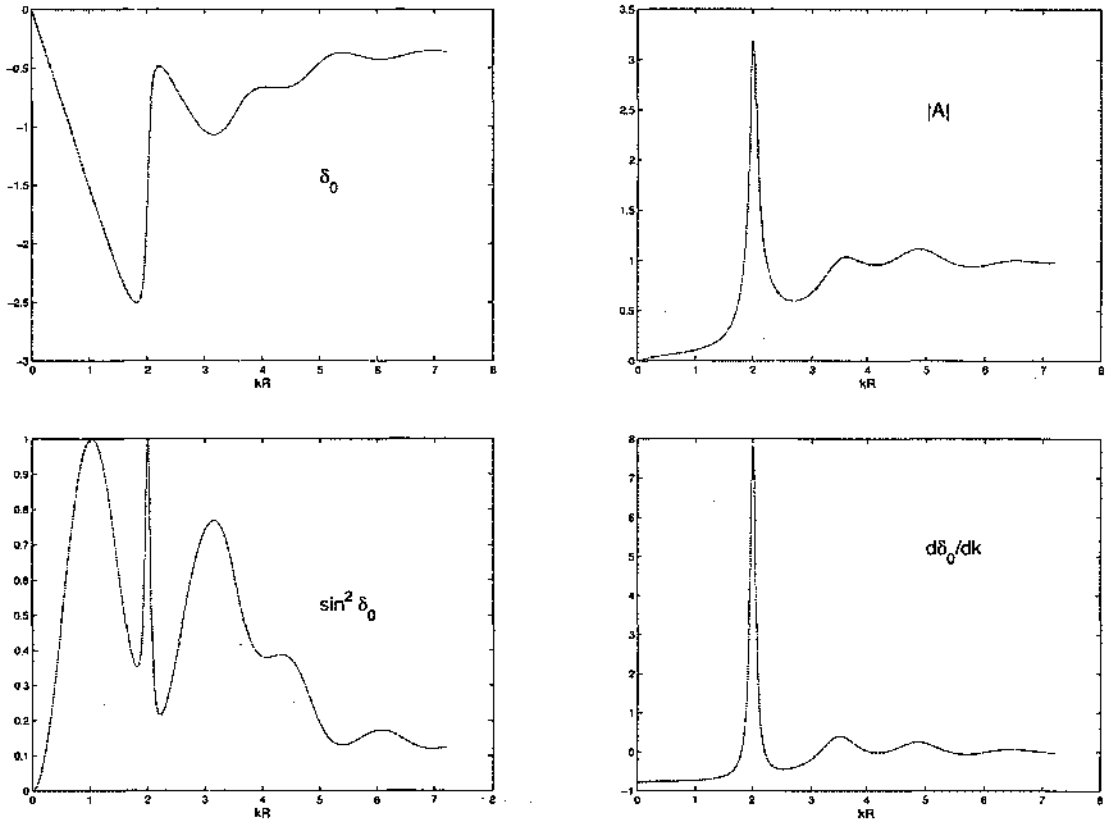

FIG. 27: Scattering from the one-dimensional potential of Figure 21 with $V_0 = 1$ and $V_1 = 20$. The resonance at $kR \simeq 1.8$ is reflected in the behavior of the phase shift δ_0, the scattering strength $\sin^2 \delta_0$, the interior wave amplitude $|A|$, and the specific time delay $d\delta_0/dk$.

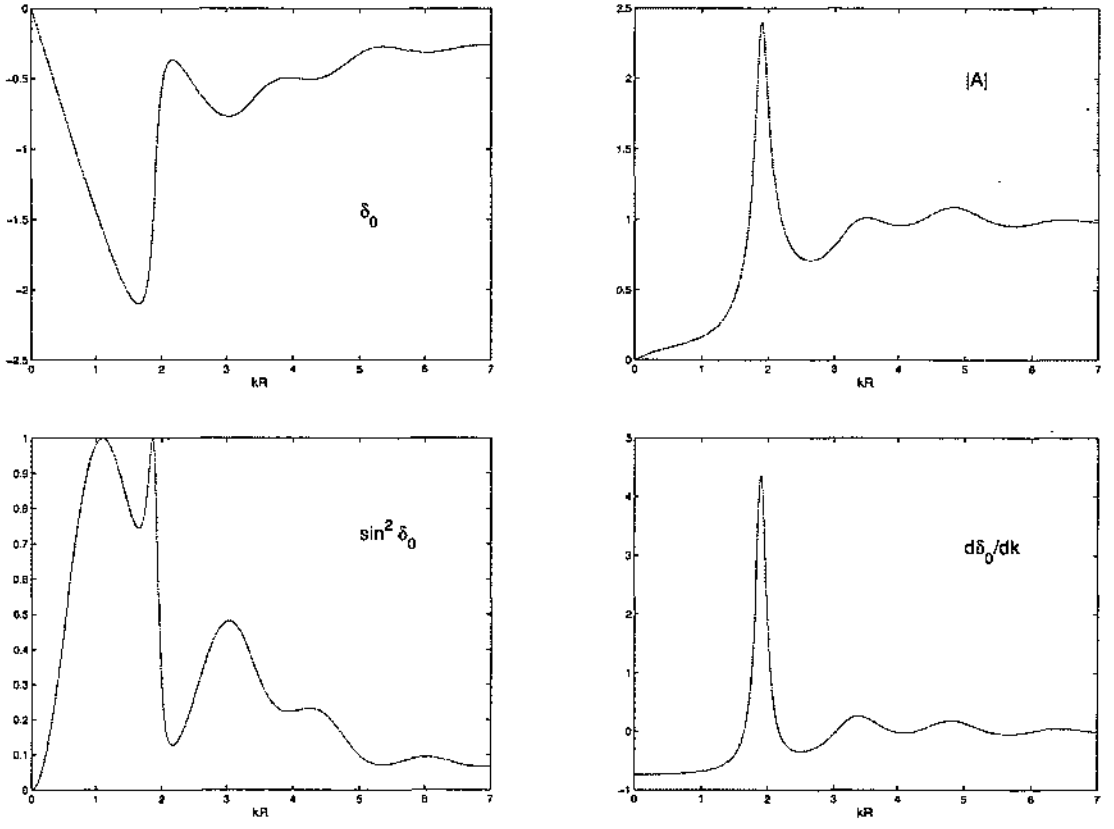

FIG. 28: Scattering from the one-dimensional potential of Figure 21 with $V_0 = 1$ and $V_1 = 15$. The resonance at $kR \simeq 1.8$ is reflected in the behavior of the phase shift δ_0, the scattering strength $\sin^2 \delta_0$, the interior wave amplitude $|A|$, and the specific time delay $d\delta_0/dk$.

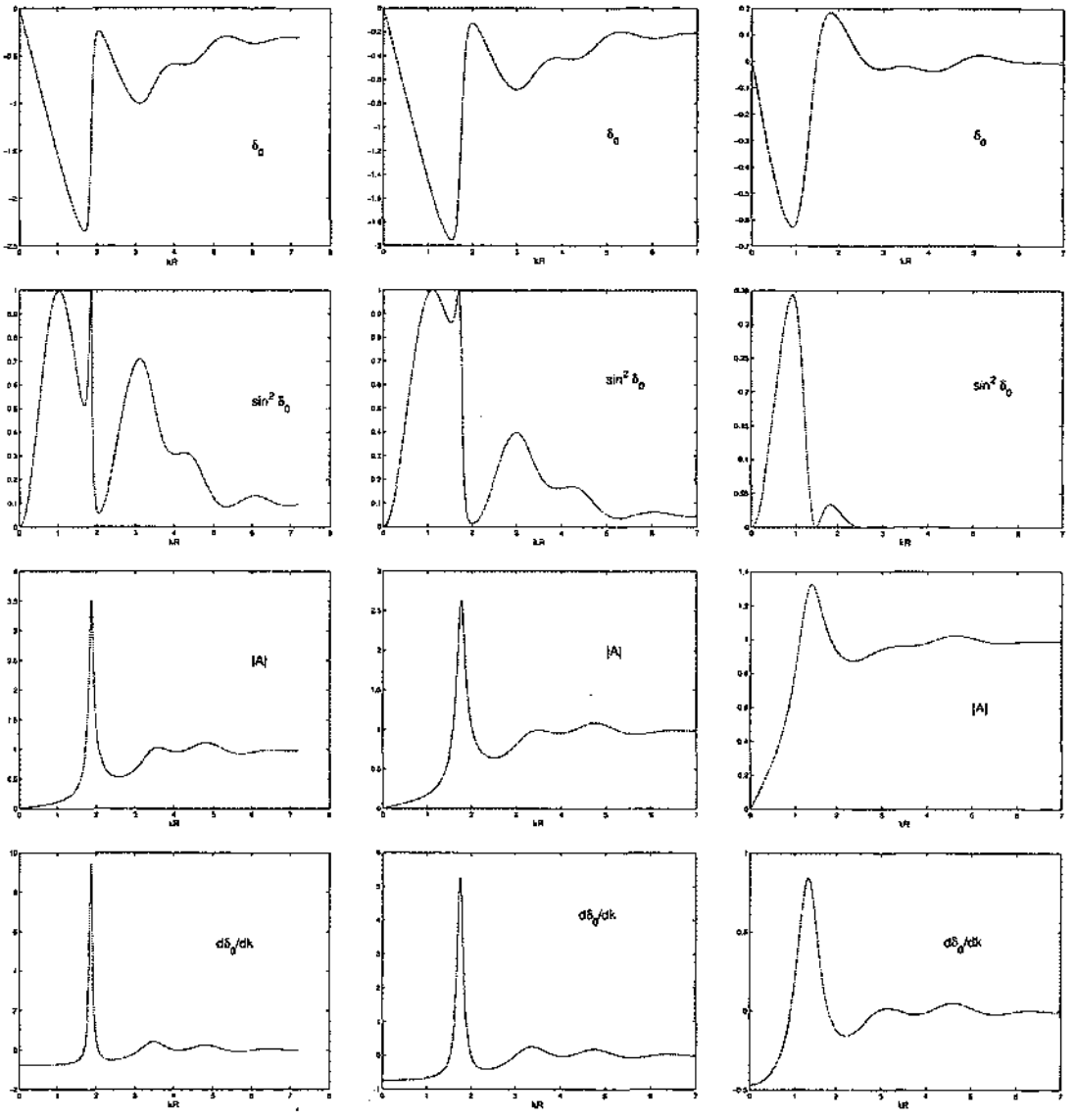

FIG. 29: Scattering on a square well for δ_0, $\sin^2\delta_0$, $|A|$, and $d\delta_0/dk$ (in each row) with barrier of different heights. The value of V_1 are 20, 15, and 4 for the top, center, and bottom, respectively. The value of V_0 is 4 in all case.

CHAPTER 3

SCALAR WAVE SCATTERING BY SPHERICALLY SYMMETRIC INHOMOGENEITIES

3.1 INTRODUCTION

"This paper is concerned with the scattering of a scalar plane wave by an inhomogeneous medium in which the velocity of propagation c is a function only of the spherical radial coordinate r, i.e., $c = c(r)$. This problem is of interest in various branches of physics: scattering by inhomogeneous spheres; scattering of acoustic waves in the ocean, electromagnetic waves in the atmosphere, and seismic waves in the Earth. Although quantum-mechanical problems involving scattering by spherically symmetric potentials have been extensively investigated, the analogous classical problems involving scattering by spherically symmetric inhomogeneities have not been as thoroughly studied. It is the purpose of this paper to show how a convenient quantum-mechanical method can be used to treat the classical problems and to apply this method to some simple solvable problems [12]."

So begins the paper by Frisk and DeSanto [12], referred to hereafter as in [12]. The problem they consider is essentially that of one uniform medium (a sphere of constant refractive index $n > 1$) embedded in an infinite medium with constant refractive index $n = 1$. This is the simplest case one can consider in an acoustic problem (or indeed a scalar electromagnetic or elastic one) with the corresponding time-independent potential scattering problem.

As noted in Chapter 2, it is of mathematical interest to be able to solve this direct scattering problem for specified analytic profiles $n(r)$, and this can indeed be carried out for certain special cases. However, since in practice (in optical and industrial applications at least) the inhomogeneous scattering media will be piecewise constant continuous, a variable approach to the problem may be to mimic the continuous cases for which, say $n'(r) < 0$ and $n'(r) > 0$, respectively, by 3-layer models for which the

$n(r)$ and $V(r)$ profiles are shown below (see Figures 30 through 33).

$$n(r) = \begin{cases} n_1, & 0 \le r < R_1, \\ n_2 \ (< n_1), & R_1 \le r < R_2, \\ 1 < n_2, & R_2 \le r, \end{cases} \tag{66}$$

so,

$$\frac{V(r)}{k_0^2} = 1 - n^2(r) = \begin{cases} 1 - n_1^2, & 0 \le r < R_1, \\ 1 - n_2^2, & R_1 \le r < R_2, \\ 0, & R_2 \le r, \end{cases} \tag{67}$$

therefore,

$$V(r) = k_0^2 - k^2(r) = k_0^2(1 - n^2(r)) \tag{68}$$

is given by

$$V(r) = \begin{cases} k_0^2(1 - n_1^2) = -V_1, & 0 \le r < R_1, \\ k_0^2(1 - n_2^2) = -V_2(> -V_1), & R_1 \le r < R_2, \\ 0, & R_2 \le r, \end{cases} \tag{69}$$

and

$$n(r) = \begin{cases} n_1, & 0 \le r < R_1, \\ n_2 \ (> n_1), & R_1 \le r < R_2, \\ 1 < n_1, & R_2 \le r. \end{cases} \tag{70}$$

So

$$V(r) = \begin{cases} k_0^2(1 - n_1^2) = -V_1, & 0 \le r < R_1, \\ k_0^2(1 - n_2^2) = -V_2(< -V_1), & R_1 \le r < R_2, \\ 0, & R_2 \le r. \end{cases} \tag{71}$$

Based on the paper [12] in which the authors consider the case of scalar plane wave scattering by a spherically symmetric scatterer, the form of the inhomogeneous Helmholtz equation and the time-independent Schrödinger wave equation are similar. Therefore, as we have already seen, we can treat the classical and quantum problems by analogous methods. In particular, for acoustic wave propagation in radially inhomogeneous media, the governing equation is

$$\rho \nabla \cdot (\rho^{-1} \nabla \Psi(\bar{r}, t)) - \frac{1}{c^2(r)} \frac{\partial^2 \Psi(\bar{r}, t)}{\partial t^2} = 0, \tag{72}$$

where $\Psi(\bar{r}, t)$ is the acoustic pressure perturbation and $\rho(r)$ is the density of the medium (see Martin [38]). If the density is constant (assumed here), (72) reduces to the standard spherically symmetric wave equation.

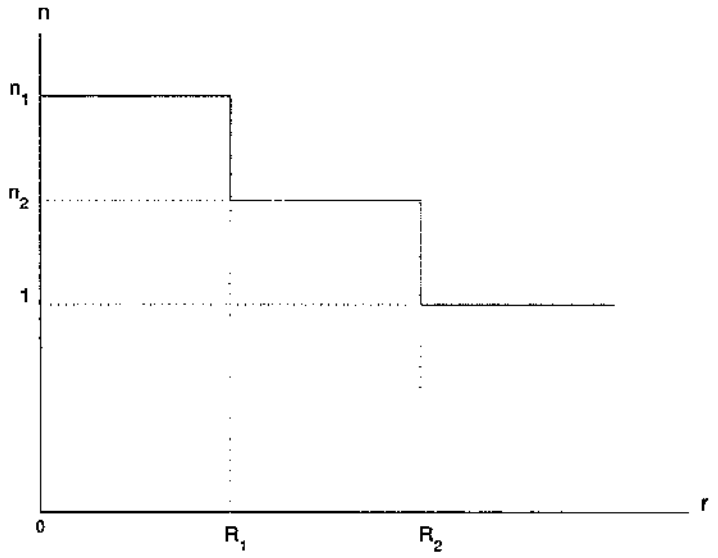

FIG. 30: Refractive index profile for $n_1 > n_2$.

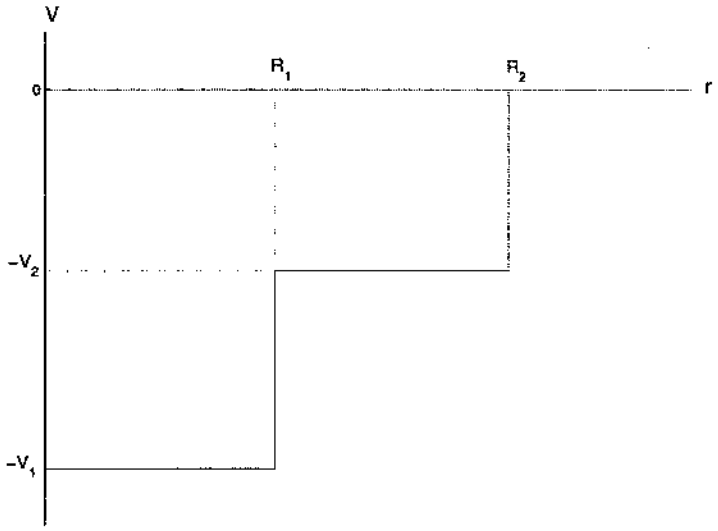

FIG. 31: $V(r)$ potential for $n_1 > n_2$.

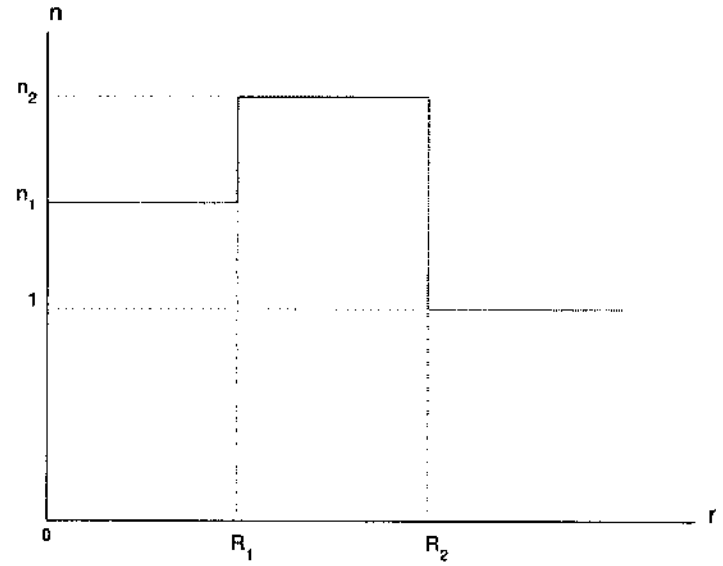

FIG. 32: Refractive index profile for $n_1 < n_2$.

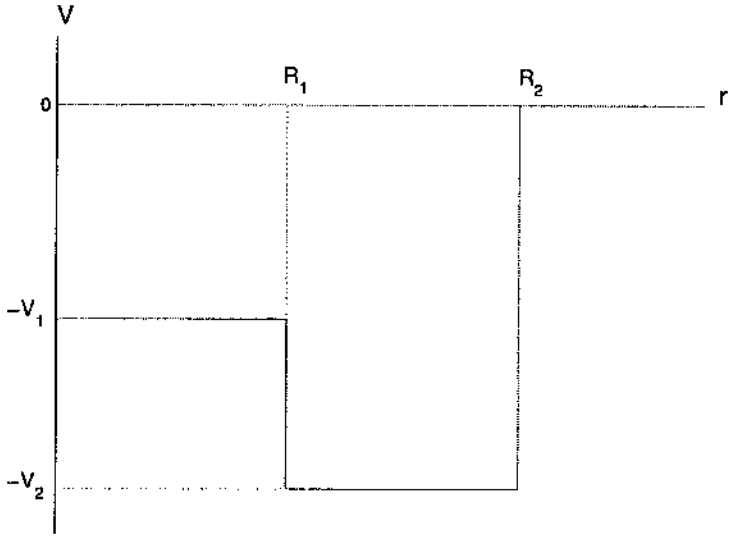

FIG. 33: $V(r)$ potential for $n_1 < n_2$.

We consider a monochromatic time-harmonic dependence of $\Psi(\bar{r},t)$ such that

$$\Psi(\bar{r},t) = \psi(\bar{r})e^{-i\omega t}. \tag{73}$$

Consequently, the spatial part of $\Psi(\bar{r},t)$ satisfies the inhomogeneous Helmholtz equation

$$\nabla^2\psi(\bar{r}) + k_0^2\psi(\bar{r}) = V(r)\psi(\bar{r}). \tag{74}$$

In this equation, $k_0 = \omega/c_0$ is the 'free space' wavenumber, where c_0 is the constant wave speed of the acoustic wave outside the scatterer. In electromagnetic terminology, c_0 corresponds to the outer region where the refractive index $n = 1$. As noted in Chapter 2, the 'potential'

$$\begin{aligned} V(r) &= k_0^2 - k^2(r) \equiv k_0^2(1 - n^2(r)) \\ &= k_0^2(1 - \frac{c_0^2}{c^2(r)}) = k_0^2 - \frac{\omega}{c^2(r)}. \end{aligned} \tag{75}$$

Thus, $k(r) = \omega/c(r)$ is the wavenumber in the scattering medium, and $k_0 = \omega/c_0$ is the wavenumber in the surrounding medium. Equation (74) corresponds to the canonical form of the time-independent Schrödinger equation, where $k_0^2 = 2mE/\hbar^2$, $V(r) = 2mU(r)/\hbar^2$, $\hbar = h/2\pi$, h being Planck's constant, and m is the mass of a particle of total energy E moving in a potential $U(r)$, i.e.

$$\nabla^2\psi(\bar{r}) + [k_0^2 - V(r)]\psi(\bar{r}) = 0. \tag{76}$$

In what follows k_0 will be written as k, and $k(r)$ will be used for $kn(r)$. Note that $V(r) \leq 0$ for $n^2(r) \geq 1$, so the quantum mechanical formulation corresponds to scattering by a spherical potential well. Therefore, the wave function can be both interpreted as the spatial part of the acoustic pressure (classically) or as the Schrödinger wave function (quantum mechanically).

The basis for this chapter is the application of the Jost function formulation of quantum scattering theory (as presented by DeAlfaro and Regge [30]) to the scattering of a scalar plane wave by a medium with spherically symmetric inhomogeneities.

After rederiving the formulation of [12], we generalize it to the above-mentioned three-layer models, utilizing the Jost function method described below. By the method of separation of variables, (76) can be written, in a spherical coordinate system

$$\psi(r) = \sum_{l=0}^{\infty}\sum_{m=-l}^{+l} A_{lm}R_l(r)Y_{lm}(\theta,\phi), \tag{77}$$

where $R_l(r) = u_l(r)/r$ and $Y_{lm}(\theta, \phi)$ is a spherical harmonic, l and m are angular momentum. Then it follows that $u_l(r)$ satisfies the "partial-wave" radial equation,

$$\frac{d^2u_l(r)}{dr^2} + [k^2 - \frac{l(l+1)}{r^2} - V(r)]u_l(r) = 0. \tag{78}$$

The Jost-function technique is very useful to solve the solution of the radial wave equation of the so-called 'partial' wave equation. The Jost function is defined as the Wronskian of two solutions of the radial equation, one satisfying boundary conditions at $r = 0$ (which is called regular solution) and the other satisfying boundary conditions at $r = \infty$ (the *Jost solution*). The total scattering cross sections are obtained from the phase shifts δ_l, which can be calculated easily once the Jost function is found.

3.1.1 THE TOTAL SCATTERING CROSS SECTION AND PHASE SHIFT

In scattering theory, the total cross-section is a measure of the probability that an interaction occurs; the larger the cross section, the greater the probability that an interaction will happen when a particle is incident on a target. Both classical and quantum mechanical scattering phenomena are characterized by the scattering cross section, σ.

We consider for particles of mass m and energy $E > 0$, scattering from a spherically symmetric potential $V(r)$, r being the radial distance from the center of the scatterer. The potential is described by a wave function $\psi(r)$ which consists of a linear combination of the incident plane wave and an outwardly propagating spherical wave and satisfies the Schrödinger wave equation,

$$-\frac{\hbar^2}{2m}\nabla^2\psi + V(r)\psi = E\psi,$$

with the boundary condition when $r \to \infty$

$$\psi_{r\to\infty} = e^{ikz} + f(\theta)\frac{e^{ikr}}{r},$$

where the incoming plane wave is incident along the direction of the z-axis and scattered as an outgoing wave, k is a wavenumber, θ is the scattering angle between r and the z-axis, and f is the complex scattering amplitude. The differential cross-section is given by

$$\frac{d\sigma}{d\Omega} = |f(\theta)|^2.$$

From the expression for $\frac{d\sigma}{d\Omega}$, we obtain the total scattering cross-section:

$$\sigma_{tot} = \int d\sigma = \int |f(\theta)|^2 d\Omega,$$

with orthogonality relation, we obtain $\sigma_{tot} = 4\pi \sum_l (2l+1)|f(\theta)|^2$, where

$$f_l(k) = \frac{1}{2ik}(e^{2i\delta_l(k)} - 1) = \frac{e^{i\delta_l(k)}}{k} \sin \delta_l,$$

is defined by the scattering phase shifts $\delta_l(k)$ which can be determined from the asymptotic form of $\psi(\mathrm{r})$ by solving the Schrödinger wave equation. For the special case $l = 0$ we have that

$$\sigma_0 = 4\pi \left| \frac{1}{2ik}(e^{2i\delta_i(k)} - 1) \right|^2, \tag{79}$$

which will be discussed again as shown in (127) [37].

The Jost function can be calculated either from the original radial differential equation with the Jost boundary conditions or from a Volterra integral equation incorporating these boundary conditions. For the case of a constant inhomogeneity for $r < R_1$ (three-dimensional square-well potential), the former approach is more straightforward, however, the latter approach may be more useful when the inhomogeneity (potential) has a more complicated functional form for which the radial equation may not have an exact solution. The solution of the integral equation is then written as a perturbation expansion, and an iteration procedure yields the solutions to the desired accuracy. The perturbation expansion for a Volterra integral equation is very useful because it converges everywhere.

In Section 3.2, the Jost-function formulation of scattering theory is presented. In Section 3.3, the Jost function from the radial differential equation for scattering from a constant spherical inhomogeneity for arbitrary l is derived, and evaluated for $l = 0$. In Section 3.4, we derive the $l = 0$ Jost integral equation for scattering from an arbitrary inhomogeneity with a cutoff. The Jost function for $l = 0$ from this integral equation is obtained using an iteration technique (only the first two iterations are considered) for scattering from a constant spherical inhomogeneity, and we compare it (and the cross sections) graphically with the exact results. In Section 3.5, the general Jost integral-equation formulation for arbitrary l is presented

for scattering from a piecewise uniform inhomogeneity and it is applied to scattering from a constant spherical inhomogeneity. In Section 3.6, the Jost integral equation for $\lambda = \frac{1}{2}$ and some approximate solutions in three-layer model are examined. In Section 3.7, the general Jost integral-equation formulation for arbitrary λ for scattering from an arbitrary inhomogeneity is defined.

3.2 JOST-FUNCTION FORMULATION OF SCATTERING THEORY

We now consider the radial equation (78) again:

$$\frac{d^2u_l(r)}{dr^2} + [k^2 - \frac{l(l+1)}{r^2} - V(r)]u_l(r) = 0.$$

For the following analysis to hold, following DeAlfaro and Regge, we must impose certain requirements on $V(r)$: it must be a real function vanishing at $r = \infty$, and must be almost everywhere continuous; furthermore, we require that

$$\int_c^\infty |V(r)|dr = M(c) < \infty;$$
$$\int_0^{c'} r|V(r)|dr = N(c') < \infty, \tag{80}$$

where c and c' are arbitrary constants greater than zero. These conditions are readily satisfied for non-singular $V(r)$ with compact support.

3.2.1 JOST BOUNDARY CONDITIONS AT $r = 0$

For small r, $|-l(l+1)/r^2| \gg |k^2 - V(r)|$, and we begin our discussion of (78) by neglecting the term $[k^2 - V(r)]$. Equation (78) then becomes

$$\frac{d^2u_l(r)}{dr^2} - \left[\frac{l(l+1)}{r^2}\right]u_l(r) = 0, \tag{81}$$

which has a regular point at $r = 0$ and the exact solution is

$$u_l(r) = \alpha r^{l+1} + \beta r^{-l}. \tag{82}$$

Using (82) as a guide, we define two linearly independent solutions of (78) with the behavior

$$\phi(r) = r^{l+1}[1 + o(1)], \tag{83a}$$

$$\phi_1(r) = r^{-l}[1 + o(1)], \tag{83b}$$

where o is the 'small' order symbol. We also define $\lambda = l + \frac{1}{2}$, so that (78) becomes even in λ:

$$\frac{d^2 u_{\lambda-\frac{1}{2}}(r)}{dr^2} + [k^2 - \frac{\lambda^2 - \frac{1}{4}}{r^2} - V(r)]u_{\lambda-\frac{1}{2}}(r) = 0. \tag{84}$$

We now consider the solutions of (84) as a function of the parameters λ and k, which in the general case may be complex variables. Thus $\phi(r) \to \phi_1(r)$ as $\lambda \to -\lambda$, and we therefore replace $\phi(r)$ and $\phi_1(r)$ by $\phi(\lambda, k, r)$ and $\phi(-\lambda, k, r)$, respectively. We write $u_{\lambda-\frac{1}{2}}(r)$ instead of $u_l(r)$ in order that the notation be consistent. We solve (84) exactly by converting it into an integral equation using the method of variation of parameters with the boundary conditions (83). We thus obtain

$$\phi(\lambda, k, r) = r^{\lambda+\frac{1}{2}} + \frac{1}{2}\lambda^{-1}\int_0^r [(\xi/r)^\lambda - (r/\xi)^\lambda] \times (r\xi)^{\frac{1}{2}}[k^2 - V(\xi)]\phi(\lambda, k, \xi)d\xi. \tag{85}$$

From (85), we can write the Jost boundary conditions at $r = 0$ as

$$\begin{aligned} &\lim_{r\to 0}\phi(\lambda, k, r) = 0; \\ &\lim_{r\to 0}\frac{d\phi(\lambda, k, r)}{dr} = \lim_{r\to 0}(\lambda + \frac{1}{2})r^{\lambda-\frac{1}{2}}. \end{aligned} \tag{86}$$

Equation (85) is a Volterra integral equation, and we write its solution as a perturbation expansion

$$\phi(\lambda, k, r) = \sum_{n=0}^{\infty}\phi_n(\lambda, k, r), \tag{87}$$

where

$$\phi_0(\lambda, k, r) = r^{\lambda+\frac{1}{2}}, \tag{88}$$

and

$$\phi_{n+1}(\lambda, k, r) = \frac{1}{2}\lambda^{-1}\int_0^r [(\xi/r)^\lambda - (r/\xi)^\lambda](r\xi)^{\frac{1}{2}} \times [k^2 - V(\xi)]\phi_n(\lambda, k, \xi)d\xi. \tag{89}$$

The perturbation expansion for $\phi(\lambda, k, r)$ is bounded term-by-term and is unrestrictedly convergent.

Since the Wronskian of the two linearly independent solutions of (84) is nonzero and constant, we can evaluate the Wronskian of $\phi(\lambda, k, r)$ and $\phi(-\lambda, k, r)$ by replacing $\phi(\lambda, k, r)$ with $r^{\lambda+\frac{1}{2}}$:

$$W[\phi(\lambda, k, r), \phi(-\lambda, k, r)] = \phi(\lambda, k, r)\phi'(-\lambda, k, r) - \phi'(\lambda, k, r)\phi(-\lambda, k, r) = -2\lambda. \tag{90}$$

3.2.2 JOST BOUNDARY CONDITIONS AT $r = \infty$

For large r, we can neglect the term

$$\left[-\frac{\lambda^2 - \frac{1}{4}}{r^2} - V(r)\right],$$

in (84), which therefore becomes

$$\frac{d^2 u_{\lambda-\frac{1}{2}}(r)}{dr^2} + k^2 u_{\lambda-\frac{1}{2}}(r) = 0. \tag{91}$$

Equation (91) has the exact solution

$$u_{\lambda-\frac{1}{2}}(r) = \alpha e^{-ikr} + \beta e^{ikr}. \tag{92}$$

Therefore, we construct a solution $f(\lambda, k, r)$ (Jost solution) of (84) with the asymptotic behavior

$$\lim_{r\to\infty} e^{ikr} f(\lambda, k, r) = 1. \tag{93}$$

We use the method of variation of parameters in a manner analogous to that of Section 3.2.1, so that (84) with the asymptotic conditions (93) becomes

$$f(\lambda, k, r) = e^{-ikr} + k^{-1} \int_r^\infty [\sin k(r' - r)] \times [V(r') + (\lambda^2 - \frac{1}{4})(r')^{-2}] f(\lambda, k, r') dr'. \tag{94}$$

We write the solution of (94) as a perturbation expansion

$$f(\lambda, k, r) = \sum_{n=0}^{\infty} g_n(\lambda, k, r), \tag{95}$$

where

$$g_0 = e^{-ikr}, \tag{96}$$

and

$$g_{n+1}(\lambda, k, r) = k^{-1} \int_r^\infty [\sin k(r' - r)] \times [V(r') + (\lambda^2 - \frac{1}{4})(r')^{-2}] g_n(\lambda, k, r') dr'. \tag{97}$$

The perturbation expansion for $f(\lambda, k, r)$ is bounded for any λ.

We state the following relation:

$$W[f(\lambda, k, r), f(\lambda, -k, r)] = 2ik, \tag{98}$$

where we have evaluated the Wronskian by substituting for $f(\lambda, \pm k, r)$ its asymptotic behavior, $e^{\pm ikr}$.

3.2.3 THE JOST FUNCTION AND THE S-MATRIX

The Jost function $f(\lambda, k)$ is defined as the Wronskian of $f(\lambda, k, r)$ and $\phi(\lambda, k, r)$

$$\begin{aligned} f(\lambda, k) &= W[f(\lambda, k, r), \phi(\lambda, k, r)] \\ &= f(\lambda, k, r)\phi'(\lambda, k, r) - f'(\lambda, k, r)\phi(\lambda, k, r). \end{aligned} \tag{99}$$

The general solution of (84) is a linear combination of any two linearly independent solutions and, in fact, we have that

$$\phi(\lambda, k, r) = \frac{1}{2ik}[f(\lambda, k)f(\lambda, -k, r) - f(\lambda, -k)f(\lambda, k, r)], \tag{100}$$

where (98) has been used.

The asymptotic form of $\phi(\lambda, k, r)$ is

$$\phi(\lambda, k, r) \sim \frac{1}{2ik}[f(\lambda, k)e^{ikr} - f(\lambda, -k)e^{-ikr}], \tag{101}$$

where we have replaced $f(\lambda, \pm k, r)$ with $e^{\pm ikr}$. If we parametrize the Jost functions in (101) as

$$\begin{aligned} f(\lambda, k) &= \tau(\lambda, k)e^{[i\delta(\lambda,k) - \frac{1}{2}i\pi(\lambda - \frac{1}{2})]}, \\ f(\lambda, -k) &= \tau(\lambda, k)e^{[-i\delta(\lambda,k) + \frac{1}{2}i\pi(\lambda - \frac{1}{2})]}, \end{aligned} \tag{102}$$

where $\tau(\lambda, k)$ is the complex amplitude, then (101) becomes

$$\phi(\lambda, k, r) \sim \frac{1}{k}\tau(\lambda, k)\sin[kr + \delta(\lambda, k) - \frac{1}{2}\pi(\lambda - \frac{1}{2})], \tag{103}$$

which agrees with the standard partial-wave analysis in quantum mechanics texts (Schiff [29], Mott and Massey [31]). The S-matrix is given by

$$S(\lambda, k) = e^{2i\delta(\lambda,k)} = \left[\frac{f(\lambda, k)}{f(\lambda, -k)}\right]e^{i\pi(\lambda - \frac{1}{2})}. \tag{104}$$

Note that the S-matrix is proportional to the ratio of the coefficients of the outgoing and incoming waves in (101).

3.3 SCATTERING FROM A CONSTANT SPHERICAL INHOMOGENEITY: DIFFERENTIAL-EQUATION APPROACH

This is the problem originally discussed by [12]. While it may seem superfluous to rederive their analysis, there are three good reasons for doing so. First, we can verify their results before proceeding with the 3-layer model. Second, the analysis is readily extended to the 3-layer model once the exact and perturbation solutions have been defined, and third, it is easy to check consistency of the latter analytically and computationally by collapsing Region 2 onto Region 1 to recover the original model.

We apply the method outlined in Section 3.2 to the problem of scattering from a constant spherical inhomogeneity (see Figure 34):

$$\begin{aligned} &\textit{Region } 1 : V(r) = -V_1, \;\; k(r) = k_1, r < R_1, \\ &\textit{Region } 2 : V(r) = 0, \qquad k(r) = k, r > R_1. \end{aligned} \tag{105}$$

The solutions in the two regions are:

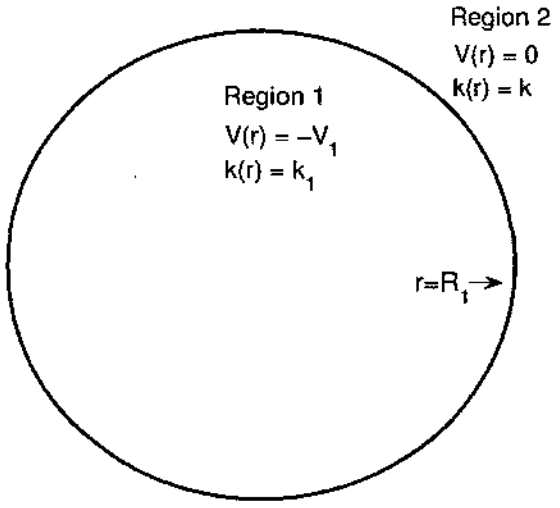

FIG. 34: A constant spherical inhomogeneity.

$$\begin{aligned} &\textit{Region } 1 : u^{(1)}_{\lambda-\frac{1}{2}}(k_1, r) = r[Aj_{\lambda-\frac{1}{2}}(k_1 r) + By_{\lambda-\frac{1}{2}}(k_1 r)], \\ &\textit{Region } 2 : u^{(2)}_{\lambda-\frac{1}{2}}(k, r) = r[Ch^{(1)}_{\lambda-\frac{1}{2}}(kr) + Dh^{(2)}_{\lambda-\frac{1}{2}}(kr)], \end{aligned} \tag{106}$$

where $j_{\lambda-\frac{1}{2}}(k_1 r)$, $y_{\lambda-\frac{1}{2}}(k_1 r)$, $h^{(1)}_{\lambda-\frac{1}{2}}(kr)$, and $h^{(2)}_{\lambda-\frac{1}{2}}(kr)$ are spherical Bessel, Neumann, and Hankel functions of the first kind and second kind, respectively.

Choosing $u^{(1)}_{\lambda-\frac{1}{2}}(k_1 r)$ to be $\phi(\lambda, k_1, r)$ and imposing the boundary conditions (86) at $r = 0$, we find that $B = 0$ and

$$\begin{aligned}
\phi(\lambda, k_1, r) &= 2^{\lambda+\frac{1}{2}}\pi^{-\frac{1}{2}}k_1^{-\lambda+\frac{1}{2}}\Gamma(\lambda+1) r j_{\lambda-\frac{1}{2}}(k_1 r), \\
\phi'(\lambda, k_1, r) &= 2^{\lambda+\frac{1}{2}}\pi^{-\frac{1}{2}}k_1^{-\lambda+\frac{1}{2}}\Gamma(\lambda+1) \times [j_{\lambda-\frac{1}{2}}(k_1 r) + k_1 r j'_{\lambda-\frac{1}{2}}(k_1 r)],
\end{aligned} \tag{107}$$

where the prime denotes differentiation with respect to the argument of the function, Γ is the gamma function, and we have used the following series representation for $j_{\lambda-\frac{1}{2}}(k_1 r)$ in [39]:

$$\begin{aligned}
j_{\lambda-\frac{1}{2}}(k_1 r) &= \sum_{n=0}^{\infty} \frac{(-1)^n \pi^{\frac{1}{2}} (k_1 r/2)^{\lambda+2n-\frac{1}{2}}}{2n!\Gamma(\lambda+n+1)}, \\
&\qquad \lambda - \frac{1}{2} \neq -1, -2, -3, \ldots .
\end{aligned} \tag{108}$$

Choosing $u^{(2)}_{\lambda-\frac{1}{2}}(kr)$ to be $f(\lambda, k, r)$ and imposing the boundary conditions (93) at $r = \infty$, we find that $C = 0$, $D = ke^{-i\frac{\pi}{2}(\lambda+\frac{1}{2})}$, and

$$f(\lambda, k, r) = ke^{-i\frac{\pi}{2}(\lambda+\frac{1}{2})} r h^{(2)}_{\lambda-\frac{1}{2}}(kr); \tag{109a}$$

$$f'(\lambda, k, r) = ke^{-i\frac{\pi}{2}(\lambda+\frac{1}{2})} [h^{(2)}_{\lambda-\frac{1}{2}}(kr) + kr h'^{(2)}_{\lambda-\frac{1}{2}}(kr)], \tag{109b}$$

where we have used the following asymptotic form for $h^{(2)}_{\lambda-\frac{1}{2}}(kr)$:

$$\lim_{kr\to\infty} h^{(2)}_{\lambda-\frac{1}{2}}(kr) = \frac{1}{kr} e^{-i[kr-\frac{\pi}{2}(\lambda+\frac{1}{2})]}. \tag{110}$$

Since the point $r = R_1$ is the common domain of $\phi(\lambda, k_1, r)$ and $f(\lambda, k, r)$, we evaluate the Jost function at $r = R_1$ and thus obtain

$$\begin{aligned}
f(\lambda, k) &= W[f(\lambda, k, r), \phi(\lambda, k_1, r)]_{r=R_1} \\
&= 2^{\lambda+\frac{1}{2}}\pi^{-\frac{1}{2}}\Gamma(\lambda+1) k_1^{-\lambda+\frac{1}{2}} k e^{-i\frac{\pi}{2}(\lambda+\frac{1}{2})} R_1 \\
&\quad \times [k_1 j'_{\lambda-\frac{1}{2}}(k_1 R_1) h^{(2)}_{\lambda-\frac{1}{2}}(kR_1) - k j_{\lambda-\frac{1}{2}}(k_1 R_1) h'^{(2)}_{\lambda-\frac{1}{2}}(kR_1)].
\end{aligned} \tag{111}$$

We also have that

$$\begin{aligned}
f(\lambda, -k) &= 2^{\lambda+\frac{1}{2}}\pi^{-\frac{1}{2}}\Gamma(\lambda+1) k_1^{-\lambda+\frac{1}{2}} k e^{-i\frac{\pi}{2}(\lambda+\frac{1}{2})} R_1 e^{i\pi(\lambda-\frac{1}{2})} \\
&\quad \times [-k_1 j'_{\lambda-\frac{1}{2}}(k_1 R_1) h^{(1)}_{\lambda-\frac{1}{2}}(kR_1) + k j_{\lambda-\frac{1}{2}}(k_1 R_1) h'^{(1)}_{\lambda-\frac{1}{2}}(kR_1)].
\end{aligned} \tag{112}$$

where we have used the following identities:

$$\begin{aligned} h^{(2)}_{\lambda-\frac{1}{2}}(kre^{i\pi}) &= h^{(2)}_{\lambda-\frac{1}{2}}(-kr) \\ &= (-1)^{\lambda-\frac{1}{2}} h^{(1)}_{\lambda-\frac{1}{2}}(kr) \\ &= e^{i\pi(\lambda-\frac{1}{2})} h^{(1)}_{\lambda-\frac{1}{2}}(kr); \\ h^{(2)'}_{\lambda-\frac{1}{2}}(-kr) &= (-1)^{\lambda+\frac{1}{2}} h^{(1)'}_{\lambda-\frac{1}{2}}(kr) \\ &= e^{i\pi(\lambda+\frac{1}{2})} h^{(1)'}_{\lambda-\frac{1}{2}}(kr) \\ &= -e^{i\pi(\lambda-\frac{1}{2})} h^{(1)'}_{\lambda-\frac{1}{2}}(kr), \lambda - \frac{1}{2} = 0, 1, 2, \ldots. \end{aligned} \tag{113}$$

The S-matrix is then given by

$$S(\lambda, k) = -\frac{k j_{\lambda-\frac{1}{2}}(k_1 R_1) h'^{(2)}_{\lambda-\frac{1}{2}}(kR_1) - k_1 j'_{\lambda-\frac{1}{2}}(k_1 R_1) h^{(2)}_{\lambda-\frac{1}{2}}(kR_1)}{k j_{\lambda-\frac{1}{2}}(k_1 R_1) h'^{(1)}_{\lambda-\frac{1}{2}}(kR_1) - k_1 j'_{\lambda-\frac{1}{2}}(k_1 R_1) h^{(1)}_{\lambda-\frac{1}{2}}(kR_1)}. \tag{114}$$

We can calculate the Jost function for $\lambda = \frac{1}{2}$ from (111):

$$f(\frac{1}{2}, k) = \frac{1}{2} e^{-ikR_1}[(1 - \frac{k}{k_1})e^{-ik_1R_1} + (1 + \frac{k}{k_1})e^{ik_1R_1}], \tag{115}$$

where the following relations have been used (see TABLE 1):

TABLE 1: Alternative expressions for $j_0(k_1R_1)$, $j'_0(k_1R_1)$, $h^{(2)}_0(kR_1)$, and $h'^{(2)}_0(kR_1)$.

Function		Expression
$j_0(k_1R_1)$	=	$\sin k_1R_1/(k_1R_1)$
$j'_0(k_1R_1)$	=	$\cos k_1R_1/(k_1R_1) - [\sin k_1R_1/(k_1R_1)^2]$
$h^{(2)}_0(kR_1)$	=	$-e^{-ikR_1}/(ikR_1)$
$h^{(2)'}_0(kR_1)$	=	$e^{-ikR_1}[1 + 1/(ikR_1)]/(kR_1)$

3.4 JOST INTEGRAL EQUATION FOR $\lambda = \frac{1}{2}$ AND SOME APPROXIMATE SOLUTIONS

If we assume there is an R such that $V(r) = 0$ for $r > R$ (certainly true in optics!) and let

$$g(\frac{1}{2}, k, r) = e^{ikr} f(\frac{1}{2}, k, r),$$

then (94) becomes the Jost integral equation for $\lambda = \frac{1}{2}$:

$$g(\frac{1}{2}, k, r) = 1 + (2ik)^{-1} \int_r^R [1 - e^{2ik(r-r')}] V(r') g(\frac{1}{2}, k, r') dr'. \tag{116}$$

We write the solution of (116) as a perturbation expansion

$$g(\frac{1}{2}, k, r) = \sum_{n=0}^{\infty} g_n(\frac{1}{2}, k, r), \tag{117}$$

where

$$g_0(\frac{1}{2}, k, r) = 1 \tag{118}$$

and

$$g_n(\frac{1}{2}, k, r) = 1 + (2ik)^{-1} \int_r^R [1 - e^{2ik(r-r')}] V(r') g_{n-1}(\frac{1}{2}, k, r') dr'. \tag{119}$$

From (86), we have

$$\begin{aligned} &\lim_{r \to 0} \phi(\frac{1}{2}, k, r) = 0, \\ &\lim_{r \to 0} \frac{\phi'(\frac{1}{2}, k, r)}{dr} = 1. \end{aligned} \tag{120}$$

$f(\frac{1}{2}, k, r)$ and $f'(\frac{1}{2}, k, r)$ are finite and we can evaluate $f(\frac{1}{2}, k)$ at $r = 0$ using (120), thus obtaining the useful relation

$$f(\frac{1}{2}, k) = f(\frac{1}{2}, k, 0) = g(\frac{1}{2}, k, 0). \tag{121}$$

We now redevelop the case of scattering from a constant spherical inhomogeneity, for which we have already calculated $f(\frac{1}{2}, k)$ exactly in Section 3.3. We can use the exact solution of the Jost function to check for the accuracy of the iteration procedure. We write down the solution again in the following form:

$$\begin{aligned} f(\frac{1}{2}, k) = &\cos[(k_1/k)kR_1] \cos kR_1 + (k/k_1) \sin[(k_1/k)kR_1] \\ &\times \sin kR_1 + i\{-\cos[(k_1/k)kR_1] \sin kR_1 \\ &+ (k/k_1) \sin[(k_1/k)kR_1] \cos kR_1\}. \end{aligned} \tag{122}$$

The $\lambda = \frac{1}{2}$ Jost integral (116) for this case is

$$g(\frac{1}{2}, k, r) = 1 - V_1(2ik)^{-1} \int_r^{R_1} [1 - e^{2ik(r-r')}] g(\frac{1}{2}, k, r') dr'. \tag{123}$$

The first iteration $g_I(\frac{1}{2}, k, 0)$ of (123) is

$$\begin{aligned} g_I(\frac{1}{2}, k, 0) &= g_0(\frac{1}{2}, k, 0) + g_1(\frac{1}{2}, k, 0) \\ &= 1 - \frac{1}{4}[(\frac{k_1}{k})^2 - 1][1 - \cos 2kR_1] + \frac{i}{2}[(\frac{k_1}{k})^2 - 1][kR_1 - \frac{1}{2}\sin 2kR_1]. \end{aligned} \tag{124}$$

The second iteration $g_{II}(\frac{1}{2}, k, 0)$ is given by

$$\begin{aligned} g_{II}(\frac{1}{2}, k, 0) &= g_0(\frac{1}{2}, k, 0) + g_1(\frac{1}{2}, k, 0) + +g_2(\frac{1}{2}, k, 0) \\ &= 1 - \frac{1}{4}[(\frac{k_1}{k})^2 - 1][1 - \cos 2kR_1] - \frac{1}{8}[(\frac{k_1}{k})^2 - 1]^2\{kR_1(kR_1 + \sin 2kR_1) \\ &+ \frac{3}{2}(\cos 2kR_1 - 1)\} + \frac{i}{2}\{[(\frac{k_1}{k})^2 - 1][kR_1 - \frac{1}{2}\sin 2kR_1] \\ &- \frac{1}{2}[(\frac{k_1}{k})^2 - 1]^2[kR_1(1 + \frac{1}{2}\cos 2kR_1) - \frac{3}{2}\sin 2kR_1]\}. \end{aligned} \tag{125}$$

Since wavelengths and wavenumbers vary inversely, there is an approximate theory for the scattering of plane wave by considering the ratios of wavelengths in the scattering region and in the surrounding region [28]. In this chapter, we also consider the ratios of the wavenumbers for short and long wavelengths.

In Figures 35 through 38, we have plotted $f(\frac{1}{2}, k)$, $g_I(\frac{1}{2}, k, 0)$, and $g_{II}(\frac{1}{2}, k, 0)$ as a function of kR_1 for the ratios of the wavenumbers in the scattering medium and in the surrounding medium, $k_1/k = 0.5$, 1.1, 1.5, and 2.0, respectively. The results show that the iteration technique becomes less accurate when the ratio of k_1/k is not around 1. For $k_1/k = 1.1$, the approximation is good for the entire range of kR_1. For $k_1/k = 0.5$, the approximation is good until $kR_1 \approx \pi$. For $k_1/k = 1.5$, and 2.0, the approximation is good until $kR_1 \approx 3\pi/4$.

For real λ and k, we have

$$f(\lambda, -k) = f^*(\lambda, k), \tag{126}$$

and therefore

$$\begin{aligned} \sigma_0/\pi R_1^2 &= |1 - e^{2i\delta(\frac{1}{2}, k)}|^2/(kR_1)^2 \\ &= |1 - [f(\frac{1}{2}, k)/f^*(\frac{1}{2}, k)]|^2/(kR_1)^2, \end{aligned} \tag{127}$$

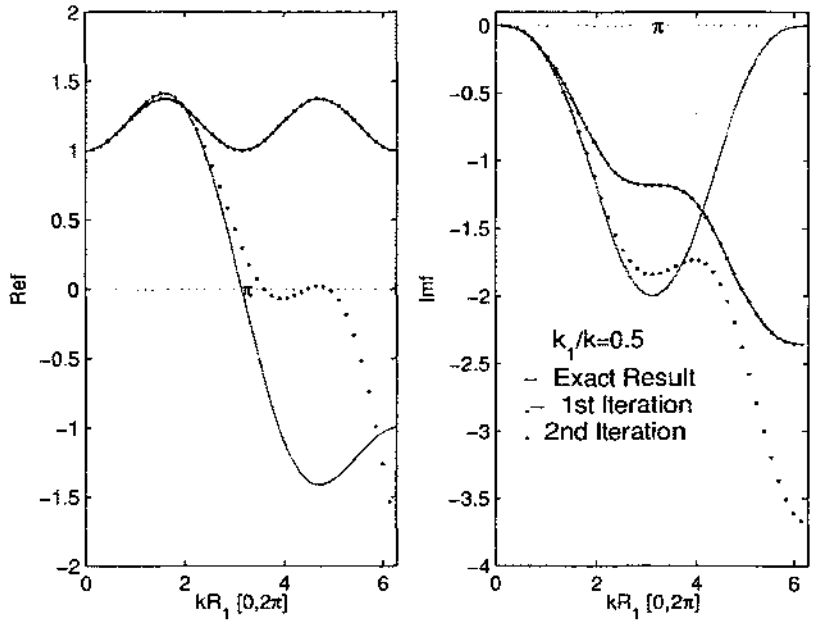

FIG. 35: $f(\frac{1}{2},k)$ vs kR_1 for scattering from a constant spherical inhomogeneity, $k_1/k = 0.5$.

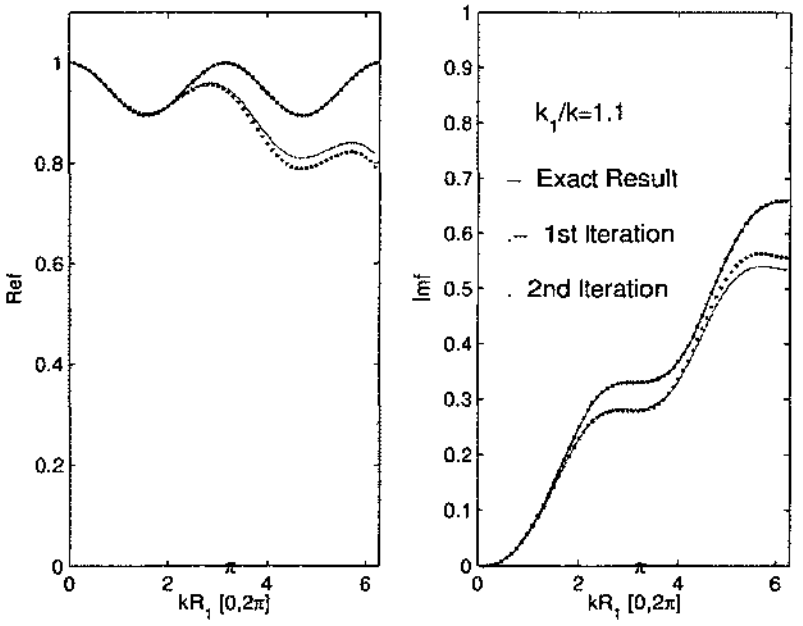

FIG. 36: $f(\frac{1}{2},k)$ vs kR_1 for scattering from a constant spherical inhomogeneity, $k_1/k = 1.1$.

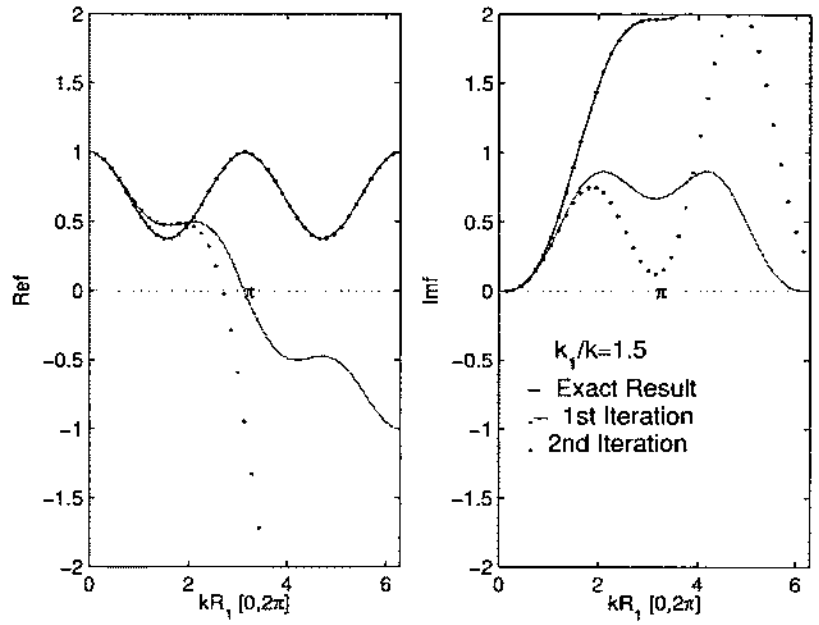

FIG. 37: $f(\frac{1}{2},k)$ vs kR_1 for scattering from a constant spherical inhomogeneity, $k_1/k = 1.5$.

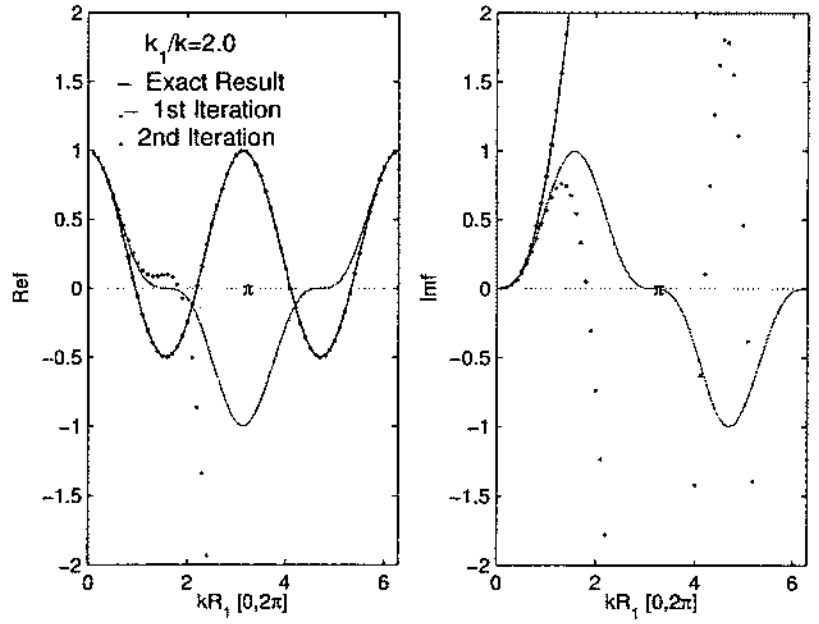

FIG. 38: $f(\frac{1}{2},k)$ vs kR_1 for scattering from a constant spherical inhomogeneity, $k_1/k = 2.0$.

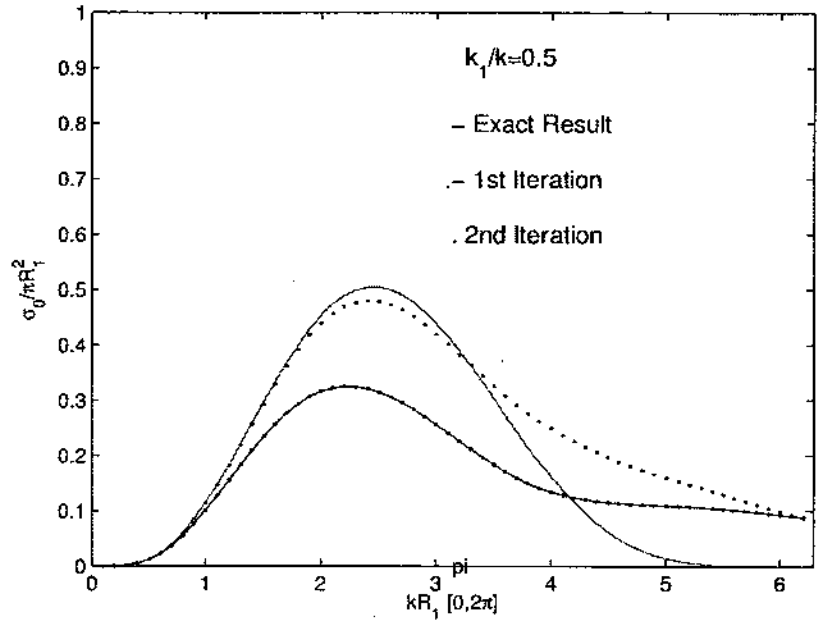

FIG. 39: $\sigma_0/\pi R_1^2$ vs kR_1 for scattering from a constant spherical inhomogeneity, $k_1/k = 0.5$.

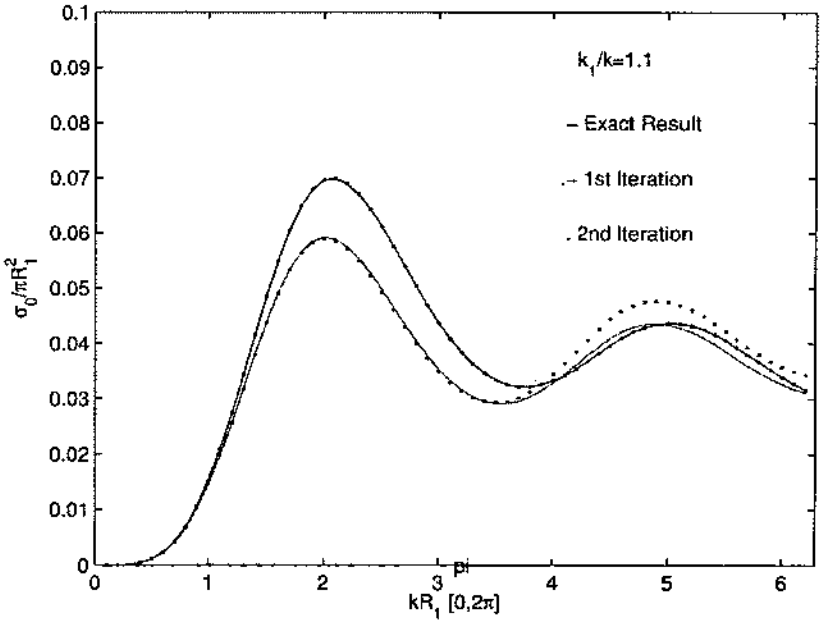

FIG. 40: $\sigma_0/\pi R_1^2$ vs kR_1 for scattering from a constant spherical inhomogeneity, $k_1/k = 1.1$.

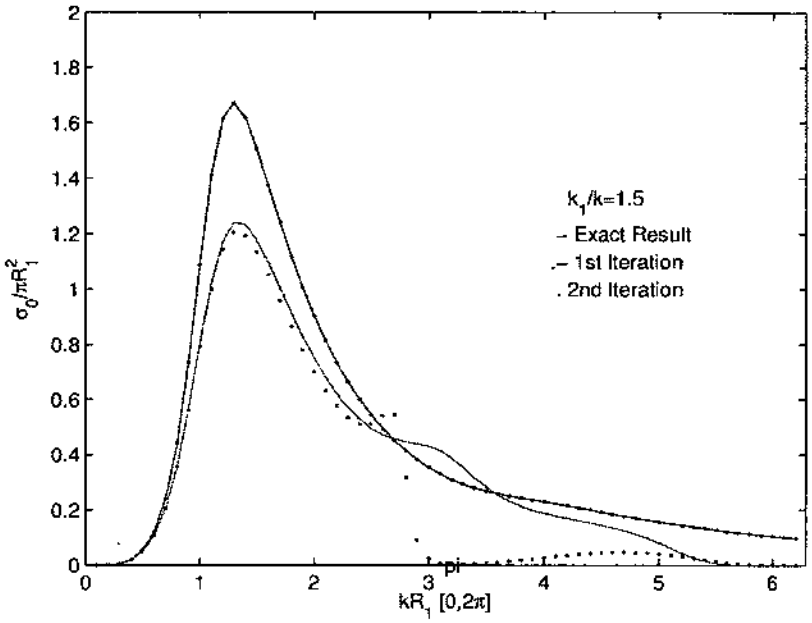

FIG. 41: $\sigma_0/\pi R_1^2$ vs kR_1 for scattering from a constant spherical inhomogeneity, $k_1/k = 1.5$.

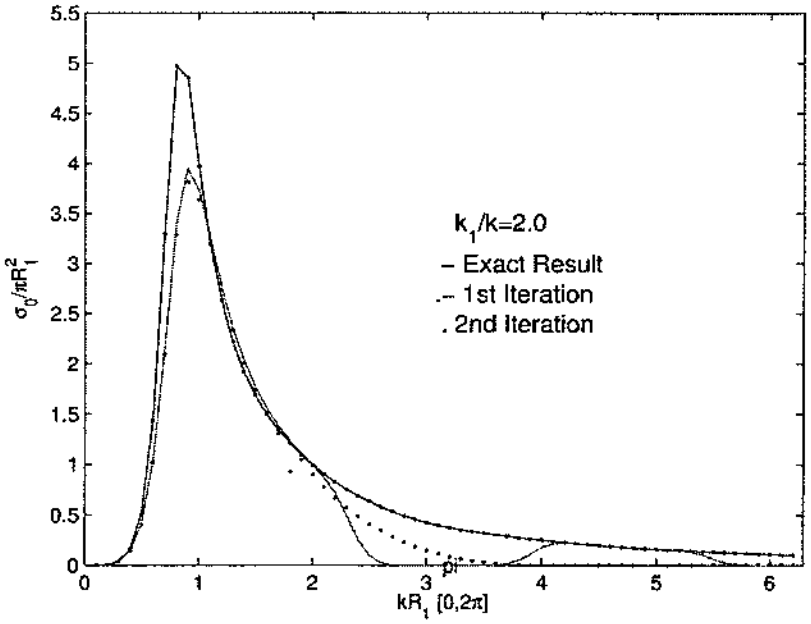

FIG. 42: $\sigma_0/\pi R_1^2$ vs kR_1 for scattering from a constant spherical inhomogeneity, $k_1/k = 2.0$.

where σ_0 is the $l = 0$ total cross section. Using (122), (124), (125), and (127), in Figures 39 through 42, the exact result, first iteration, and second iteration for $\sigma_0/\pi R_1^2$ for $k_1/k = 0.5$, 1.1, 1.5, and 2.0 are respectively presented. It appears that the iteration procedure is more accurate for the cross section than the Jost function itself. For long-wavelengths ($kR_1 \ll 1$), the iteration technique is good for any ratio of wavenumbers in the scattering and surrounding media. For shorter wavelengths, the ratio k_1/k close to 1 (e.g., $k_1/k = 1.1$) gives a good approximation to the total cross section $l = 0$ for the entire range of kR_1; however, the smaller k_1/k (e.g., $k_1/k = 0.5$) gives a good approximation to σ_0 until $kR_1 \approx 7\pi/6$ and the larger k_1/k (e.g., $k_1/k = 1.5, 2.0$) gives a good approximation to σ_0 until $kR_1 \approx 3\pi/4$.

3.5 SCATTERING FROM A PIECEWISE CONSTANT BY MULTI-LAYER SPHERICALLY SYMMETRIC INHOMOGENEITIES

We apply the method outlined in Section 3.2 to the problem of scattering from a piecewise constant in a multi-layer spherical inhomogeneities (see Figure 43): For a three-layer inhomogeneity we define the following potential

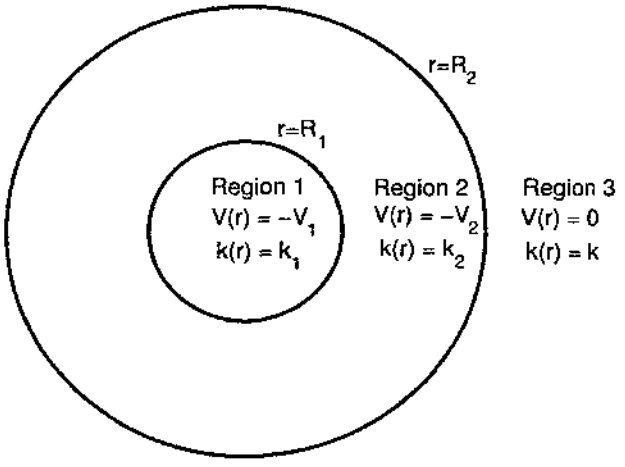

FIG. 43: A piecewise constant spherical inhomogeneity.

$$Region\ 1 : V(r) = -V_1, k(r) = k_1, r < R_1,$$
$$Region\ 2 : V(r) = -V_2, k(r) = k_2, R_1 < r < R_2,$$
$$Region\ 3 : V(r) = 0, k(r) = k, r > R_2. \tag{128}$$

The solutions in the three regions are:

$$Region\ 1 : u^{(1)}_{\lambda-\frac{1}{2}}(k_1, r) = r[Aj_{\lambda-\frac{1}{2}}(k_1 r) + By_{\lambda-\frac{1}{2}}(k_1 r)],$$
$$Region\ 2 : u^{(2)}_{\lambda-\frac{1}{2}}(k_2, r) = r[Cj_{\lambda-\frac{1}{2}}(k_2 r) + Dy_{\lambda-\frac{1}{2}}(k_2 r)],$$
$$Region\ 3 : u^{(3)}_{\lambda-\frac{1}{2}}(k, r) = r[Eh^{(1)}_{\lambda-\frac{1}{2}}(kr) + Fh^{(2)}_{\lambda-\frac{1}{2}}(kr)]. \tag{129}$$

where again $j_{\lambda-\frac{1}{2}}(k_1 r)$ and $j_{\lambda-\frac{1}{2}}(k_2 r)$, $y_{\lambda-\frac{1}{2}}(k_1 r)$ and $y_{\lambda-\frac{1}{2}}(k_2 r)$, and $h^{(1)}_{\lambda-\frac{1}{2}}(kr)$ and $h^{(2)}_{\lambda-\frac{1}{2}}(kr)$ are spherical Bessel, Neumann, and Hankel functions of the first kind and second kind, respectively.

We proceed as in the two-layer model. Choosing $u^{(1)}_{\lambda-\frac{1}{2}}(k_1, r)$ to be $\phi_1(\lambda, k_1, r)$ and imposing the boundary conditions (86) at $r = 0$, we find that $B = 0$ and

$$\phi_1(\lambda, k_1, r) = 2^{\lambda+\frac{1}{2}}\pi^{-\frac{1}{2}}k_1^{-\lambda+\frac{1}{2}}\Gamma(\lambda+1)rj_{\lambda-\frac{1}{2}}(k_1 r),$$
$$\phi_1'(\lambda, k_1, r) = 2^{\lambda+\frac{1}{2}}\pi^{-\frac{1}{2}}k_1^{-\lambda+\frac{1}{2}}\Gamma(\lambda+1) \times [j_{\lambda-\frac{1}{2}}(k_1 r) + k_1 r j'_{\lambda-\frac{1}{2}}(k_1 r)]. \tag{130}$$

Choosing $u^{(2)}_{\lambda-\frac{1}{2}}(k_2, r)$ to be $\phi_2(\lambda, k_2, r)$ and imposing the continuity at the boundary $r = R_1$ by matching the continuity of ϕ_1 with ϕ_2 and ϕ_1' with ϕ_2', we have

$$\phi_2(\lambda, k_2, r) = r[Cj_{\lambda-\frac{1}{2}}(k_2 r) + Dy_{\lambda-\frac{1}{2}}(k_2 r)],$$
$$\phi_2'(\lambda, k_2, r) = C[j_{\lambda-\frac{1}{2}}(k_2 r) + k_2 r j'_{\lambda-\frac{1}{2}}(k_2 r)] + D[y_{\lambda-\frac{1}{2}}(k_2 r) + k_2 r y'_{\lambda-\frac{1}{2}}(k_2 r)], \tag{131}$$

where

$$C = -\frac{m(j_{\lambda-\frac{1}{2}}(k_1 R_1)y'_{\lambda-\frac{1}{2}}(k_2 R_1) - \frac{k_1}{k_2}j'_{\lambda-\frac{1}{2}}(k_1 R_1)y_{\lambda-\frac{1}{2}}(k_2 R_1))}{j'_{\lambda-\frac{1}{2}}(k_2 R_1)y_{\lambda-\frac{1}{2}}(k_2 R_1) - j_{\lambda-\frac{1}{2}}(k_2 R_1)y'_{\lambda-\frac{1}{2}}(k_2 R_1)},$$
$$D = \frac{m(j_{\lambda-\frac{1}{2}}(k_1 R_1)j'_{\lambda-\frac{1}{2}}(k_2 R_1) - \frac{k_1}{k_2}j'_{\lambda-\frac{1}{2}}(k_1 R_1)j_{\lambda-\frac{1}{2}}(k_2 R_1))}{j'_{\lambda-\frac{1}{2}}(k_2 R_1)y_{\lambda-\frac{1}{2}}(k_2 R_1) - j_{\lambda-\frac{1}{2}}(k_2 R_1)y'_{\lambda-\frac{1}{2}}(k_2 R_1)},$$
$$(m = 2^{\lambda+\frac{1}{2}}\pi^{-\frac{1}{2}}k_1^{-\lambda+\frac{1}{2}}\Gamma(\lambda+1)). \tag{132}$$

Choosing $u^{(3)}_{\lambda-\frac{1}{2}}(k, r)$ to be $f(\lambda, k, r)$ and imposing the boundary conditions (93), we find that $E = 0$, $F = ke^{-i\frac{\pi}{2}(\lambda+\frac{1}{2})}$, and

$$f(\lambda, k, r) = ke^{-i\frac{\pi}{2}(\lambda+\frac{1}{2})}rh^{(2)}_{\lambda-\frac{1}{2}}(kr),$$
$$f'(\lambda, k, r) = ke^{-i\frac{\pi}{2}(\lambda+\frac{1}{2})}[h^{(2)}_{\lambda-\frac{1}{2}}(kr) + krh'^{(2)}_{\lambda-\frac{1}{2}}(kr)], \tag{133}$$

where we have used the following asymptotic form for $h^{(2)}_{\lambda-\frac{1}{2}}(kr)$:

$$\lim_{kr\to\infty} h^{(2)}_{\lambda-\frac{1}{2}}(kr) = \frac{1}{kr}e^{-i[kr-\frac{\pi}{2}(\lambda+\frac{1}{2})]}.$$

Since the point $r = R_2$ is the common domain of $\phi_2(\lambda, k_2, r)$ and $f(\lambda, k, r)$, we evaluate the Jost function at $r = R_2$ and thus obtain

$$\begin{aligned}
f(\lambda,k) &= W[f(\lambda,k,r),\phi_2(\lambda,k_2,r)]_{r=R_2} \\
&= f(\lambda,k,r)\phi_2'(\lambda,k_2,r) - f'(\lambda,k,r)\phi_2(\lambda,k_2,r) \\
&= 2^{\lambda+\frac{1}{2}}\pi^{-\frac{1}{2}}\Gamma(\lambda+1)k_1^{-\lambda+\frac{1}{2}}ke^{-i\frac{\pi}{2}(\lambda+\frac{1}{2})}R_2^2 \\
&\times \{h^{(2)}_{\lambda-\frac{1}{2}}(kR_2)k_2[a_1 j_{\lambda-\frac{1}{2}}(k_1R_1) + \frac{k_1}{k_2}a_3 j'_{\lambda-\frac{1}{2}}(k_1R_1)] \\
&- h^{(2)'}_{\lambda-\frac{1}{2}}(kR_2)k[a_2 j_{\lambda-\frac{1}{2}}(k_1R_1) + \frac{k_1}{k_2}a_4 j'_{\lambda-\frac{1}{2}}(k_1R_1)]\} \\
&/[j'_{\lambda-\frac{1}{2}}(k_2R_1)y_{\lambda-\frac{1}{2}}(k_2R_1) - j_{\lambda-\frac{1}{2}}(k_2R_1)y'_{\lambda-\frac{1}{2}}(k_2R_1)]. \qquad (134)
\end{aligned}$$

We also have that

$$\begin{aligned}
f(\lambda,-k) &= 2^{\lambda+\frac{1}{2}}\pi^{-\frac{1}{2}}\Gamma(\lambda+1)k_1^{-\lambda+\frac{1}{2}}ke^{-i\frac{\pi}{2}(\lambda+\frac{1}{2})}R_2^2e^{i\pi(\lambda-\frac{1}{2})} \\
&\times \{-h^{(1)}_{\lambda-\frac{1}{2}}(kR_2)k_2[a_1 j_{\lambda-\frac{1}{2}}(k_1R_1) + \frac{k_1}{k_2}a_3 j'_{\lambda-\frac{1}{2}}(k_1R_1)] \\
&+ h^{(1)'}_{\lambda-\frac{1}{2}}(kR_2)k[a_2 j_{\lambda-\frac{1}{2}}(k_1R_1) + \frac{k_1}{k_2}a_4 j'_{\lambda-\frac{1}{2}}(k_1R_1)]\} \\
&/[j'_{\lambda-\frac{1}{2}}(k_2R_1)y_{\lambda-\frac{1}{2}}(k_2R_1) - j_{\lambda-\frac{1}{2}}(k_2R_1)y'_{\lambda-\frac{1}{2}}(k_2R_1)], \qquad (135)
\end{aligned}$$

where we have used the following identities:

$$\begin{aligned}
h^{(2)}_{\lambda-\frac{1}{2}}(kre^{i\pi}) &= h^{(2)}_{\lambda-\frac{1}{2}}(-kr) \\
&= (-1)^{\lambda-\frac{1}{2}}h^{(1)}_{\lambda-\frac{1}{2}}(kr) \\
&= e^{i\pi(\lambda-\frac{1}{2})}h^{(1)}_{\lambda-\frac{1}{2}}(kr) \\
h^{(2)'}_{\lambda-\frac{1}{2}}(-kr) &= (-1)^{\lambda+\frac{1}{2}}h^{(1)'}_{\lambda-\frac{1}{2}}(kr) \\
&= e^{i\pi(\lambda+\frac{1}{2})}h^{(1)'}_{\lambda-\frac{1}{2}}(kr) \\
&= -e^{i\pi(\lambda-\frac{1}{2})}h^{(1)'}_{\lambda-\frac{1}{2}}(kr), \lambda-\frac{1}{2} = 0,1,2,\ldots. \qquad (136)
\end{aligned}$$

The S-matrix is then given by

$$\begin{aligned} S(\lambda,k) = -\{&kh^{(2)'}_{\lambda-\frac{1}{2}}(kR_2)[a_2 j_{\lambda-\frac{1}{2}}(k_1R_1) + \frac{k_1}{k_2}a_4 j'_{\lambda-\frac{1}{2}}(k_1R_1)] \\ &- k_2 h^{(2)}_{\lambda-\frac{1}{2}}(kR_2)[a_1 j_{\lambda-\frac{1}{2}}(k_1R_1) + \frac{k_1}{k_2}a_3 j'_{\lambda-\frac{1}{2}}(k_1R_1)]\} \\ /\{&kh^{(1)'}_{\lambda-\frac{1}{2}}(kR_2)[a_2 j_{\lambda-\frac{1}{2}}(k_1R_1) + \frac{k_1}{k_2}a_4 j'_{\lambda-\frac{1}{2}}(k_1R_1)] \\ &- k_2 h^{(1)}_{\lambda-\frac{1}{2}}(kR_2)[a_1 j_{\lambda-\frac{1}{2}}(k_1R_1) + \frac{k_1}{k_2}a_3 j'_{\lambda-\frac{1}{2}}(k_1R_1)]\}, \end{aligned} \tag{137}$$

where

$$\begin{aligned} a_1 &= j'_{\lambda-\frac{1}{2}}(k_2R_1)y'_{\lambda-\frac{1}{2}}(k_2R_2) - y'_{\lambda-\frac{1}{2}}(k_2R_1)j'_{\lambda-\frac{1}{2}}(k_2R_2), \\ a_2 &= j'_{\lambda-\frac{1}{2}}(k_2R_1)y_{\lambda-\frac{1}{2}}(k_2R_2) - j_{\lambda-\frac{1}{2}}(k_2R_2)y'_{\lambda-\frac{1}{2}}(k_2R_1), \\ a_3 &= y_{\lambda-\frac{1}{2}}(k_2R_1)j'_{\lambda-\frac{1}{2}}(k_2R_2) - j_{\lambda-\frac{1}{2}}(k_2R_1)y'_{\lambda-\frac{1}{2}}(k_2R_2), \\ a_4 &= j_{\lambda-\frac{1}{2}}(k_2R_1)y_{\lambda-\frac{1}{2}}(k_2R_2) - y_{\lambda-\frac{1}{2}}(k_2R_1)j_{\lambda-\frac{1}{2}}(k_2R_2). \end{aligned}$$

We can calculate the Jost function for $\lambda = \frac{1}{2}$ from (134):

$$\begin{aligned} f(\frac{1}{2},k) =&\frac{1}{4}e^{-ikR_2}\{([\frac{(k-ik_2)}{k_1} + \frac{(ik+k_2)}{k_2}]e^{k_2(R_2-R_1)} \\ &+ [\frac{(k+ik_2)}{k_1} + \frac{(k_2-ik)}{k_2}]e^{-k_2(R_2-R_1)})e^{ik_1R_1} \\ &+ ([\frac{(ik+k_2)}{k_2} - \frac{(k-ik_2)}{k_1}]e^{k_2(R_2-R_1)} \\ &+ [\frac{(k_2-ik)}{k_2} - \frac{(k+ik_2)}{k_1}]e^{-k_2(R_2-R_1)})e^{-ik_1R_1}\}, \end{aligned} \tag{138}$$

where we have used the following relations (see TABLE 2):

3.6 JOST INTEGRAL EQUATION FOR $\lambda = \frac{1}{2}$ AND SOME APPROXIMATE SOLUTIONS IN THE 3-LAYER MODEL

We now apply the method in Section 3.4 to the case of scattering from a piecewise constant by multi-layer spherical inhomogeneity. We have already calculated $f(\frac{1}{2},k)$ exactly in Section 3.5. We can use the exact solution of the Jost function to check for the accuracy of the iteration procedure. We write the solution (123) again in the

TABLE 2: Alternative expressions for $j_0(kR)$, $j_0'(kR)$, $h_0^{(2)}(kR)$, and $h_0^{\prime(2)}(kR)$.

Function		Expression
$j_0(kR)$	=	$\sin kR/(kR)$
$j_0'(kR)$	=	$\cos kR/(kR) - [\sin kR/(kR)^2]$
$h_0^{(2)}(kR)$	=	$-e^{-ikR}/(ikR)$
$h_0^{(2)'}(kR)$	=	$e^{-ikR}[1 + 1/(ikR)]/(kR)$

following form: The first iteration $g_I(\frac{1}{2}, k, 0)$ of (123) is

$$\begin{aligned} g_I(\frac{1}{2}, k, 0) &= g_0(\frac{1}{2}, k, 0) + g_1(\frac{1}{2}, k, 0) \\ &= 1 - \frac{1}{4}\{[(\frac{k_1}{k})^2 - 1][1 - \cos 2kR_1] + [1 - (\frac{k_2}{k})^2][\cos 2kR_2 - \cos 2kR_1]\} \\ &+ \frac{i}{2}\{[(\frac{k_1}{k})^2 - 1][kR_1 - \frac{1}{2}\sin 2kR_1] \\ &+ [1 - (\frac{k_2}{k})^2][k(R_2 - R_1) - \frac{1}{2}(\sin 2kR_2 - \sin 2kR_1]\}. \end{aligned} \tag{139}$$

The second iteration $g_{II}(\frac{1}{2},k,0)$ is

$$
\begin{aligned}
g_{II}(\frac{1}{2},k,0) &= g_0(\frac{1}{2},k,0)+g_1(\frac{1}{2},k,0)++g_2(\frac{1}{2},k,0)\\
&= 1+\frac{1}{4}\{[(\frac{k_1}{k})^2-1][\cos 2kR_1-1]+[1-(\frac{k_2}{k})^2][\cos 2kR_2-\cos 2kR_1]\}\\
&-\frac{1}{8}\{[(\frac{k_1}{k})^2-1]^2(kR_1[kR_1+\sin 2kR_1]+\frac{3}{2}[\cos 2kR_1-1])\\
&+[(\frac{k_1}{k})^2-1][1-(\frac{k_2}{k})^2](k(R_2-R_1)[2kR_1-k(R_2-R_1)-\sin 2kR_1]\\
&-[\cos 2k(R_2-R_1)-1]+\frac{3}{2}[\cos 2kR_2-\cos 2kR_1]\\
&+k(R_2-R_1)[\sin 2kR_2+\sin 2kR_1]+kR_1[\sin 2kR_2-\sin 2kR_1])\\
&+[1-(\frac{k_2}{k})^2]^2(k(R_2-R_1)[2k(R_2-R_1)-\sin 2k(R_2-R_1)\\
&+\sin 2kR_2-\sin 2kR_1]+[\cos 2k(R_2-R_1)-1])\}\\
&+i\{\frac{1}{2}([(\frac{k_1}{k})^2-1][kR_1-\frac{1}{2}\sin 2kR_1]\\
&+[1-(\frac{k_2}{k})^2][k(R_2-R_1)-\frac{1}{2}[\sin 2kR_2-\sin 2kR_1]])\\
&-\frac{1}{8}([(\frac{k_1}{k})^2-1]^2(kR_1[\cos 2kR_1+2]-\frac{3}{2}\sin 2kR_1)\\
&+[(\frac{k_1}{k})^2-1][1-(\frac{k_2}{k})^2](kR_1[\cos 2kR_2-\cos 2kR_1]\\
&+k(R_2-R_1)[\cos 2kR_2+\cos 2kR_1]\\
&-k(R_2-R_1)[\cos 2kR_1-1]-\frac{3}{2}[\sin 2kR_2-\sin 2kR_1])\\
&-[1-(\frac{k_2}{k})^2]^2(k(R_2-R_1)[[\cos 2k(R_2-R_1)-\cos 2kR_2+\cos 2kR_1]))\}.
\end{aligned}
\tag{140}
$$

In Figures 44 through 51, we consider both increasing and decreasing refractive indices profiles. We have plotted $f(\frac{1}{2},k)$, $g_I(\frac{1}{2},k,0)$, and $g_{II}(\frac{1}{2},k,0)$ as a function of kR_1 for the ratios of the wavenumbers in the scattering medium between $r<R_1$ and $R_1<r<R_2$ and kR_2 for the ratios of the wavenumbers in the scattering medium between $R_1<r<R_2$ and $r>R_2$ for $k_1/k=0.7, k_2/k=0.9$; $k_1/k=0.9, k_2/k=0.7$; $k_1/k=1.1, k_2/k=1.3$; $k_1/k=1.3, k_2/k=1.1$; $k_1/k=1.2, k_2/k=1.5$; $k_1/k=1.5, k_2/k=1.2$; $k_1/k=1.5, k_2/k=2.0$ and $k_1/k=2.0, k_2/k=1.5$, respectively. The results show that the iteration procedure becomes less accurate when k_1/k and k_2/k increase.

For real λ and k, we have

$$f(\lambda, -k) = f^*(\lambda, k), \tag{141}$$

and therefore

$$\begin{aligned} \sigma_0/\pi R_1^2 &= |1 - e^{2i\delta(\frac{1}{2},k)}|^2/(kR_1)^2 \\ &= |1 - [f(\frac{1}{2},k)/f^*(\frac{1}{2},k)]|^2/(kR_1)^2, \end{aligned} \tag{142}$$

where σ_0 is the $l = 0$ total cross section. Using (138), (139), (140), and (142), in Figures 52 through 59, we have plotted the exact result, first iteration, and second iteration for $\sigma_0/\pi R_1^2$ for $k_1/k = 0.7, k_2/k = 0.9$; $k_1/k = 1.1, k_2/k = 1.3$; $k_1/k = 1.5, k_2/k = 1.2$; and $k_1/k = 2.0, k_2/k = 1.5$, respectively. For $k_1/k = 0.7, k_2/k = 0.9$, the approximation is good only for $kR_1 \ll 1$. For $k_1/k = 1.1, k_2/k = 1.3$, the approximation is good for the entire range. For $k_1/k = 1.5, k_2/k = 1.2$ and $k_1/k = 2.0, k_2/k = 1.5$, it gives a good approximation when $kR_1 \lesssim \pi/3$.

Based on these results, for long-wavelengths ($kR_1 \ll 1$) the iteration procedure gives a better approximation for the Jost function than for the total cross section, σ_0. For shorter wavelengths, all ratios of the wavenumbers give a good approximation to σ_0 from $kR_1 \approx \pi$; moreover, the approximation becomes more accurate in this range when the ratio of the wavenumbers is larger.

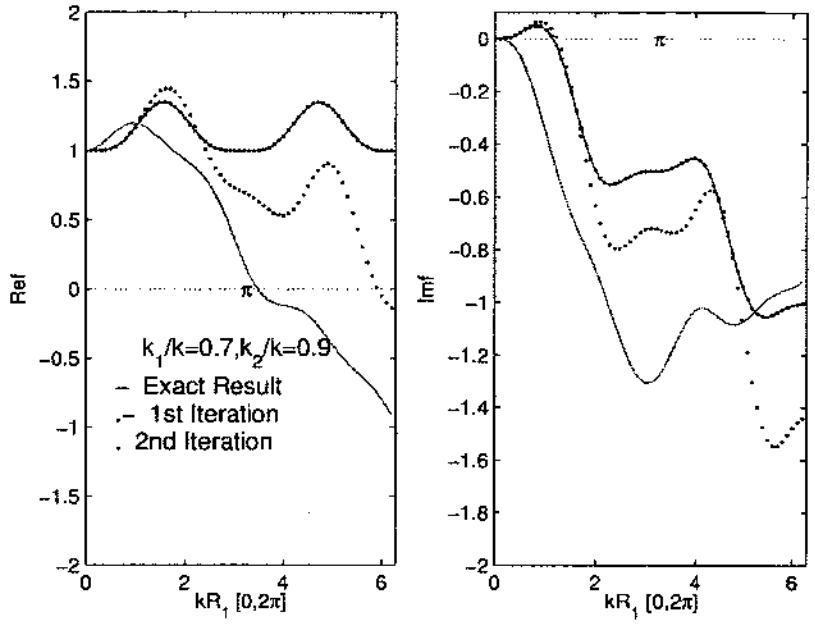

FIG. 44: $f(\frac{1}{2},k)$ vs kR_1 for scattering from a piecewise constant spherical inhomogeneity, $k_1/k = 0.7, k_2/k = 0.9$.

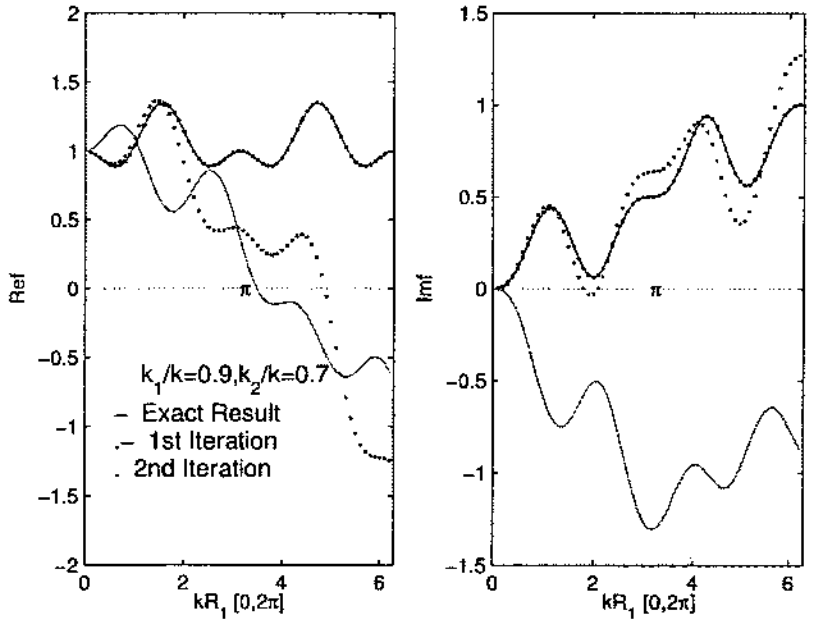

FIG. 45: $f(\frac{1}{2},k)$ vs kR_1 for scattering from a piecewise constant spherical inhomogeneity, $k_1/k = 0.9, k_2/k = 0.7$.

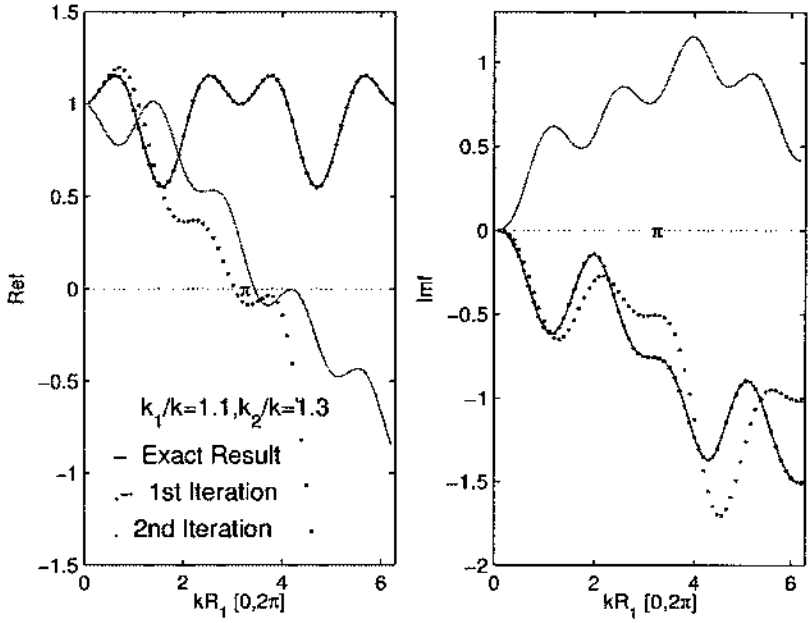

FIG. 46: $f(\frac{1}{2}, k)$ vs kR_1 for scattering from a piecewise constant spherical inhomogeneity, $k_1/k = 1.1, k_2/k = 1.3$.

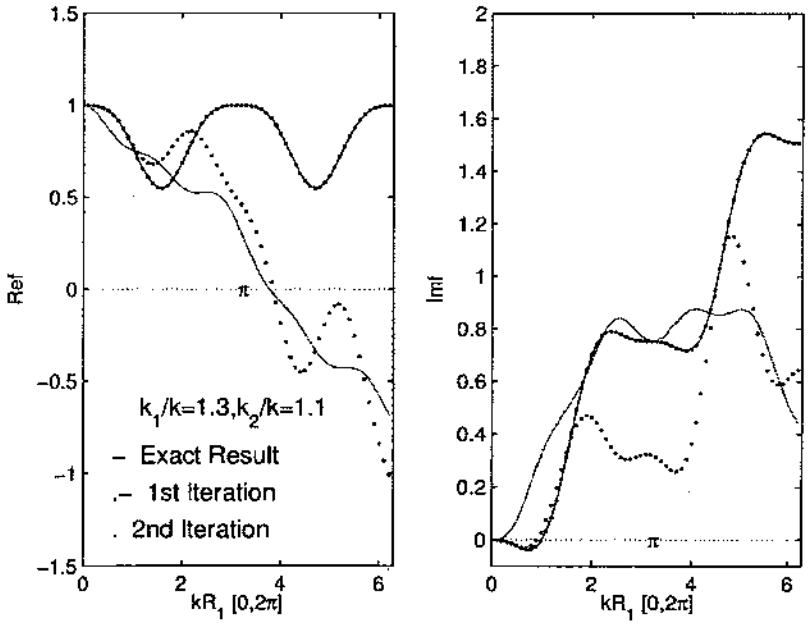

FIG. 47: $f(\frac{1}{2}, k)$ vs kR_1 for scattering from a piecewise constant spherical inhomogeneity, $k_1/k = 1.3, k_2/k = 1.1$.

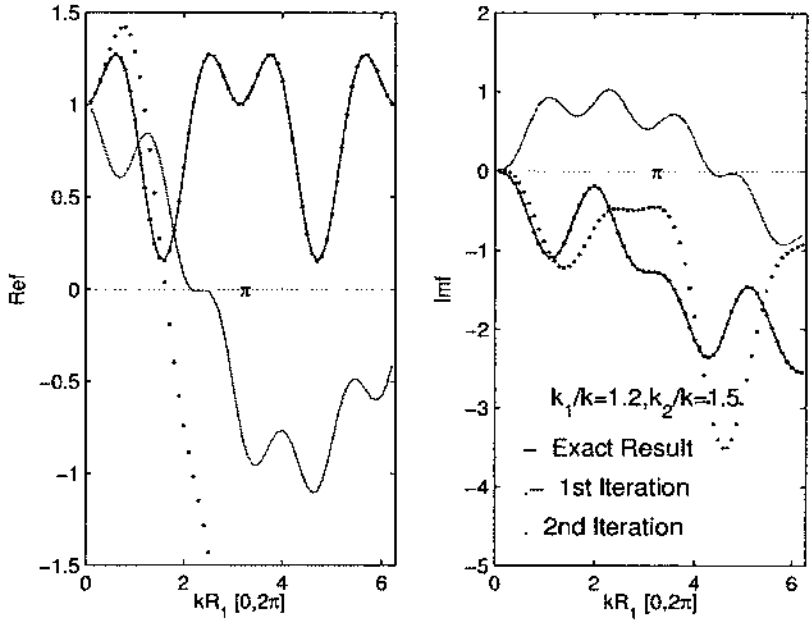

FIG. 48: $f(\frac{1}{2},k)$ vs kR_1 for scattering from a piecewise constant spherical inhomogeneity, $k_1/k = 1.2, k_2/k = 1.5$.

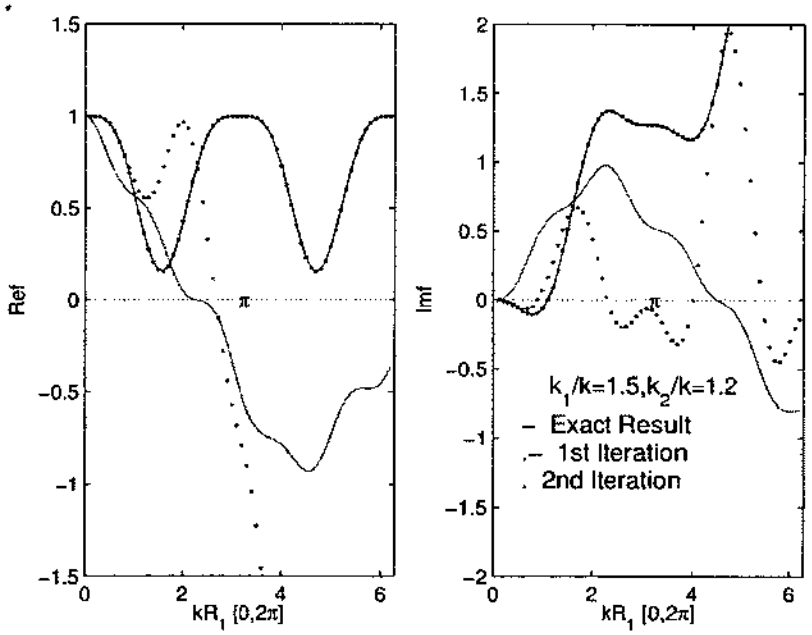

FIG. 49: $f(\frac{1}{2},k)$ vs kR_1 for scattering from a piecewise constant spherical inhomogeneity, $k_1/k = 1.5, k_2/k = 1.2$.

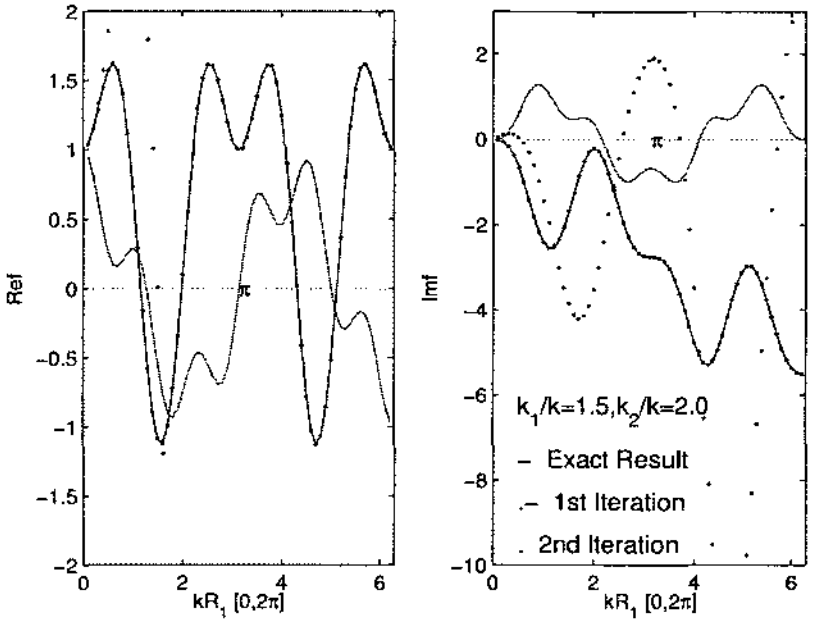

FIG. 50: $f(\frac{1}{2}, k)$ vs kR_1 for scattering from a piecewise constant spherical inhomogeneity, $k_1/k = 1.5, k_2/k = 2.0$.

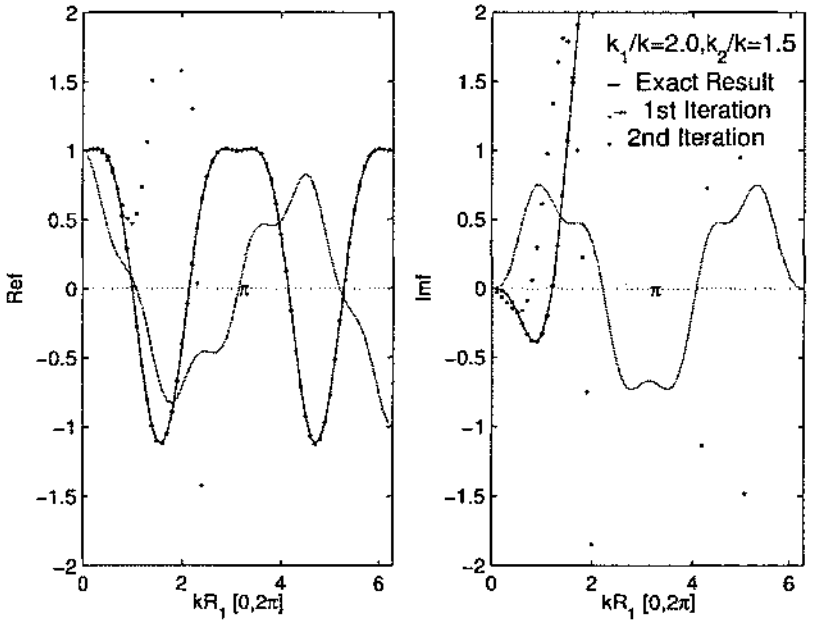

FIG. 51: $f(\frac{1}{2}, k)$ vs kR_1 for scattering from a piecewise constant spherical inhomogeneity, $k_1/k = 2.0, k_2/k = 1.5$.

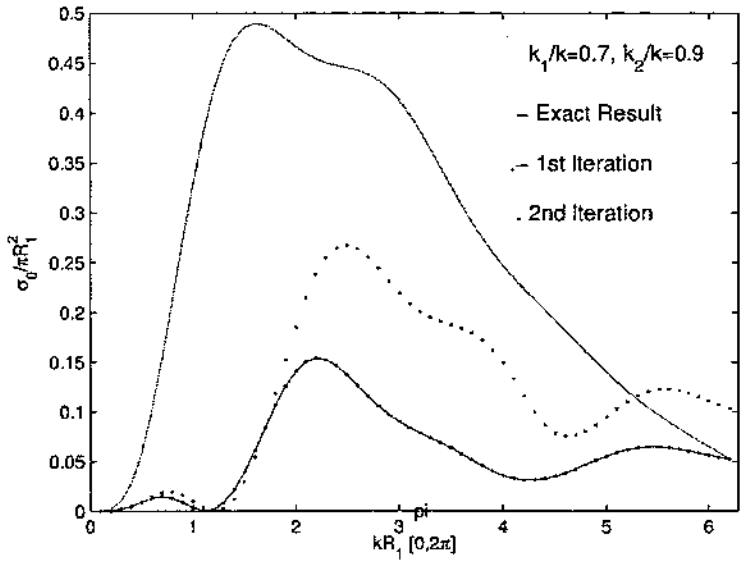

FIG. 52: $\sigma_0/\pi R_1^2$ vs kR_1 for scattering from a piecewise constant spherical inhomogeneity, $k_1/k = 0.7, k_2/k = 0.9$.

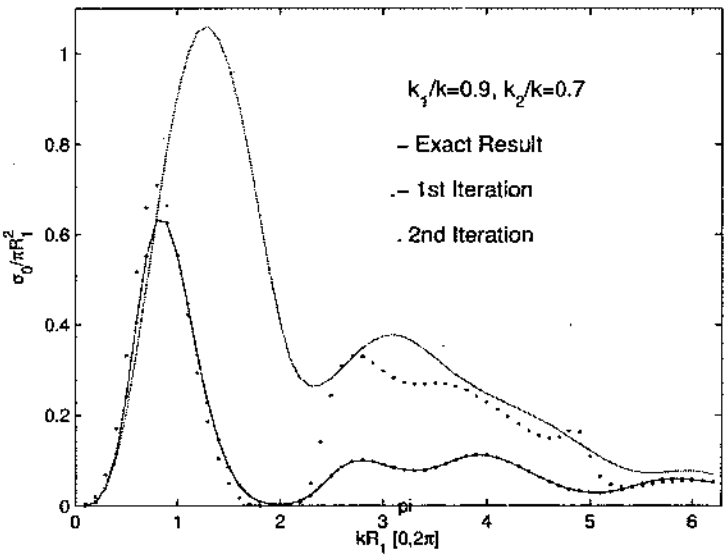

FIG. 53: $\sigma_0/\pi R_1^2$ vs kR_1 for scattering from a piecewise constant spherical inhomogeneity, $k_1/k = 0.9, k_2/k = 0.7$.

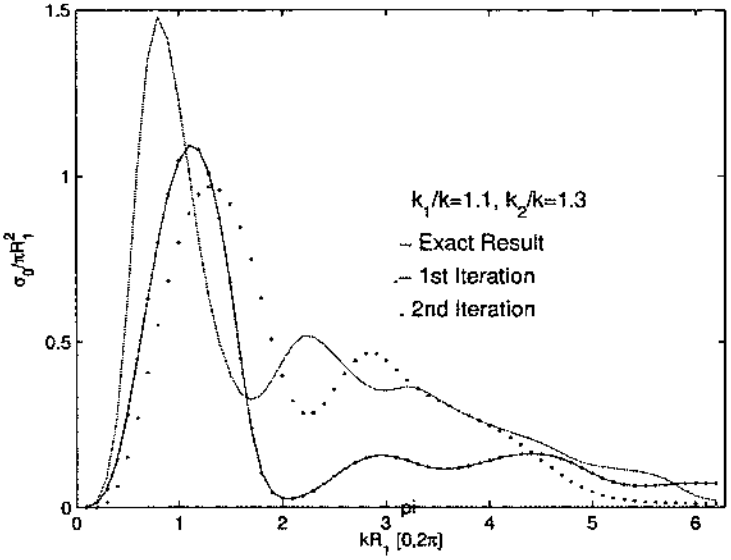

FIG. 54: $\sigma_0/\pi R_1^2$ vs kR_1 for scattering from a piecewise constant spherical inhomogeneity, $k_1/k = 1.1, k_2/k = 1.3$.

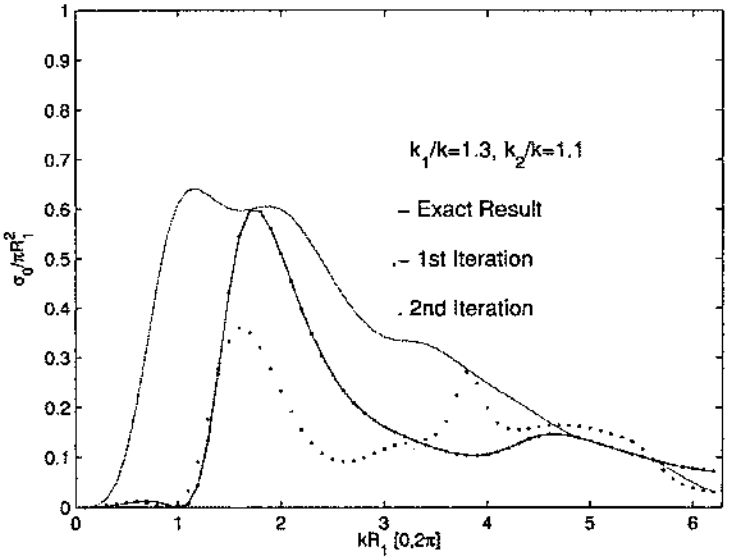

FIG. 55: $\sigma_0/\pi R_1^2$ vs kR_1 for scattering from a piecewise constant spherical inhomogeneity, $k_1/k = 1.3, k_2/k = 1.1$.

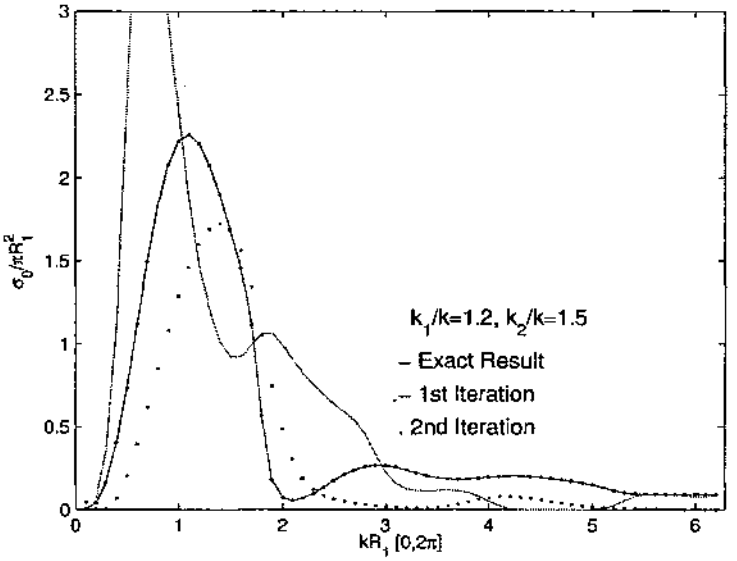

FIG. 56: $\sigma_0/\pi R_1^2$ vs kR_1 for scattering from a piecewise constant spherical inhomogeneity, $k_1/k = 1.2, k_2/k = 1.5$.

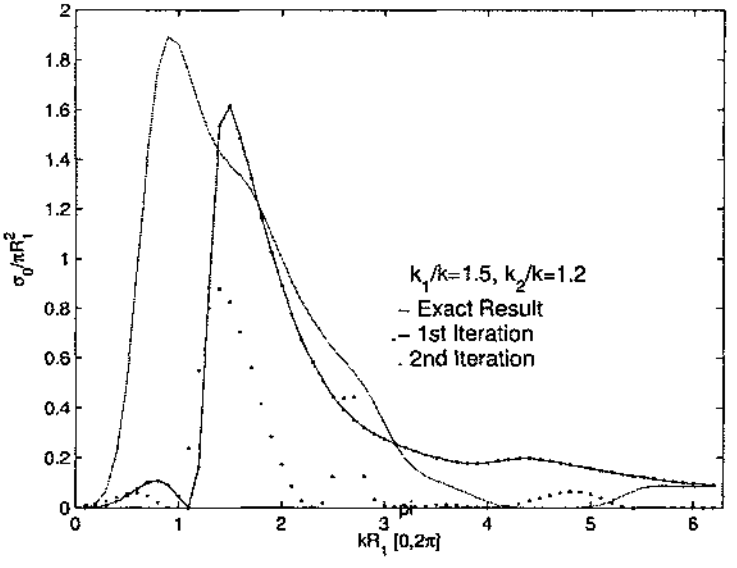

FIG. 57: $\sigma_0/\pi R_1^2$ vs kR_1 for scattering from a piecewise constant spherical inhomogeneity, $k_1/k = 1.5, k_2/k = 1.2$.

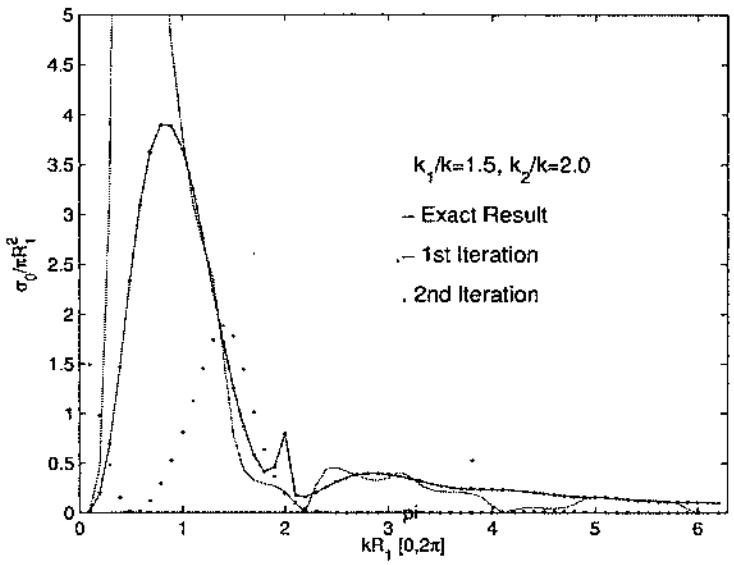

FIG. 58: $\sigma_0/\pi R_1^2$ vs kR_1 for scattering from a piecewise constant spherical inhomogeneity, $k_1/k = 1.5, k_2/k = 2.0$.

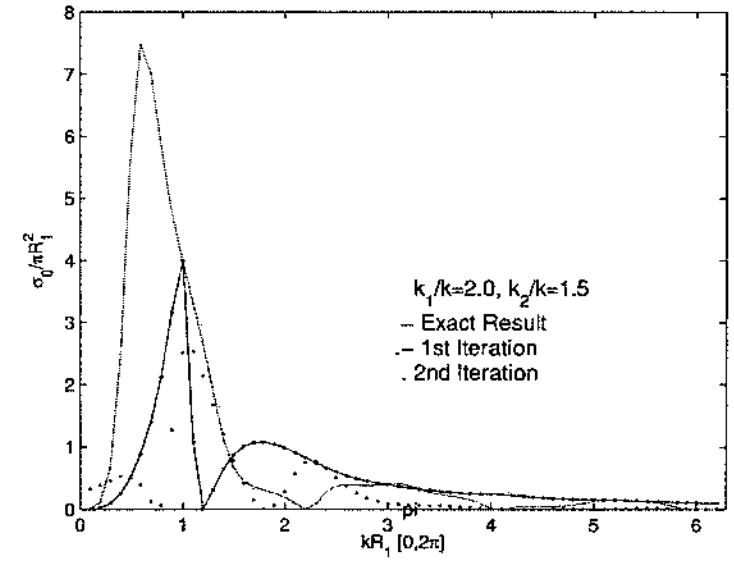

FIG. 59: $\sigma_0/\pi R_1^2$ vs kR_1 for scattering from a piecewise constant spherical inhomogeneity, $k_1/k = 2.0, k_2/k = 1.5$.

3.7 GENERAL JOST INTEGRAL-EQUATION FORMULATION FOR ARBITRARY λ FOR SCATTERING FROM AN ARBITRARY INHOMOGENEITY

3.7.1 2-LAYER MODEL

From (85) and (94) for $\phi(\lambda, k, r)$ and $f(\lambda, k, r)$, we can derive the general Jost integral-equation formulation for arbitrary λ for scattering from an arbitrary inhomogeneity. For any $V(r)$ satisfying requirements (80), we can solve (85) and (94) using an iteration procedure that used in Section 3.4. After we know $\phi(\lambda, k, r)$ and $f(\lambda, k, r)$, we can calculate $\phi'(\lambda, k, r)$ and $f'(\lambda, k, r)$ and therefore $f(\lambda, k)$, which can be calculated at any point in common domain of $\phi(\lambda, k, r)$ and $f(\lambda, k, r)$. In the case of scattering from a constant spherical inhomogeneity, we have the following two integral equations:

$$\begin{aligned}\phi(\lambda, k, r) =& r^{\lambda+\frac{1}{2}} + \frac{1}{2}\lambda^{-1}\int_0^{R_1}[(\xi/r)^\lambda - (r/\xi)^\lambda] \times (r\xi)^{\frac{1}{2}}[k^2 + V_1]\phi(\lambda, k, \xi)d\xi \\ &+ \frac{1}{2}\lambda^{-1}\int_{R_1}^{r}[(\xi/r)^\lambda - (r/\xi)^\lambda](r\xi)^{\frac{1}{2}}k^2\phi(\lambda, k, \xi)d\xi; \end{aligned} \tag{143}$$

$$\begin{aligned}f(\lambda, k, r) =& e^{-ikr} + k^{-1}\int_r^{R_1}[\sin k(r' - r)] \times [-V_1 + (\lambda^2 - \frac{1}{4})/(r')^2]f(\lambda, k, r')dr' \\ &+ k^{-1}\int_{R_1}^{\infty}[\sin k(r' - r)] \times [(\lambda^2 - \frac{1}{4})/(r')^2]f(\lambda, k, r')dr'. \end{aligned} \tag{144}$$

The Jost function can be evaluated at any point $r \geq R$, since we have restricted $f(\lambda, k, r)$ to the region $r > R$.

3.7.2 3-LAYER MODEL

In the case of scattering from a piecewise constant spherical inhomogeneity, the two integral equations (143) and (144) become:

$$\begin{aligned}\phi(\lambda, k, r) =& r^{\lambda+\frac{1}{2}} + \frac{1}{2}\lambda^{-1}\int_0^{R_1}[(\xi/r)^\lambda - (r/\xi)^\lambda] \times (r\xi)^{\frac{1}{2}}[k^2 + V_1]\phi(\lambda, k, \xi)d\xi \\ &+ \frac{1}{2}\lambda^{-1}\int_{R_1}^{R_2}[(\xi/r)^\lambda - (r/\xi)^\lambda] \times (r\xi)^{\frac{1}{2}}[k^2 + V_2]\phi(\lambda, k, \xi)d\xi \\ &+ \frac{1}{2}\lambda^{-1}\int_{R_2}^{r}[(\xi/r)^\lambda - (r/\xi)^\lambda](r\xi)^{\frac{1}{2}}k^2\phi(\lambda, k, \xi)d\xi; \end{aligned} \tag{145}$$

$$f(\lambda,k,r) = e^{-ikr} + k^{-1}\int_{r}^{R_1}[\sin k(r'-r)]\times[-V_1+(\lambda^2-\frac{1}{4})/(r')^2]f(\lambda,k,r')dr'$$
$$+ k^{-1}\int_{R_1}^{R_2}[\sin k(r'-r)]\times[-V_2+(\lambda^2-\frac{1}{4})/(r')^2]f(\lambda,k,r')dr'$$
$$+ k^{-1}\int_{R_2}^{\infty}[\sin k(r'-r)]\times[(\lambda^2-\frac{1}{4})/(r')^2]f(\lambda,k,r')dr'. \qquad (146)$$

3.8 SUMMARY

In this chapter, we have seen that the Jost-function formulation of quantum scattering theory can be applied to classical problems concerned with the scattering of a plane scalar wave by a medium with a spherically symmetric inhomogeneity of finite extent. We have applied this technique to solve the radial differential equation for the scattering from a constant spherical inhomogeneity and a piecewise-constant multilayer spherical inhomogeneity. When the Jost function cannot be solved exactly, we can use the Jost integral formula to convert it into an integral equation corresponding to these boundary conditions. As shown in Sections 3.3 and 3.4, we can use an iteration procedure to solve the $l = 0$ Jost integral equation for a discontinuous area inhomogeneity as shown in 2-layer and 3-layer models. Although the iterative technique is not the most effective method in all cases, it may be useful when we have a more complicated function. Based on the results that we have for a constant spherical inhomogeneity, the iteration technique is good for the problem with long wavelengths ($kR_1 \ll 1$) for any k_1/k. For shorter wavelengths, small k_1/k (e.g., $k_1/k = 1.1$) gives a good approximation to σ_0 for the entire range of kR_1 considered ($0 \leq R_1 \leq 2\pi$); however, large k_1/k (e.g., $k_1/k = 1.5, 2.0$) gives a good approximation to σ_0 in the range of $0 < kR_1 \lesssim 3\pi/4$. In case of a piecewise constant spherical inhomogeneity, the iteration procedure gives a better approximation for the problem with long wavelengths ($kR_1 \ll 1$) only for small ratios of k_1/k and k_2/k (e.g., $k_1/k = 0.7, k_2/k = 0.9; k_1/k = 1.1, k_2/k = 1.3$). For a larger k_1/k and k_2/k (e.g., $k_1/k = 1.5, k_2/k = 1.2$), it gives a good approximation when $kR_1 \lesssim 2\pi/3$. The approximation for the Jost function becomes less accurate for larger ratios of wavenumber k_1/k and k_2/k (e.g., $k_1/k = 2.0, k_2/k = 1.5$). When the ratios of wavenumbers k_1/k are greater than k_2/k, we have a better approximation. However, the approximation for the Jost function is still better than the total cross section for the large wavelengths. For shorter wavelengths, all ratios of the wavenumbers give a better approximation

to σ_0 for approximately $kR_1 \gtrsim 2\pi/3$.

We note that our plots of the $l = 0$ cross section differ from those for the square-well potential presented in standard quantum mechanics texts (e.g., see Merzbacher [37]). The reason for this difference is the fact that in quantum scattering theory, we are concerned with the behavior of the cross section as a function of kR_1 for a fixed value of $V_1R_1^2$ (i.e., we have fixed the parameters of the potential), whereas in classical scattering theory we are concerned with the behavior of the cross section as a function of kR_1 for a fixed value of the relative index of refraction k_1/k. Also, in classical scattering theory, the phase shift and cross section are zero as $kR_1 \to 0$, while in quantum scattering theory, the phase shift and therefore the cross section for $kR_1 \to 0$ are dependent on the value of $V_1R_1^2$ and can, in fact, be nonzero, depending on the presence of bound states and the phase shift normalization at infinite energy [12].

CHAPTER 4

THE S-MATRIX FOR THE CASE OF A COATED SPHERE.

4.1 INTRODUCTION

In recent years, there has been interest in the light scattering properties of mammalian cells. Typically, for such calculations, a mammalian cell was imagined as a homogeneous sphere immersed in a waterlike medium such that the (relative) refractive index of the cell was slightly greater than unity. A more realistic model for some mammalian cells would be a sphere (nucleus) with a given refractive index, surrounded by a coating (cytoplasm) with a slightly lower refractive index. The mammalian cells of interest are typically 10-15 μ in diameter with nuclei whose diameters are about two thirds of the total cell diameter. Another example of the use of coated spheres was mentioned in the introduction in connection with optical tweezer technology. Optical tweezers are scientific instruments that use a highly focused laser beam to provide an attractive or repulsive force (typically on the order of pico-newtons depending on the refractive index) mismatch to physically hold and move microscopic dielectric objects. In the late 1980's, optical tweezers were used to trap an individual tobacco mosaic virus and Escherichia coli bacterium. They have also been used to trap neutral atoms, and for cell sorting in biology, i.e., by creating a large optical intensity pattern over the sample area, cells can be sorted by their intrinsic optical characteristics. Optical tweezers have also been used to probe the cytoskeleton, measure the viscoelastic properties of biopolymers, and study cell motility. Most recently, a biomolecular assay was developed in which clusters of ligand coated nano-particles were both optically trapped and optically detected. Coated spheres can also be used as enhanced probes for optical trapping (Bormuth et al. [25], Hu et al. [26]).

We start by examining the paper by Nussenzveig [15] and extending it to include a delta-function potential on the surface of the potential well discussed in [15]. We review some of the properties of the S-matrix and its poles (especially (152) before

proceeding further. The S-matrix for the general case of $l \neq 0$ is derived, and then specialized to $l = 0$ (the case discussed in [15]), of course with the addition of the delta function potential on the surface of the well.

4.2 THE SCATTERING MATRIX

Consider first as a review and for simplicity, a scalar plane wave incident upon an *impenetrable* sphere of radius a. The solution of the Helmholtz equation (outside the sphere is)

$$\psi_k(r,\theta) = \frac{1}{2}\sum_{l=0}^{\infty}(2l+1)i^l[h_l^{(2)}(kr) + S_l(\beta)h_l^{(1)}(kr)]P_l(cos\theta), \tag{147}$$

where $h_l^{(1)}(kr)$ and $h_l^{(2)}(kr)$ are spherical Hankel functions of the first and second kind respectively, and

$$S_l(\beta) = -\frac{h_l^{(2)}(\beta)}{h_l^{(1)}(\beta)}; \beta \equiv ka = \frac{2\pi a}{\lambda}. \tag{148}$$

The quantity $S_l(\beta)$ is the element (for a given l-value) of the scattering or S-matrix. For 'elastic' (or non-absorptive) scattering, $S_l(\beta)$ is a phase factor, and a very important one - it completely determines the nature of scattering in a potential field. As $|r| = r \rightarrow \infty$,

$$h_l^{(1)}(kr) \sim (-i)^{l+1}\frac{e^{ikr}}{kr}; h_l^{(2)}(kr) \sim i^{l+1}\frac{e^{-ikr}}{kr}, \tag{149}$$

hence inside the summation we have the term

$$\frac{(-1)^{l+1}}{kr}S_l(\beta)[e^{ikr} + \frac{(-1)^{l+1}e^{-ikr}}{S_l(\beta)}]. \tag{150}$$

Again, the reader should note that several possible contexts can be considered here. The modified partial wave number $\lambda = l + 1/2$ is in general considered to be complex, with k being a real quantity, but here we consider k to be a complex quantity also. Thus, so called 'bound states' (of interest in quantum mechanics) are characterized by a pure imaginary wavenumber $k = ik_i$, $k_i > 0$ corresponding to energy $E = k^2 < 0$. In order for such a solution to be square-integrable in (a, ∞), it is necessary that the second term vanish in (150) above. Formally, this will be the case if $\beta = ka$ is a pole of $S_l(\beta)$. This is the essential significance of the poles of the S-matrix in what follows.

For a spherical square well or barrier, corresponding to a transparent sphere with constant refractive index n, the form of the scattering matrix elements for scalar waves is more complicated than (152). In fact, in terms of spherical Bessel functions (j_l) and spherical Hankel functions ($h_l^{(1)}, h_l^{(2)}$), the S-matrix is

$$S_l(\beta) = -\frac{\beta j_l(\alpha) h_l'^{(2)}(\beta) - \alpha j_l'(\alpha) h_l^{(2)}(\beta)}{\beta j_l(\alpha) h_l'^{(1)}(\beta) - \alpha j_l'(\alpha) h_l^{(1)}(\beta)}. \tag{151}$$

Equation (151) is an expression of the matching at the finite boundary of the potential of the regular internal solution with the appropriate external solution of the Schrödinger equation. Using the notation of Nussenzveig [15], the expression (151) is equivalent to

$$S_l(\beta) = -\frac{h_l^{(2)}(\beta)}{h_l^{(1)}(\beta)} \left[\frac{\ln' h_l^{(2)}(\beta) - n \ln' j_l(\alpha)}{\ln' h_l^{(1)}(\beta) - n \ln' j_l(\alpha)} \right], \tag{152}$$

where $\ln'$ represents the logarithmic derivative operator, j_l is a spherical Bessel function. The 'size parameter' $\beta = ka$ plays the role of a dimensionless external wavenumber, and $\alpha = n\beta$ is the corresponding *internal* wavenumber. Not surprisingly, $S_l(\beta)$ may be equivalently expressed in terms of cylindrical Bessel and Hankel functions of half-integer order.

As noted by [15] that for $l = 0$ the S-matrix element takes the simpler form

$$S_0(\beta) = e^{-2i\beta} \frac{\alpha \cot \alpha + i\beta}{\alpha \cot \alpha - i\beta}, \tag{153}$$

and is extended later in this chapter. To obtain the analytic continuation of $S_l(\beta)$, it is sufficient to consider (151) as a function of the complex variable β. It follows from the properties of the spherical Bessel functions that (151) is a meromorphic function of β, which satisfies the well-known relations

$$S_l(\beta) S_l(-\beta) = S_l(\beta) S_l^*(\beta^*) = 1. \tag{154}$$

According to (154), if β is a pole of $S_l(\beta)$, so is $-\beta^*$, while $-\beta$ and β^* are zeros. Therefore, it suffices to determine the poles on the imaginary axis and in the right half plane. The l^{th} "partial wave" in the series solution (C2, see Appendix C) and (147) is associated with an *impact parameter* $b(l) = (l + 1/2)/k$, i.e., only 'rays' "hitting" the sphere ($b \leq a$) are significantly scattered, and the number of terms that must be retained in the series to get an accurate result is slightly larger than β. Unfortunately, for visible light scattered by water droplets in the atmosphere, β

is approximately several thousand and the partial wave series converges very slowly. This is certainly a non-trivial problem! In the next section, we examine the resolution of this difficultly for both the scalar and the vector wave problem.

Ref. [15] is concerned with S-matrix poles associated with the case of non-relativistic scattering by a central potential of finite radius for angular momentum $l = 0$. In this case, as is well known, the S-matrix is a diagonal matrix, with elements

$$S_l(k) = e^{2i\delta_l(k)}, \tag{155}$$

where $\delta_l(k)$ are the phase-shifts corresponding to the angular momentum l and wave number k in the cases of interest.

Summarizing from [15], the properties of the poles of the S-matrix are described in the following:

(i) The poles are located either on the positive imaginary axis or in the lower half-plane.

(ii) A pole on the positive imaginary axis, $k = i\kappa_n$ ($\kappa_n > 0$), corresponds to a bound state with energy $E = k^2$.

(iii) Complex poles are usually interpreted either by means of so-called "quasi-stationary" or "virtual" states (or in terms of resonance scattering). The first interpretation involves the analytic continuation of Schrödinger's wave function to "complex energies". A pole at the point $k = k' - i\kappa$ ($\kappa > 0$) is associated with the 'complex energy':

$$E = E_r - \frac{i}{2}\Gamma. \tag{156}$$

If $k' > 0$, the corresponding "wave function" is said to represent a "decaying state," with decay constant Γ and "energy" E (defined with an uncertainty given by Γ). In quantum mechanics, poles with $k' < 0$ are associated with "capture" processes. In both cases, it is assumed that $E > 0$ (see Section 5.2 in [15]). The complex poles in (157) for the resonance scattering associated with a "Breit-Wigner peak" in the scattering cross-section are interpreted in the next section (and see also Appendix C).

The poles and zeros of the S-matrix are symmetrically situated with respect to the imaginary k-axis, because by virtue of (154), if the S-matrix has a pole at the point k, then it also has a pole at the point $-\bar{k}$ and it has zeros at the points $-k$ and $\bar{k}$. For potentials satisfying the conditions stated at the beginning of this section, only a finite number of bound states can be supported and these give rise to the poles

lying on the positive imaginary axis. However, an infinite number of poles can occur in the lower half k-plane. If they do not lie on the negative imaginary k-axis, they occur in pairs symmetric with respect to this axis, as discussed above. If they lie on the negative imaginary k-axis, they are often referred to as *virtual state* poles; the wave functions corresponding to these states cannot be normalized. Poles lying in the lower half k-plane and close to the real positive k-axis give rise to resonance effects in the cross section equation. Poles lying in the lower half k-plane and far away from the real positive k-axis contribute to the smooth "background" or "non-resonant" scattering. The distribution of poles in the complex k-plane has been discussed in detail for scattering by a square well potential in a few cases [33].

4.3 THE BREIT-WIGNER FORM

Consider an isolated pole in the S-matrix which lies in the lower half k-plane close to the positive real k-axis. This pole gives rise to resonance scattering at the nearby real energy. Suppose that the pole occurs at the complex energy (recall (157))

$$E = E_r - \frac{i}{2}\Gamma$$

where E_r is the resonance position, and Γ is the resonance width, and both are real and positive numbers. For the unitarity relation, we see that corresponding to this pole there is a *zero* in the S-matrix (at a complex energy given by $E = E_r + i\Gamma/2$) in the upper half k-plane. For energies E on the real axis in the neighborhood of this pole the S-matrix can be written in a form which is both unitary and explicitly contains the pole and zero:

$$S_l(\beta) = e^{2i\delta_l^0(k)} \frac{E - E_r - i\Gamma/2}{E - E_r + i\Gamma/2}. \tag{157}$$

The quantity $\delta_l^0(k)$ in this equation is called the "background" or "non-resonant" phase shift. Provided that the energy E_r is not close to threshold, $E = 0$, nor to another resonance then the background phase shift is slowly varying with energy. Comparing (155) and (157) we obtain the following expression for the phase shift:

$$\delta_l(k) = \delta_l^0(k) + \delta_l^r(k). \tag{158}$$

The quantity

$$\delta_l^r(k) = \arctan\left(\frac{\Gamma/2}{E_r - E}\right), \tag{159}$$

is called the "resonant" phase shift which is seen to increase through π radians as the energy E increases from well below to well above the resonance position E_r.

It can be shown that if $\delta_0^0(k)$ is zero, the partial-wave cross section σ_l is given by the Lorentzian shape

$$\sigma_l = \frac{4\pi}{k^2}(2l+1)\left[\frac{\Gamma^2/4}{(E-E_r)^2+\Gamma^2/4}\right]. \tag{160}$$

This is known as the Breit-Wigner resonance form [40].

4.4 THE S-MATRIX THEORY OF A SQUARE WELL PLUS DELTA FUNCTION POTENTIAL

The governing radial Schrödinger equation is

$$\frac{d^2R_l(r)}{dr^2} + [k^2 - \frac{l(l+1)}{r^2} - V(r)]R_l(r) = 0. \tag{161}$$

We suppose that

$$V(r) = -\frac{V_0}{a^2}\theta(a-r) - \frac{\mu}{a}\delta(r-a), \tag{162}$$

where the step function

$$\theta(\xi) = \begin{cases} 1, & \xi > 0 \\ 0, & \xi < 0 \end{cases} \tag{163}$$

and V_0, μ are dimensionless. Since $\theta(\xi)$ is dimensionless, and $\delta(\xi)$, from its limiting definition (i.e. as a delta distribution), has dimension of $(\text{length})^{-1}$, (161) has dimension of $R_l(r)/(length)^2$. We proceed to work in terms of the dimensionless spatial independent variables $x = kr$, and $x_0 = ka$. Equation (161) becomes

$$\frac{d^2R_l(r)}{dr^2} + [1 - \frac{l(l+1)}{r^2} - \frac{V_0}{x_0^2}\theta(\frac{x_0-x}{k}) - \frac{\mu}{x_0}\delta(x-x_0)]R_l(r) = 0, \tag{164}$$

where $\delta(k(r-a)) = |k|^{-1}\delta(r-a)$, so $\delta(r-a) = k\delta(x-x_0)$, and we assume without loss of generality that $k > 0$.

The solutions to the equation

$$\frac{d^2u_l(r)}{dx^2} + [1 - \frac{l(l+1)}{r^2}]u_l(r) = 0, \tag{165}$$

are Riccati-Bessel functions, $C_l(x) = xj_l(x)$ and $D_l(x) = -xy_l(x)$ in terms of spherical Bessel function of the first and second kind. To match the solutions at $x = x_0$, we require that

$$(i) \quad \lim_{\epsilon \to o^+}\{R_l(x_0+\epsilon) - R_l(x_0-\epsilon)\} = 0, \tag{166}$$

together with

$$(ii) \quad \lim_{\epsilon \to o^+} \int_{x_0-\epsilon}^{x_0+\epsilon} \left\{ \frac{d^2 R_l(x)}{dx^2} + [1 - \frac{l(l+1)}{x^2} + \frac{V_0}{x_0^2}\theta(\frac{x_0 - x}{k}) + \frac{\mu}{x_0}\delta(x - x_0)] R_l(x) \right\} = 0. \tag{167}$$

This implies that

$$\left[\frac{d}{dx} R_l(x)\right]\Big|_{x_0-\epsilon}^{x_0+\epsilon} + \left[\frac{V_0}{x_0^2}(0) + \frac{\mu}{x_0}\right] R_l(x_0) = 0. \tag{168}$$

The result for $\delta(x - x_0)$ follows because

$$\int_{x_0-\epsilon}^{x_0+\epsilon} \delta(x - x_0) R_l(x) dx = R_l(x_0). \tag{169}$$

For $\theta(\frac{x_0-x}{k})$,

$$\int_{x_0-\epsilon}^{x_0+\epsilon} \theta(\frac{x_0 - x}{k}) R_l(x) dx = \int_{x_0-\epsilon}^{x_0} R_l(x) dx + \int_{x_0}^{x_0+\epsilon} 0 dx = 0, \tag{170}$$

since $R_l(x)$ is continuous in any $(x_0 - \epsilon, x) \subset (0, \infty)$. Therefore,

$$\frac{dR_l(x_0^+)}{dx} - \frac{dR_l(x_0^-)}{dx} = -\frac{\mu}{x_0} R_l(x_0). \tag{171}$$

For $0 < x < x_0$, (164) is

$$\frac{d^2 R_l(r)}{dx^2} + [1 - \frac{l(l+1)}{x^2} + \frac{V_0}{x_0^2}] R_l(r) = 0. \tag{172}$$

For $x > x_0$, we have

$$\frac{d^2 R_l(r)}{dx^2} + [1 - \frac{l(l+1)}{x^2}] R_l(r) = 0. \tag{173}$$

We can rescale the first of these by requiring that $x = \alpha y$, such that the differential operator becomes

$$\frac{d^2}{dy^2} + 1 - \frac{l(l+1)}{y^2},$$

i.e., from

$$\frac{d}{dx} = \frac{1}{\alpha}\frac{d}{dy},$$

yields the condition

$$\alpha = \frac{x_0}{(x_0^2 + V_0)^{1/2}},$$

where $\alpha > 0$. Therefore, for $0 < x < x_0$,

$$\left[\frac{d^2}{dy^2} + 1 - \frac{l(l+1)}{y^2}\right] R_l(y) = 0, \tag{174}$$

which possesses linear independent solutions $C_l(y)$ and $D_l(y)$, where $y = \alpha^{-1}x$ and $y > x$ for $V_0 > 0$.

For $x < x_0$,

$$R_l(y) = AC_l(y). \tag{175}$$

For $x > x_0$,

$$R_l(x) = B[C_l(x) + \tan\delta_l(k)D_l(x)], \tag{176}$$

where in (176) the standard formulation in terms of the phase shift $\delta_l(k)$ has been used. We now rewrite (175) as

$$R_l(x) = AC_l(\alpha^{-1}x). \tag{177}$$

By applying the continuity conditions (166) and (167) to (175) and (176) at $x = x_0$ gives

$$AC_l(mx_0) = B[C_l(x_0) + \tan\delta_l(k)D_l(x_0)], \tag{178}$$

and

$$B[C_l'(x_0) + \tan\delta_l(k)D_l'(x_0)] - AmC_l'(mx_0) = A\frac{\mu}{x_0}C_l(mx_0), \tag{179}$$

where $m = \alpha^{-1} = \frac{(x_0^2+V_0)^{1/2}}{x_0}$ and $\alpha^{-1} > 1$ if $V_0 > 0$. Equating B/A from (178) and (179) provides that

$$\tan\delta_l(k) = \frac{C_l(mx_0)C_l'(x_0) - mC_l'(mx_0)C_l(x_0) + \frac{\mu}{x_0}C_l(mx_0)C_l(x_0)}{mC_l'(mx_0)D_l(x_0) - C_l(mx_0)D_l'(x_0) - \frac{\mu}{x_0}C_l(mx_0)D_l(x_0)}. \tag{180}$$

4.4.1 $l = 0$ WITH DELTA FUNCTION $\mu \neq 0$ AND SQUARE WELL

Using (180) with $l = 0$ and the following identities:

$$j_0(x) = \frac{\sin(x)}{x}, \tag{181a}$$

$$y_0(x) = -\frac{\cos(x)}{x}. \tag{181b}$$

Then

$$\begin{aligned} C_0(mx_0) &= mx_0j_0(mx_0) = \sin(mx_0), \\ D_0(x_0) &= -x_0y_0(x_0) = \cos(x_0), \\ C_0'(mx_0) &= j_0(mx_0) + mx_0j_0'(mx_0) = \cos(mx_0), \\ D_0'(x_0) &= -[y_0(x_0) + x_0y_0'(x_0)] = -sin(x_0). \end{aligned}$$

Therefore, (180) becomes

$$\tan\delta_0(k) = \frac{\sin(mx_0)\cos(x_0) - m\cos(mx_0)\sin(x_0) + \frac{\mu}{x_0}\sin(mx_0)\sin(x_0)}{m\cos(mx_0)\cos(x_0) + \sin(mx_0)\sin(x_0) - \frac{\mu}{x_0}\sin(mx_0)\cos(x_0)}. \quad (182)$$

Now the S-matrix

$$S_0(k) = e^{2i\delta_0} = \frac{1 + i\tan\delta_0}{1 - i\tan\delta_0}. \quad (183)$$

Therefore,

$$S_0(k) = \frac{e^{-ix_0}[m\cos(mx_0) + i\sin(mx_0) - \frac{\mu}{x_0}\sin(mx_0)]}{e^{ix_0}[m\cos(mx_0) - i\sin(mx_0) - \frac{\mu}{x_0}\sin(mx_0)]}. \quad (184)$$

Letting $\alpha = mx_0$, $\beta = x_0$, $m = \frac{\alpha}{\beta}$ with $\beta = ka$, we can write (184) into the form (in Nussenzveig's notation)

$$S_0(\beta) = e^{-2i\beta}\left(\frac{\alpha\cot\alpha + i\beta - \mu}{\alpha\cot\alpha - i\beta - \mu}\right), \quad (185)$$

$$= e^{-2i\beta}\left(\frac{\alpha\cot\alpha + i(\beta + i\mu)}{\alpha\cot\alpha - i(\beta - i\mu)}\right), \quad (186)$$

$$= e^{-2i\beta}\left(\frac{\alpha\cot\alpha + i\tilde{\beta}^*}{\alpha\cot\alpha - i\tilde{\beta}}\right). \quad (187)$$

where $\tilde{\beta} = \beta - i\mu$. Poles of the S-matrix are given by

$$\alpha\cot\alpha = i\tilde{\beta} = i\beta + \mu \quad (188)$$

where $\alpha = \sqrt{k^2 + V_0}a$, $\beta = ka$, and in Nussenzveig's notation, $A^2 = V_0\beta^2/k^2 = V_0a^2$ (the "volume" of the well, or proportional to it), so $A = \sqrt{V_0}a$. Therefore,

$$\alpha^2 = \beta^2 + A^2, \quad (189)$$

$$\alpha^2\cot^2\alpha = (i\beta + \mu)^2, \quad (190)$$

from which we have

$$\alpha^2\cot^2\alpha = -\beta^2 + 2i\beta\mu + \mu^2 = A^2 - \alpha^2 \pm 2i\sqrt{\alpha^2 - A^2}\mu + \mu^2,$$

where $\beta = \pm\sqrt{\alpha^2 - A^2}$. Then,

$$\cot^2\alpha = \frac{A^2}{\alpha^2} - 1 + \frac{[\mu^2 \pm 2i\mu\sqrt{\alpha^2 - A^2}]}{\alpha^2},$$

$$\csc^2\alpha = \frac{A^2 + [\mu^2 \pm 2i\mu\sqrt{\alpha^2 - A^2}]}{\alpha^2},$$

$$\frac{\alpha^2}{\sin^2\alpha} = A^2 + [\mu^2 \pm 2i\mu\sqrt{\alpha^2 - A^2}],$$

$$\alpha^{-1}\sin\alpha = \pm[A^2 + \mu^2 \pm 2i\mu\sqrt{\alpha^2 - A^2}]^{-1/2}, \tag{191}$$

where the $\pm$ signs must be chosen such that $\alpha\cot\alpha = i\beta - \mu$ is satisfied.

The problem is now reduced to the determination of the roots of (191) as a function of the parameter A, and hence to determine the poles of $S_0(\beta)$ in the β-plane. Some of these poles, together with the corresponding values of A are shown in the next section.

4.5 SUMMARY

Figures 60 through 64 show the poles of the S-matrix corresponding to several values of μ. This is ongoing work, and clearly it will be necessary to interpret the effects of the coating potential (or delta function potential) on the poles of S, and their implications for electromagnetic resonances. This, it is hoped, will be the subject of future work.

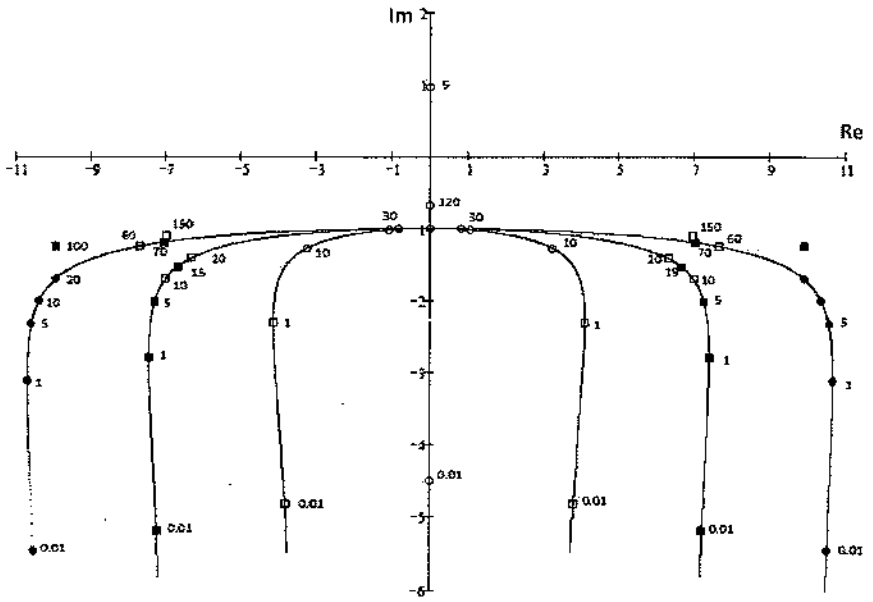

FIG. 60: The S-matrix poles in the complex $\beta = ka$ plane for $\mu = 0$. The numbers beside the poles give the corresponding values of A. The curves in full line are the paths described by the poles.

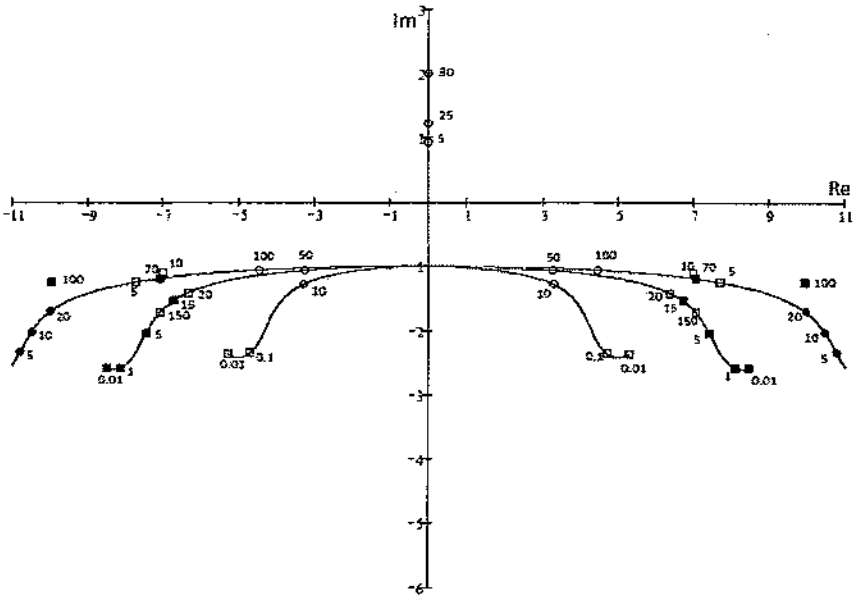

FIG. 61: The S-matrix pole in the complex $\beta = ka$ plane for $\mu = 0.1$. The numbers beside the poles give the corresponding values of A. The curves in full line are the paths described by the poles.

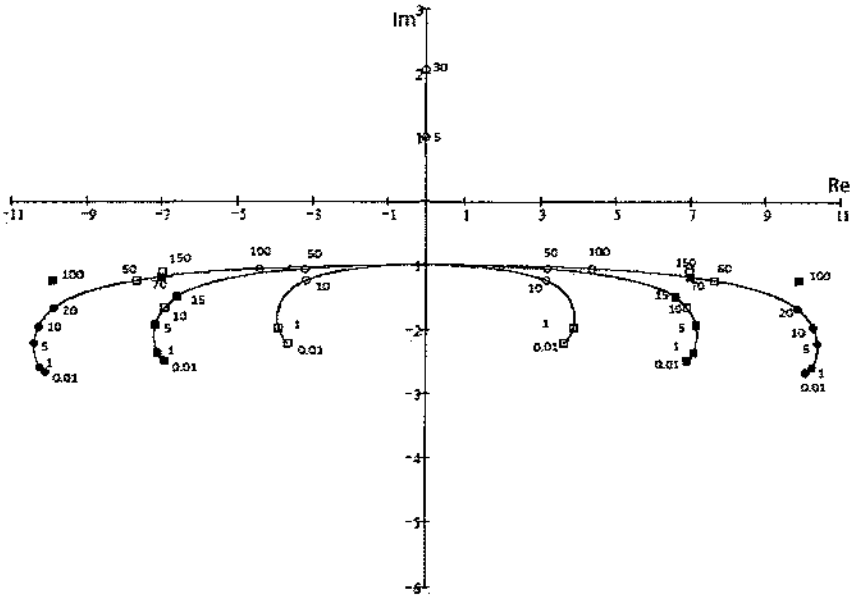

FIG. 62: The S-matrix pole in the complex $\beta = ka$ plane for $\mu = -0.1$. The numbers beside the poles give the corresponding values of A. The curves in full line are the paths described by the poles.

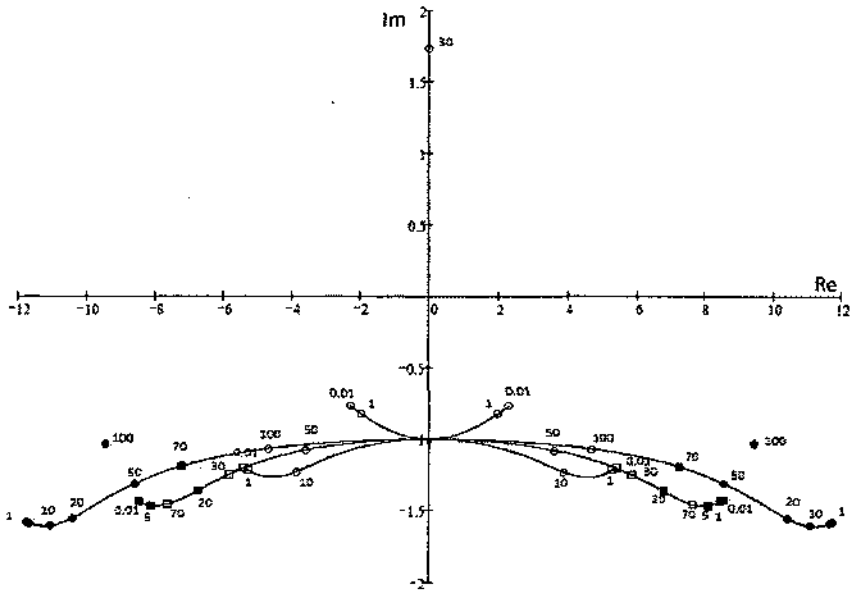

FIG. 63: The S-matrix pole in the complex $\beta = ka$ plane for $\mu = 1$. The numbers beside the poles give the corresponding values of A. The curves in full line are the paths described by the poles.

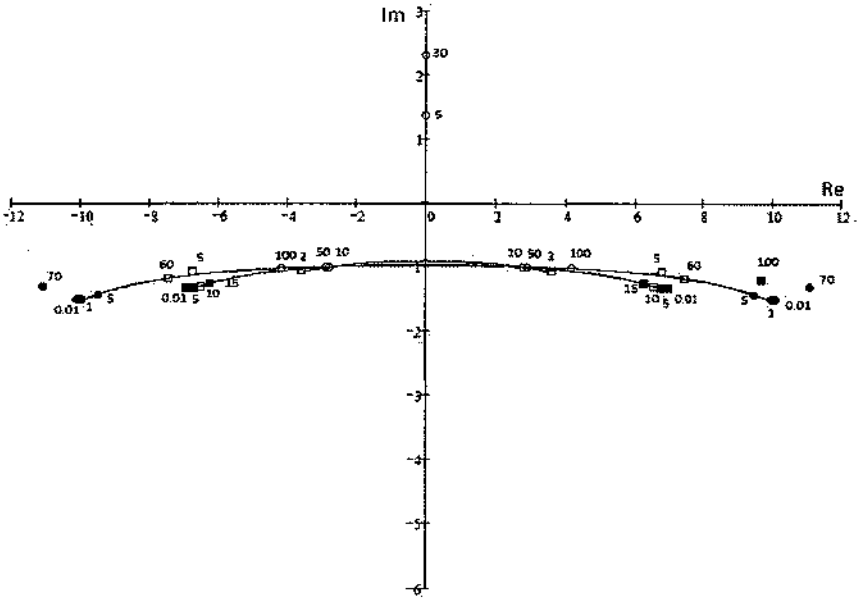

FIG. 64: The S-matrix pole in the complex $\beta = ka$ plane for $\mu = -1$. The numbers beside the poles give the corresponding values of A. The curves in full line are the paths described by the poles.

CHAPTER 5

CONCLUSIONS

In this dissertation we have analyzed, for piecewise-uniform media, electromagnetic scattering resonances (MDRs), phase shifts, cross sections and the S-matrix and its poles using the analogy between the radial Schrödinger equation and the differential equations for the radial Debye potentials. These resonances are shown to be analogous to quantum-mechanical shape resonances and correspond to the poles of the S-matrix. These resonances exist as quasi-bound states, temporarily trapped in a potential well of the type illustrated in Figure 4 for a constant refractive index associated with a spherical dielectric particle, and in Figures 13 and 14 for a piecewise constant refractive index associated with a multi-layer spherical dielectric particle.

These resonances are very significant for understanding the basic nature of light scattering from any object, although for obvious reasons the spherical symmetry imposed here renders the analysis mathematically tractable. It is a simple matter to determine the effective upper and lower bounds for the resonance levels from the top and the bottom of the potential well. The lower energy levels must tunnel through a wider barrier, so the lower levels have a longer lifetime. We have also noted that for the occurrence of a shape resonance (or bound state) in a potential well, the wave function must decrease exponentially in the classically forbidden regions outside the well. The application of this condition leads directly from (21a) for TE mode and (21b) for TM mode in the 2-layer model, and from (33a) and (33b) for TE mode ((34a) and (34b) for TM mode) in the 3-layer model. It is expected that this interpretation of resonances as the quasi-bound states of a potential well can be applied to more complicated systems than a uniform dielectric sphere or even a multilayered spherically symmetric sphere.

Moreover, the resonances for the zero angular momentum ($l = 0$) case in the square well can be 'morphed' into approximations for the $l \neq 0$ case (in principle) by adjusting the parameters of a simple well-barrier model accordingly. For any particular choice of these parameters, the properties of any resonances are readily established.

We have also indicated how the Jost-function formulation of quantum scattering theory can be applied to classical problems involving the scattering of a scalar plane wave by a medium with multilayered spherically symmetric inhomogeneities, as shown in Figure 43. This technique can be used to solve the radial differential equation for multilayered spherical inhomogeneities. Given the complicated form of the matching Jost boundary conditions, the technique of converting it into an integral equation corresponding with these boundary conditions is a very useful one. The results show that the $l = 0$ Jost integral equation for the cutoff inhomogeneities can be approximated analytically and numerically by using an iteration procedure in both 2-layer and 3-layer models. Typically (and perhaps not surprisingly) the iteration technique appears to work best for weak inhomogeneities, i.e., for the quantity $k_i/k - 1$ to be sufficiently small, where $i = 1, 2$ in the three-layer case. Also, consistent with the $l = 0$ case examined, it is known that from standard quantum mechanical arguments that the largest l-value that contributes significantly to the partial wave expansion for the scattering amplitude is on the order of k (the size of the inhomogeneity), or here, kR_i, $i = 1, 2$. Thus the accuracy of the iterations is seen to be better (in the two-layer case at least) for longer wavelengths ($\max kR_2 << 1$). With the more complex two-layer inhomogeneity more iterations will, it is expected, produce more accurate results, though at considerable loss of analytic tractability. We can apply the Jost integral equations for arbitrary l for scattering from an arbitrary inhomogeneity as future work.

In the last chapter, we have discussed some of the analytical properties of the S-matrix of a square well with an attractive delta function potential located at the edge of the well. For the special case of $l = 0$, the poles of the S-matrix have been located and tracked in the complex β-plane (where $\beta = ka$) as the strength μ of the delta function is varied. This is ongoing work and is therefore currently incomplete. Extension to higher angular momentum values is possible, but rather complicated. Several Appendices provide more background for some of the topics discussed here. In particular, Appendix D provides details for determining the S-matrix (and its poles) for a large class of piecewise differentiable potentials (and hence piecewise differentiable refractive index profiles). This, it is hoped, will be the subject of future work.

BIBLIOGRAPHY

[1] James A. Lock, "Excitation efficiency of a morphology-dependent resonance by a focused gaussian beam," *Journal of the Optical Society of America A*, vol. 15, pp. 2986-2994, 1998.

[2] A. L. Aden and M. Kerker, "Scattering of electromagnetic waves from two concentric spheres," *Journal of Applied Physics*, vol. 22, pp. 1242 -1246, 1951.

[3] M. Kerker, *The scattering of light and other electromagnetic radiation*, Academic Press, New York, 1969.

[4] L. Leonhardt and T. G. Philbin, *Geometry and light: the science of invisibility*, Dover Publications, 2010.

[5] G. Roll and G. Schweiger, "Geometrical optics model of mie resonances," *Journal of the Optical Society of America A*, vol. 17, pp. 1301-1311, 2000.

[6] John A. Adam and Philip Laven, "Rainbows from inhomogeneous transparent spheres: a ray-theoretic approach," *Applied Optics*, vol. 46, pp. 922 - 929, 2007.

[7] B. R. Johnson, "Theory of morphology-dependent resonances: shape resonances and width formulas," *Journal of the Optical Society of America A*, vol. 10, pp. 343 - 352, 1993.

[8] C. F. Bohren and D. R. Huffman, *Absorption and scattering of light by small particles*, Interscience, New York, 1983.

[9] H. C. van de Hulst, *Light scattering by small particles*, Dover, New York, 1981.

[10] Hans C. Ohanian and Carl G. Ginsburg, "Antibound 'states' and resonances," *Journal of Applied Physics*, vol. 42, pp. 310 - 315, 1974.

[11] Philip J. Wyatt, "Scattering of electromagnetic plane waves from inhomogeneous spherically symmetric objects," *Physical Review*, vol. 127, pp. 1837 - 1843, 1962.

[12] George V. Frisk and John A. DeSanto, "Scattering by spherically symmetric inhomogeneities," *Journal of Acoustical Society of America*, vol. 47, pp. 172 - 180, 1970.

[13] B. R. Johnson, "Exact theory of electromagnetic scattering by a heterogeneous multilayer sphere in the infinite-layer limit: effective-media approach," *Journal of the Optical Society of America A*, vol. 16, pp. 845 - 852, 1999.

[14] W. Edward Gettys, "Quantum theory of a square well plus delta function potential," *Journal of Applied Physics*, vol. 41, pp. 670 - 677, 1973.

[15] H.M. Nussenzveig, "The poles of the S-matrix of a rectangular potential well or barrier," *Nuclear Physics*, vol. 11, pp. 499521, 1959.

[16] W. T. Grandy, Jr, *Scattering of waves from large spheres*, Cambridge University Press, Cambridge, 2000.

[17] James C. Kitchen and J. Ronald V. Zaneveld, "A three-layered sphere model of the optical properties of phytoplankton," *the American Society of Limnology and Oceanography*, vol. 37, no. 8, pp. 1680-1690, 1992.

[18] J. A. Lock, J. M. Jamison, and C. Lin, "Rainbow scattering by a coated sphere," *Applied Optics*, vol. 33, pp. 4677-4690, 1994.

[19] A. Brunsting and P. F. Mullaney, "Light scattering from coated spheres: model for biological cells," *Applied Optics*, vol. 11, pp. 675-680, 1972.

[20] T. Kaiser, S. Lange, and G. Schweiger, "Structural resonances in a coated sphere: investigation of the volume-averaged source function and resonance positions," *Applied Optics*, vol. 33, pp. 7789-7797, 1994.

[21] R. W. Fenn and H. Oser, "Scattering properties of concentric soot-water spheres for visible and infrared light," *Applied Optics*, vol. 4, pp. 1504-1509, 1965.

[22] R. Bhandari, "Tiny core or thin layer as a perturbation in scattering by a single-layered sphere," *Journal of the Optical Society of America A*, vol. 3, pp. 319-328, 1986.

[23] A. B. Pluchino, "Surface waves and the radiative properties of micron-sized particles," *Applied Optics*, vol. 20, pp. 2986-2992, 1981.

[24] R. L. Hightower, C. B. Richardson, H.-B. Lin, J. D. Eversole, and A. J. Campillo, "Measurements of scattering of light from layered microspheres," *Optics Letters*, vol. 13, pp. 946-948, 1988.

[25] Volker Bormuth, Anita Jannasch, Marcel Ander, Carlos M. van Kats, Alfons van Blaaderen, Jonathon Howard, and Erik Scha, "Optical trapping of coated microspheres," *Optics Express*, vol. 16, pp. 4677-4690, 2008.

[26] Ying Hu, Timo A. Nieminen, Norman R. Heckenberg, and Halina Rubinsztein-Dunlop, "Antireflection coating for improved optical trapping," *Journal of Applied Physics*, vol. 103, no. 093119, 2008.

[27] P. Sanz, J. Saudo, and J. Sesma, "Trajectories of the S-matrix poles in the complex wavenumber plane," *Journal of Mathematical Physics*, vol. 22, pp. 2594 - 2597, 1981.

[28] R. W. Hart and E. W. Montroll, "On the scattering of plane waves by soft particles. I. spherical obstacles," *Journal of Applied Physics*, vol. 22, pp. 376 -386, 1951.

[29] L.I. Schiff, *Quantum mechanics*, 3rd edition, New York, McGraw-Hill, 1968.

[30] V. de Alfaro and T. Regge, *Potential scattering*, North-Holland Publishing Company, Amsterdam, 1965.

[31] N.F. Mott and H.S. W. Massey, *The theory of atomic collisons*, 3rd edition, Clarendon Press, Oxford, 1965.

[32] C. Eftimiu, "Direct and inverse scattering by a sphere of variable index of refraction," *Journal of Mathematical Physics*, vol. 23, pp. 2140-2146, 1982.

[33] J. A. Adam: 'Rainbows' in homogeneous and radially inhomogeneous spheres: connections with ray, wave and potential scattering theory. *Advances in interdisciplinary mathematical research: applications to engineering, physical and life sciences*, Springer Proceedings in Mathematics & Statistics, vol. 37, Ed. Bourama Toni, Springer, 2013.

[34] C. Eftimiu, *Inverse electromagnetic scattering for radially inhomogeneous dielectric spheres, in inverse methods in electromagnetic imaging* (1985); Proceedings of the NATO Advanced Research Workshop, Bad Windsheim, West Germany, Part 1, Dordrecht, D. Reidel Publishing Company, September, pp. 18-24, 1983.

[35] J. A. Adam and U. Nuntaplook, "Electromagnetic and potential scattering from a radially inhomogeneous sphere," submitted to *Applied Mathematics Letters*, 2013.

[36] A. O. Barut and F. Calogero, "Singularities in angular momentum of the scattering amplitude for a class of soluble potentials," *Physical Review*, vol. 128, 1962.

[37] U. E. Merzbacher, *Quantum mehcanics*, John Wiley and Sons, Inc., New York, pp. 213 - 247, 1961.

[38] P. A. Martin, "Acoustic scattering by inhomogeneous spheres," *Journal of Acoustical Society of America*, vol. 111, pp. 2013-2018, 2002.

[39] Milton Abramowitz and Irene A. Stegun, *Handbook of mathematical functions: with formulars, graphs, and mathematical tables*, Edited Edition, Dover Publications, New York, 1965.

[40] Burke, P.G., *Potential scattering in atomic physics*, Plenum, New York, 1977.

APPENDIX A

THE JOST FUNCTIONS FOR $\lambda = \frac{1}{2}$.

A.1 THE JOST FUNCTION FOR $\lambda = \frac{1}{2}$ FOR THE 2-LAYER MODEL

We can find $f(\frac{1}{2}, k)$ for scattering from a piecewise constant spherical inhonogeneity by letting $\lambda = \frac{1}{2}$ in (84), which then becomes

$$\frac{d^2u_0(r)}{dr^2} + [k^2 - V(r)]u_0(r) = 0. \tag{A1}$$

The solutions in the three regions are:

$$\begin{aligned} &Region\ 1 : \phi(\frac{1}{2}, k_1, r) = Ae^{ik_1 r} + Be^{-ik_1 r}, \\ &Region\ 2 : f(\frac{1}{2}, k, r) = Ce^{ikr} + De^{-ikr}. \end{aligned} \tag{A2}$$

Imposing the boundary conditions (86), we find that

$$A = -B = \frac{1}{2ik_1}. \tag{A3}$$

Next, we impose the boundary conditions (93), we find that $C = 0$ and $D = 1$. Since the point $r = R_1$ is the common domain of $\phi(\frac{1}{2}, k_1, r)$ and $f(\frac{1}{2}, k, r)$, we evaluate the Jost function at $r = R_1$ from and thus obtain

$$f(\frac{1}{2}, k) = \frac{1}{2}e^{-ikR_1}[(1 - \frac{k}{k_1})e^{-ik_1R_1} + (1 + \frac{k}{k_1})e^{ik_1R_1}], \tag{A4}$$

which agrees with (115).

A.2 THE JOST FUNCTION FOR $\lambda = \frac{1}{2}$ FOR THE 3-LAYER MODEL

We can also find $f(\frac{1}{2}, k)$ for scattering from a piecewise constant spherical inhonogeneity by letting $\lambda = \frac{1}{2}$ in (84), which then becomes

$$\frac{d^2u_0(r)}{dr^2} + [k^2 - V(r)]u_0(r) = 0. \tag{A5}$$

The solutions in the three regions are:

$$\begin{aligned}
&Region\ 1 : \phi_1(\frac{1}{2}, k_1, r) = Ae^{ik_1 r} + Be^{-ik_1 r},\\
&Region\ 2 : \phi_2(\frac{1}{2}, k_2, r) = Ce^{ik_2 r} + De^{-ik_2 r},\\
&Region\ 3 : f(\frac{1}{2}, k, r) = Ee^{ikr} + Fe^{-ikr}.
\end{aligned} \tag{A6}$$

Imposing the boundary conditions (86) for $\phi_1(\frac{1}{2}, k_1, r)$ and $\phi_2(\frac{1}{2}, k_2, r)$, we find that

$$A = -B = \frac{1}{2ik_1}, \tag{A7}$$

and

$$\phi_1(\frac{1}{2}, k_1, r) = \frac{\sin k_1 r}{k_1}. \tag{A8}$$

By continuity at the boundary $r = R_1$, we match $\phi_1(\frac{1}{2}, k_1, r)$ with $\phi_2(\frac{1}{2}, k_2, r)$ and $\phi_1'(\frac{1}{2}, k_1, r)$ with $\phi_2'(\frac{1}{2}, k_2, r)$, and we have that

$$\begin{aligned}
&\frac{\sin k_1 R_1}{k_1} = Ce^{ik_2 R_1} + De^{-ik_2 R_1},\\
&\cos k_1 R_1 = ik_2(Ce^{ik_2 R_1} - De^{-ik_2 R_1}).
\end{aligned}$$

Solving those two equations gives C and D as

$$\begin{aligned}
C &= \frac{1}{2}e^{-ik_2 R_1}[\frac{\sin k_1 R_1}{k_1} + \frac{\cos k_1 R_1}{ik_2}],\\
D &= \frac{1}{2}e^{ik_2 R_1}[\frac{\sin k_1 R_1}{k_1} - \frac{\cos k_1 R_1}{ik_2}].
\end{aligned} \tag{A9}$$

Therefore, in Region 2 we have that

$$\begin{aligned}
\phi_2(\frac{1}{2}, k_2, r) = \frac{1}{2}e^{-ik_2 R_1}[\frac{\sin k_1 R_1}{k_1} + \frac{\cos k_1 R_1}{ik_2}]e^{ik_2 r}\\
+ \frac{1}{2}e^{ik_2 R_1}[\frac{\sin k_1 R_1}{k_1} - \frac{\cos k_1 R_1}{ik_2}]e^{-ik_2 r}.
\end{aligned} \tag{A10}$$

Next, we impose the boundary conditions (93), we find that $E = 0$ and $F = 1$, and we have

$$f(\frac{1}{2}, k, r) = e^{-ikr}. \tag{A11}$$

Since the point $r = R_2$ is the common domain of $\phi_2(\frac{1}{2}, k_2, r)$ and $f(\frac{1}{2}, k, r)$, we evaluate the Jost function at $r = R_2$ from

$$f(\frac{1}{2}, k) = W[f(\frac{1}{2}, k, r), \phi_2(\frac{1}{2}, k_2, r)]_{r=R_2}. \tag{A12}$$

Therefore,

$$f(\frac{1}{2},k) = \frac{i}{2}(k+k_2)e^{i[(k_2-k)R_2-k_2R_1]}[\frac{\sin k_1R_1}{k_1}+\frac{\cos k_1R_1}{ik_2}] + \frac{i}{2}(k-k_2)e^{-i[(k_2+k)R_2-k_2R_1]}[\frac{\sin k_1R_1}{k_1}-\frac{\cos k_1R_1}{ik_2}], \quad \text{(A13)}$$

which we can write in terms of complex exponentials also

$$\begin{aligned} f(\frac{1}{2},k) = \frac{1}{4}e^{-ikR_2}\{([\frac{(k-ik_2)}{k_1}+\frac{(ik+k_2)}{k_2}]e^{k_2(R_2-R_1)} \\ +[\frac{(k+ik_2)}{k_1}+\frac{(k_2-ik)}{k_2}]e^{-k_2(R_2-R_1)})e^{ik_1R_1} \\ +([\frac{(ik+k_2)}{k_2}-\frac{(k-ik_2)}{k_1}]e^{k_2(R_2-R_1)} \\ +[\frac{(k_2-ik)}{k_2}-\frac{(k+ik_2)}{k_1}]e^{-k_2(R_2-R_1)})e^{-ik_1R_1}\}, \end{aligned} \quad \text{(A14)}$$

and which agrees with (138).

APPENDIX B

ELECTROMAGNETIC AND POTENTIAL SCATTERING FROM A RADIALLY INHOMOGENEOUS SPHERE

B.1 INTRODUCTION

In a paper by Adam and Nuntaplook submitted to Applied Mathematics Letters, the refractive index profile $n(r)$ (which may be complex) is a function of the radial coordinate only, and the sphere has radius a. For $r > a$, $n(r) \equiv 1$. A time-harmonic dependence of the field quantities, $\exp(-i\omega t)$ is assumed throughout. The governing equation for the electric field $E(r, \theta, \phi)$ is

$$\nabla \times \nabla \times \mathbf{E} - k^2 n^2(r)\mathbf{E} = \mathbf{0}. \tag{B1}$$

The wavenumber k is $2\pi/\lambda$, λ being the wavelength. As shown in [7], the solution may be found by expanding the electric field in terms of vector spherical harmonics in terms of the so-called transverse electric (TE) and transverse magnetic (TM) modes, respectively:

$$\mathbf{M}_{l,m}(r, \theta, \phi) = \frac{e^{im\phi}}{kr} S_l(r)\mathbf{X}_{l,m}(\theta), \tag{B2a}$$

$$\mathbf{N}_{l,m}(r, \theta, \phi) = \frac{e^{im\phi}}{k^2 n^2(r)} \left[\frac{1}{r}\frac{dT_l(r)}{dr}\mathbf{Y}_{l,m}(\theta) + \frac{T_l(r)}{r^2}\mathbf{Z}_{l,m}(\theta)\right]. \tag{B2b}$$

The vector angular functions in (B2a) and (B2b) are defined in a spherical coordinate system as

$$\mathbf{X}_{l,m}(\theta) = \langle 0, i\pi_{l,m}(\theta), -\tau_{l,m}(\theta)\rangle, \tag{B3a}$$

$$\mathbf{Y}_{l,m}(\theta) = \langle 0, \tau_{l,m}(\theta), -i\tau_{l,m}(\theta)\rangle, \tag{B3b}$$

$$\mathbf{Z}_{l,m}(\theta) = \langle l(l+1) P_l^m(\cos\theta), 0, 0\rangle, \tag{B3c}$$

where $P_l^m(\cos\theta)$ is an associated Legendre polynomial of degree l and order m. The corresponding scalar angular functions are defined as

$$\pi_{l,m}(\theta) = \frac{m}{\sin\theta} P_l^m(\cos\theta), \tag{B4a}$$

$$\tau_{l,m}(\theta) = \frac{dP_l^m(\cos\theta)}{d\theta}. \tag{B4b}$$

The functions $S_l(r)$ and $T_l(r)$ are called the radial Debye potentials, and they respectively satisfy the equations

$$\frac{d^2S_l(r)}{dr^2} + \left[k^2n^2(r) - \frac{l(l+1)}{r^2}\right] S_l(r) = 0, \tag{B5a}$$

$$\frac{d^2T_l(r)}{dr^2} - \left(\frac{2}{n(r)}\frac{dn(r)}{dr}\right)\frac{dT_l(r)}{dr} + \left[k^2n^2(r) - \frac{l(l+1)}{r^2}\right] T_l(r) = 0. \tag{B5b}$$

In addition to the appropriate matching conditions at $r = a$, these potentials must also satisfy the boundary conditions $S_l(0) = 0$ and $T_l(0) = 0$. Equation (B5b) may be rewritten in terms of the dependent variable $U_l(r)$, where $T_l(r) = n(r)\,U_l(r)$ to become

$$\frac{d^2U_l(r)}{dr^2} + \left[k^2n^2(r) - n(r)\frac{d^2}{dr^2}\left(\frac{1}{n(r)}\right) - \frac{l(l+1)}{r^2}\right] U_l(r) = 0. \tag{B6}$$

provided that $n(0) \neq 0$, $U_l(0) = 0$. Both (B5a) and (B6) may be placed in the form of the canonical time-independent Schrödinger equation, namely

$$\frac{d^2S_l(r)}{dr^2} + \left[k^2 - V_S(r) - \frac{l(l+1)}{r^2}\right] S_l(r) = 0, \tag{B7a}$$

$$\frac{d^2U_l(r)}{dr^2} + \left[k^2 - V_U(r) - \frac{l(l+1)}{r^2}\right] U_l(r) = 0, \tag{B7b}$$

where the k-dependent 'scattering potentials' $V_S(r)$ and $V_U(r)$ are defined in $[0, a]$ as

$$V_S(r) = k^2\left[1 - n^2(r)\right], \tag{B8a}$$

$$V_U(r) = k^2\left[1 - n^2(r) + \frac{n(r)}{k^2}\frac{d^2}{dr^2}\left(\frac{1}{n(r)}\right)\right]. \tag{B8b}$$

for the TE and TM modes, respectively (the potentials are both identically zero for $r > a$). These potentials are identical for the case of a uniform refractive index.

$V_U(r)$ will be regarded as a small perturbation of the potential $V_S(r)$, so we also define

$$\varepsilon(r) \equiv V_U(r) - V_S(r) = n(r) \frac{d^2}{dr^2}\left(\frac{1}{n(r)}\right). \tag{B9}$$

B.2 PHASE SHIFTS

It is a standard result for potentials vanishing sufficiently fast at infinity [29 - 31] that as $r \to \infty$

$$S_l(r) \sim \sin\left(kr - \frac{\pi l}{2} + \delta_l^S(k)\right), \tag{B10a}$$

$$U_l(r) \sim \sin\left(kr - \frac{\pi l}{2} + \delta_l^U(k)\right). \tag{B10b}$$

Here $\delta_l^S(k)$ and $\delta_l^U(k)$ are the phase shifts induced by each potential respectively. Multiplying (B7a) and (B7b) by $U_l(r)$ and $S_l(r)$ respectively, subtracting and integrating we obtain

$$U_l(r) \frac{dS_l(r)}{dr} - S_l(r) \frac{dU_l(r)}{dr} = -\int_0^r \varepsilon(\eta) S_l(\eta) U_l(\eta) d\eta. \tag{B11}$$

Utilizing the asymptotic expressions in (B10), we have, in the limit as $r \to \infty$,

$$k \sin\left[\delta_l^U(k) - \delta_l^S(k)\right] = -\int_0^\infty \varepsilon(r) S_l(r) U_l(r) dr = -\int_0^a \varepsilon(r) S_l(r) U_l(r) dr, \tag{B12}$$

since $n(r)$ is constant for $r > ka$ (or $r > a$). Thus far, this equation is exact. If we now consider $\varepsilon(r)$ to be sufficiently small that $U_l(r) \approx S_l(r)$, then $\left|\delta_l^U(k) - \delta_l^S(k)\right| << 1$ and we have the relation

$$\delta_l^U(k) \approx \delta_l^S(k) \pm \frac{1}{k}\int_0^a \varepsilon(r) [S_l(r)]^2 dr. \tag{B13}$$

Whether $\delta_l^U(k) > \delta_l^S(k)$ or not clearly depends on the concavity of $n(r)$. A further approximation can be made if the scattering potential $V_S(r)$ is constant (specifically, $V_S = k^2(1 - N^2)$ for $n = N$, $r \le a$), for then the solution for (B7a) can be expressed in terms of a Riccati-Bessel function of the first kind, i.e.

$$S_l(r) = \left(\frac{\pi N k r}{2}\right)^{1/2} J_{l+1/2}(Nkr). \tag{B14}$$

Then we have that

$$\delta_l^U(k) \approx \delta_l^S(k) \pm \frac{\pi N}{2} \int_0^a \left\{ n(r) \frac{d^2}{dr^2} \left(\frac{1}{n(r)} \right) \right\} \left[J_{l+1/2}(Nkr) \right]^2 r dr \equiv \delta_l^S(k) \pm \frac{\pi N}{2} \mathcal{I}(a). \tag{B15}$$

In the case of a small perturbation about $V_S = 0$, i.e. for which $n = N = 1$, the term $\delta_l^S(k)$ in (B15) is zero, and the resulting approximation for $\delta_l^U(k)$ is related to the first Born approximation in quantum scattering theory [32]. In particular, if $\varepsilon(r) = Dr^{-s}$, D being some constant, a closed form solution for I an be found as $a \to \infty$ [31], namely

$$\mathcal{I}(\infty) = \int_0^\infty \left[J_{l+1/2}(Nkr) \right]^2 r^{1-s} dr = \frac{1}{2} \left(\frac{Nk}{2} \right)^{s-2} \frac{\Gamma(s-1)\Gamma\left(l - \frac{1}{2}s + \frac{3}{2}\right)}{\left[\Gamma\left(\frac{1}{2}s\right)\right]^2 \Gamma\left(l + \frac{1}{2}s + \frac{1}{2}\right)}, \tag{B16}$$

provided $s > 1$ and $2l > s - 3$. The question may be asked: what $n(r)$ profiles give rise to $\varepsilon(r) = Dr^{-s}$ (where $D > 0$)? Writing $p(r) = [n(r)]^{-1}$ we are led to consider solutions of the equation

$$r^s \frac{d^2 p(r)}{dr^2} - Dp(r) = 0. \tag{B17}$$

The general solution to this equation may be expressed in terms of modified Bessel functions, but we do not pursue this here.

B.3 A LIOUVILLE TRANSFORMATION

As defined in (B8a) and (B8b), the 'potentials' $V_S(r)$ and $V_U(r)$ are also k-dependent, which is not the case in potential scattering theory [30]. This has an important consequence: unlike the quantum mechanical case, here pure 'bound state' solutions, that is, real square-integrable solutions corresponding to $k^2 < 0$ (Imk > 0) do not exist. This can readily be proven [32 - 33] for the TE mode (equation (B7a)) that

$$\int_0^\infty \left[\left| \frac{dS_l(r)}{dr} \right|^2 + \frac{l(l+1)}{r^2} |S_l(r)|^2 \right] dr = k^2 \int_0^\infty n^2(r) |S_l(r)|^2 dr. \tag{B18}$$

This cannot be satisfied for $k^2 < 0$ for a real and positive refractive index $n(r)$. In [34] the corresponding result is established from (7b) for $U_l(r)$. Furthermore, a Liouville transformation may be used to define a new k-independent potential [32]. Using the following simultaneous changes of independent and dependent variables in equation (5a)

$$r \to \rho : \rho(r) = \int_0^r n(s)ds, \tag{B19a}$$

$$u_l \to \psi_l : \psi_l(\rho) = (n(r))^{1/2} u_l(r). \tag{B19b}$$

Clearly, $n(r)$ must be integrable and non-negative (in naturally-occurring circumstances $n \geq 1$ and $n(r) = 1$ for $r > a$); also $\rho(0) = 0$. It is easy to establish the following results:

$$\begin{aligned}
(i)\ \rho(r) &= \rho_0 + r - a,\ r \geq a,\ \text{where } \rho_a = \int_0^a n(s)ds; \\
(ii)\ \rho(r) &\sim r,\ r \to \infty; \\
(iii)\ r(\rho) &= \int_0^\rho \frac{ds}{v(s)},\ \text{where } v(\rho) = n(r(\rho)).
\end{aligned}$$

Furthermore, by applying (B19a) and (B19b) to (B7a) we find that

$$\left[\frac{d^2}{d\rho^2} - \frac{l(l+1)}{R^2(\rho)} + k^2\right] \psi_l(r) = V(\rho)\,\psi_l(\rho), \tag{B20}$$

where

$$R(\rho) = v(\rho)\,r(\rho) \sim n(0)\,\rho,\ \rho \to 0,\ \text{and } V(\rho) = [v(\rho)]^{-1/2} \frac{d^2}{d\rho^2} [v(\rho)]^{1/2}. \tag{B21}$$

Clearly, $v(\rho)$ should be at least twice differentiable. Now the new 'potential' $V(\rho)$ is independent of the wavenumber k. Note also that $V(\rho) = 0$ for $\rho > \rho_a$. It is of interest to determine the 'shape' of the potential $V(\rho)$ by inverting $\rho(r)$ for various choices of physical $n(r)$ profiles for $r \in [0, a]$ (with $n(0) = n_0$, $n(a) = n_a$ and $n(r) = 1$ for $r > a$). In what follows only the non-zero potential shapes with be stated (corresponding to $\rho \in [0, \rho_a]$. Thus [32] for

$$n(r) = n_a \left[1 - c^2 \left(\frac{r-a}{a}\right)^2\right]^{-1};\ V(\rho) = \frac{c^2}{n_a^2} > 0, \tag{B22a}$$

where c is a real constant, i.e. the potential is a spherical barrier. For the profile [6]

$$n(r) = (A + Br)^{-1},\ A = n_0^{-1},\ B = \frac{n_0 - n_a}{a n_0 n_a};\ V(\rho) = \frac{B^2}{4} > 0, \tag{B22b}$$

also a barrier. For the important Maxwell Fish-Eye profile [4],

$$n(r) = n_0 \left(1 + Br^2\right)^{-1},\ B = \frac{n_0 - n_a}{a^2 n_a};\ V(\rho) = -\frac{B}{n_0^2}. \tag{B22c}$$

In this case, the new potential is a spherical well or barrier as $n_0 > n_a$ or $n_0 < n_a$, respectively. In the latter case, the singularity occurring in $n(r)$ is moot since it arises for $r > a$. In all the other cases investigated thus far [35], including $n(r) = n_0 \exp(-\alpha r)$; $n_0 \cos \alpha r$ and $n_0 \cosh \alpha r$, the potentials $V(\rho)$ are rather complicated functions, and there are no significant advantages to using the Liouville transformation in these cases. It is therefore of interest to examine what profiles $n(r)$ give rise to constant potentials $V(\rho)$. In (B21), let $y(\rho) = [v(\rho)]^{1/2}$ and $V(\rho) = V_0$, where V_0 is a constant of either sign. Then it follows that

$$\frac{d^2y}{d\rho^2} - V_0 y = 0, \tag{B23}$$

the general solution being expressible in terms of real or complex exponential functions as $V_0 > 0$ (potential barrier) or $V_0 < 0$ (potential well) respectively. In r-space, $V_0 < 0$ corresponds to a constant refractive index $n = N = (1 + |V_0| k^{-2})^{1/2} > 1$, so we proceed with this physically realistic case. Writing the general solution of (B23) as

$$y(\rho) = C \cos\left(|V_0|^{1/2} \rho + \eta\right), \tag{B24}$$

where C and η are constants, it follows that

$$r(\rho) = \int_0^\rho \frac{ds}{v(s)} = \left(C^2 |V_0|^{1/2}\right)^{-1} \left[\tan\left(|V_0|^{1/2} \rho + \eta\right) - \tan\eta\right]. \tag{B25}$$

This can be inverted to yield

$$\rho(r) = \int_0^r n(s) ds = |V_0|^{-1/2} \left\{\arctan\left[C^2 |V_0|^{1/2} r + \tan\eta\right] - \eta\right\}. \tag{B26}$$

Therefore

$$n(r) = \rho'(r) = \frac{C}{1 + [Br + \tan\eta]^2}, \tag{B27a}$$

where $C = n_0 \sec^2 \eta$ and η can be determined from the requirement that $n(a) = n_a$. This is a generalization of the Maxwell Fish-Eye profile in (B22c). The corresponding result for $V_0 > 0$ is

$$n(r) = \frac{C}{1 - [Br + \tanh\eta]^2}. \tag{B27b}$$

Note that in this case a singularity exists for $r > 0$ at $r = B^{-1}(1 - \tanh\eta)$.

APPENDIX C

THE EXTRACT FROM THE ARTICLE BY ADAM (2013)

C.1 SCATTERING BY A TRANSPARENT SPHERE: SCALAR WAVE DESCRIPTION

The essential mathematical problem for scalar wave can be thought of either in terms of classical mathematical physics, e.g., the scattering of sound waves, or in quantum mechanical terms, e.g., the non-relativistic scattering of particles by a square potential well (or barrier) of radius a and depth (or height) V_0. In either case we can consider a scalar plane wave impinging in the direction $\theta = 0$ on a sphere of radius a. In what follows, a boldface letter refers to a vector quantity, thus here, $\mathbf{r} =< |r|, \theta, \phi >$ (or$< r, \theta, \phi >$) denotes a position vector in space (using a spherical coordinate system). Suppose that we had started with the 'classical wave equation' with dependent variable $\bar{\psi}(r,t) = \psi(r)e^{-i\omega t}$. For the scalar electromagnetic problem, the angular frequency ω, wavenumber k and (constant) refractive index n are related by $\omega = kc/n$, c being the speed of light in vacuo. Then for a penetrable (= "transparent") sphere, the spatial part of the wave function $\psi(r)$ satisfies the scalar Helmholtz equation

$$\nabla^2\psi + k^2n^2\psi = 0, r < a, \tag{C1a}$$

$$\nabla^2\psi + k^2\psi = 0, r > a. \tag{C1b}$$

Again, k is the wavenumber and $n > 1$ is the (for now, constant) refractive index of the sphere. We can expand the wave function $\psi(\mathbf{r})$ as

$$\psi(\mathbf{r}) = \sum_{l=0}^{\infty} B_l(k)u_l(r)r^{-1}Y_l^m(\theta,\phi) \equiv \sum_{l=0}^{\infty} A_l(k)u_l(r)r^{-1}P_l(\cos\theta) \tag{C2}$$

where $r = |\mathbf{r}|$, as noted above and the coefficients $A_l(k)$ will be 'unfolded' below (The coefficients A_l and B_l are related by a multiplicative normalization constant that need not concern us here.) The reason that the spherical harmonics $Y_l^m(\theta,\phi)$ reduce to the Legendre polynomials in the above expression is because the cylindrical symmetry

imposed on the system by the incident radiation renders it axially symmetric (that is, independent of the azimuthal angle ϕ). The equation satisfied by $u_l(r)$ is

$$\frac{d^2u_l(r)}{dr^2} + [k^2 - V(r) - \frac{l(l+1)}{r^2}]u_l(r) = 0, \tag{C3}$$

where the potential $V(r)$ is now k-dependent, i.e.

$$V(r) = \begin{cases} k^2(1-n^2), & r < a, \\ 0, & r > a. \end{cases} \tag{C4}$$

Since $n > 1$ within the sphere, this potential corresponds to that of a spherical potential well of depth $V_0 = k^2(n^2 - 1)$. This leads very naturally to a discussion of the effective potential, wherein the potential $V(r)$ is combined with the 'centrifugal barrier' term $l(l+1)/r^2$.

C.2 MORPHOLOGY-DEPENDENT RESONANCES: THE EFFECTIVE POTENTIAL $U_l(r)$ (CONSTANT n)

A rather detailed study of the radial wave equations was carried out by Johnson, specifically for the Mie 'solution' of electromagnetic theory. A crucial part of his analysis was the use of the effective potential for the TE mode of the Mie solution, but without any loss of generality we may still refer to the scalar problem here. This potential is defined as

$$U_l(r) = \begin{cases} V(r) + l(l+1)/r^2 = k^2(1-n^2) + l(l+1)/r^2, & r \le a, \\ l(l+1)/r^2 \approx \lambda^2/r^2, & r > a. \end{cases} \tag{C5}$$

It should be noted here that λ as defined here is *not* the wavelength of the incident radiation. For large enough values of l, $[l(l+1)]^{1/2} \approx l + 1/2$. It is clear that $U_l(r)$ has a discontinuity at $r = a$ because of the 'addition' of a potential well to the centrifugal barrier. Thus there arises a tall and thin enhancement corresponding to a barrier surrounding a well, and this suggests the possible existence of resonances, particularly between the top of the former and bottom of the latter, where there are three turning points (where the energy k^2 is equal to $U_l(r)$). Such resonances are called "shape resonances" (or sometimes "morphology-dependent resonances"); they are quasi-bound states in the potential well that escape by tunneling through the centrifugal barrier. The widths of these resonances depend on where they are located; the smaller the number of nodes of the radial wave function within the

well, the deeper that state lies in the well. This in turn determines the width (and lifetime) of the state, because the tunneling amplitude is "exponentially sensitive" to the barrier height and width. Since the latter decreases rapidly with the depth of the well, the smaller is the barrier transmissivity and the lowest-node resonances become very narrow for large values of $\beta = ka$. The lifetime of the resonance (determined by the rate of tunneling through the barrier) is inversely proportional to the width of the resonance, so these deep states have the longest lifetimes. (To avoid confusion of the node number n with the refractive index, the latter has temporarily been written as N.)

Note that as k^2 is reduced, the bottom B of the potential rises (and for some value of k the energy will coincide with the bottom of the well); however, at the top of the well, $U_l(a) = \lambda^2/a^2$ is independent of k^2, but if k^2 is increased it will eventually coincide with the top of the well (T). Consider a value of k^2 between the top and the bottom of the well: within this range there will be three radial turning points, the middle one obviously occurring at $r = a$ and the largest at $r = b$ for which $U_l(a) = \lambda^2/a^2$. The smallest of the three ($r_{\min}$) is found by solving the equation

$$k^2 = \frac{\lambda^2}{r_{\min}^2} - (n^2 - 1)k^2, \tag{C6}$$

to obtain, in terms of the impact parameter $b(\lambda) = \lambda/k$

$$r_{\min} = \frac{\lambda}{nk} \equiv \frac{b}{n}. \tag{C7}$$

By applying Snell's law for given b, it is readily shown that the distance of nearest approach of the equivalent ray to the center of the sphere is just $r_{\min}$; indeed, there are in general many nearly-total internal reflections (because of internal incidence beyond the critical angle for total internal reflection) within the sphere between $r = b/n$ and $r = a$. This is analogous to orbiting in a ray picture; on returning to its original location after one circumnavigation just below the sphere surface, a ray must do so with constructive interference. The very low leakage of these states allows the resonance amplitude and energy to build up significantly during a large resonance lifetime which in turn can lead to nonlinear optical effects. In acoustics these are called "whispering gallery modes".

The energy at the bottom of the well (i.e. $\lim_{r\to a^-} U_l(r)$) corresponding to the turning point at $r = a$ is determined by the impact parameter inequalities $a < b < na$,

or in terms of $\lambda = kb$,

$$U_l(a^-) = (\frac{\lambda}{na})^2 < k^2 < (\frac{\lambda}{a})^2 = U_l(a^+). \tag{C8}$$

This is the energy range between the top and bottom of the well (and in which the resonances occur). To cross the "forbidden region" $a < r < b$ requires tunneling through the centrifugal barrier and near the resonance energies the usual oscillatory/exponential matching procedures can lead to very large ratios of internal to external amplitudes; these resonances correspond to "quasi-bound" states of electromagnetic radiation (that would be bound in the limit of zero leakage).

We now make a transition to discuss some of the related mathematical properties associated with resonances. In so doing, the reader should be alerted to a somewhat flexible notation used in connection with the scattering function (or S-matrix element). This is variously denoted by $S_l(\lambda, k)$ or $S_l(\beta)$, where $\beta = ka$, depending on the context. Mathematically, the resonances are complex eigenfrequencies associated with the poles λ_n of the scattering function $S_l(\lambda, k)$ in the first quadrant of the complex λ-plane; these are known as *Regge poles* (for real k). Corresponding to the energy interval $[U_l(a^-), U_l(a^+)]$, the real parts of these poles lie in the interval $(\beta, n\beta)$ (or equivalently, (ka, nka)); this corresponds to the tunneling region. The imaginary parts of the poles are directly related to resonance widths (and therefore lifetimes). As the node number n decreases, $\mathrm{Re}\lambda_n$ increases and $\mathrm{Im}\lambda_n$ decreases very rapidly (reflecting the exponential behavior of the barrier transmissivity). As β increases, the poles λ_n trace out Regge trajectories, and $\mathrm{Im}\lambda_n$ tend exponentially to zero. When $\mathrm{Re}\lambda_n$ passes close to a "physical" value, $\lambda = l + 1/2$, it is associated with a resonance in the l^{th} partial wave; the larger the value of β, the sharper the resonance becomes for a given node number n.

C.3 POLES AND RESONANCES ON THE k-PLANE AND E-PLANE

For algebraic simplicity, we consider the (simple) poles of the S-matrix for the one dimensional scalar problem. In this approach, the analysis is based on a slightly different formulation of the governing time-independent 'Schrödinger' equation, namely

$$\frac{1}{2}\frac{d^2u(x)}{dx^2} + [k^2 - V(x)]u(x) = 0. \tag{C9}$$

For a square well of depth $V_0 > 0$ (i.e. $V_0 = -V_0$, $|x| < a/2$ and is zero elsewhere),

the incident 'wave' is represented by

$$u(x) = Ae^{ikx}, x < -a/2, \tag{C10}$$

and a transmitted wave

$$u(x) = Ae^{ik(x-a)}S(E), x > a/2. \tag{C11}$$

The transmission coefficient $S(E)$ is the one-dimensional scattering matrix in this problem. It can be shown that

$$S(E) = \left\{ \cos \kappa a - \frac{i}{2}(\frac{k}{\kappa} + \frac{\kappa}{k}) \sin \kappa a \right\}^{-1}, \tag{C12}$$

where $k = \sqrt{2E}$ and $\kappa = \sqrt{2(E + V_0)}$. Note the similarity of this expression with the denominator of the S-matrix in (153). The transmissivity of the well is defined as

$$T(E) = |S(E)|^2 = \left\{ 1 + \frac{V_0^2 \sin^2 \kappa a}{4E(E + V_0)} \right\}^{-1}. \tag{C13}$$

This expression has maxima equal to one whenever $\sin \kappa a = 0$, i.e. when $\kappa a = n\pi$, $n = 1, 2, 3, \ldots$. Equivalently, $E = n^2\pi^2/2a^2 - V_0 > 0$. These maxima correspond to resonances (perfect transmission) in this system. The well contains an integral number of half wavelengths when this condition is satisfied.

We examine $S(E)$ as an analytic function of the energy E in what follows. For $E > 0$, $0 < T(E) \leq 1$. Therefore, poles of $T(E)$ (and $S(E)$) can only occur when $-V_0 < E < 0$. In fact $S(E)$ has a pole whenever

$$\cos \kappa a - \frac{i}{2}\left(\frac{k}{\kappa} + \frac{\kappa}{k}\right) \sin \kappa a = 0, \tag{C14}$$

i.e., when

$$\cot \kappa a = \frac{1}{2}\left(\frac{\kappa}{k} - \frac{k}{\kappa}\right). \tag{C15}$$

Furthermore, from the identity $2 \cot 2\theta = (\cot \theta - \tan \theta)$ the solutions of (C15) can be recast in terms of odd and even parity bound state solutions, i.e.

$$\kappa \cot\left(\frac{\kappa a}{2}\right) = ik, \tag{C16a}$$

$$\kappa \tan\left(\frac{\kappa a}{2}\right) = -ik. \tag{C16b}$$

(Again, notice the similarity of (C16a) and (C16b) with (153)). Suppose now that a resonance occurs at $E = E_r \equiv k_r^2/2 > 0$. In the vicinity of such value of the resonance energy, we may expand the expression $(\frac{k}{\kappa} + \frac{\kappa}{k}) \tan \kappa a$ as

$$\left(\frac{k}{\kappa} + \frac{\kappa}{k}\right) \tan \kappa a = \frac{d}{dE}\left[\left(\frac{k}{\kappa} + \frac{\kappa}{k}\right) \tan \kappa a\right]_{E_r} (E - E_r) + O(E - E_r)^2. \tag{C17}$$

To first order in $E - E_r$, on simplifying, we find that

$$\left(\frac{k}{\kappa} + \frac{\kappa}{k}\right) \tan \kappa a = a\left[\frac{d\kappa}{dE}\left(\frac{k}{\kappa} + \frac{\kappa}{k}\right)\right]_{E_r} (E - E_r) \equiv \frac{4}{\Gamma}(E - E_r). \tag{C18}$$

We can rewrite equation (C12) as

$$S(E) = \sec \kappa a \left\{1 - \frac{i}{2}\left(\frac{k}{\kappa} + \frac{\kappa}{k}\right) \tan \kappa a\right\}^{-1} \approx \sec \kappa a \left\{1 - i\frac{2}{\Gamma}(E - E_r)\right\}^{-1} \tag{C19a}$$

$$= \sec \kappa a \left(\frac{i\Gamma/2}{E - E_r + i\Gamma/2}\right) \approx \left(\frac{i\Gamma/2}{E - E_r + i\Gamma/2}\right).$$

To this order of approximation, then, the pole of $S(E)$ lies in the fourth quadrant of the complex E-plane. There is a branch cut along the real axis, $E > 0$ since if $E = |E|e^{i\theta}$, and $E^{1/2} = |E|^{1/2}e^{i\theta/2}$, in the limit $\theta \to 2\pi^-$, $\sqrt{E} = -|E|^{1/2}$. As can be seen from the term e^{ikx} in (C11), therefore, $E < 0$ corresponds to a decaying transmitted wave, and (C9) then defines the conditions for the bound states to exist within the potential well. These conditions are exactly the equations (C16a) and (C16b) above.

Similarly, for the more general three-dimensional case we would expect that, near a resonance, $S_l(E)$ also has a pole in the fourth quadrant. This pole is in the analytic continuation of $S_l(E)$ from above to below the positive real axis, and lies on the second Riemann sheet of $S_l(E)$. The bound states of the well correspond to poles of $S_l(E)$ on the negative real energy axis. The closer the resonances are to the real axis, the 'stronger' they become, that is, the more they behave like very long lived bound states.

Finally, a nice connection can be made to the phase shift from (C13). Retaining E as the independent variable, we can write

$$S(E) = e^{i\delta(E)}|T(E)|^{1/2}. \tag{C20}$$

For notational convenience, we write (C12) as $S(E) = [A(E) - iB(E)]^{-1}$, with obvious choices for A and B. Then it follows that

$$\tan \delta(E) = \frac{B(E)}{A(E)} = \frac{1}{2}\left(\frac{k}{\kappa} + \frac{\kappa}{k}\right) \tan \kappa a \approx \frac{2}{\Gamma}(E - E_r), \tag{C21}$$

on using (C18). Hence

$$\delta(E) \approx \arctan[\frac{2}{\Gamma}(E - E_r)]. \tag{C22}$$

Note also that

$$\frac{d\delta(E)}{dE} = \frac{2\Gamma}{\Gamma^2 + 4(E - E_r)^2}, \tag{C23}$$

(again, exhibiting the Breit-Wigner form) and this derivative has a maximum value when $E = E_r$, that is at a resonance, so $\delta(E)$ varies rapidly there.

APPENDIX D

THE S-MATRIX IN A LARGE CLASS OF PIECEWISE DIFFERENTIABLE POTENTIALS

D.1 ANALYTIC CONTINUATION OF THE S-MATRIX IN l AND k

Based on the paper by [36], consider the radial Schrödinger equation with $k \in C$ (in units such that $\bar{h}^2 = 2m + 1$),

$$(\frac{d^2}{dr^2} + k^2 - \frac{\lambda^2 - \frac{1}{4}}{r^2} - V(r))\phi(k, \lambda, r) = 0. \tag{D1}$$

Here $V(r)$ is a potential that either vanishes outside a sphere of a radius r_0, or is $O(r^{-2})$ for $r > r_0$. Thus the potential can be expressed as

$$V(r) = V_0(r)\theta(r_0 - r) + \frac{\Lambda}{r^2}\theta(r - r_0).$$

The general solution in $r > r_0$

$$\phi(k, \lambda, r) = B_1(k, \nu)(kr)^{\frac{1}{2}} J_\nu(kr) + B_2(k, \nu)(kr)^{\frac{1}{2}} J_{-\nu}(kr), \tag{D2}$$

where

$$\nu = \begin{cases} \lambda = l + \frac{1}{2}, \text{ if } V(r) = 0, r > r_0, \\ (\lambda^2 + \Lambda)^{\frac{1}{2}}, \text{ if } V(r) = \Lambda r^{-2}, r > r_0. \end{cases} \tag{D3}$$

J_ν and $J_{-\nu}$ are the Bessel functions which are linearly independent if $\nu \neq Z$. They are entire functions of ν in plane of $\nu \otimes kr$ domain except for a possible branch point at $kr = 0$. If $z = kr$, the circuit relation about $z = 0$ is

$$J_\nu(ze^{im\pi}) = e^{im\pi\nu} J_\nu(z), m \in C. \tag{D4}$$

Asymptotically, from (D4) as $r \to \infty$

$$\phi(k, \lambda, r) \sim B_1(k, \nu) \sin(kr - \frac{\pi\nu}{2} + \frac{\pi}{4}) + B_2(k, \nu) \sin(kr + \frac{\pi\nu}{2} + \frac{\pi}{4}). \tag{D5}$$

In terms of phase shifts $\delta(k, \nu)$, however,

$$\phi(k, \lambda, r) \sim C(k, \nu) \sin(kr - \frac{\pi\nu}{2} + \frac{\pi}{4} + \delta(k, \nu)). \tag{D6}$$

The wave amplitude (if $\nu \neq \lambda$)

$$A(k,\nu) = \frac{1}{2ik}(e^{2i\delta(k,\nu)} - 1) = \frac{1}{k} e^{i\delta(k,\nu)} \sin\delta(k,\nu). \tag{D7}$$

Note: δ is not unique. From (D6) and (D7), we obtain the S-matrix

$$S(k,\nu) = \frac{1+iK}{1-iK}, \tag{D8}$$

where the reaction matrix K is defined as

$$K = \tan\delta(k,\nu) = \frac{B_1(k,\nu)\sin[\frac{1}{2}\pi(\lambda-\nu)] + B_2(k,\nu)\sin[\frac{1}{2}\pi(\lambda+\nu)]}{B_1(k,\nu)\cos[\frac{1}{2}\pi(\lambda-\nu)] + B_2(k,\nu)\cos[\frac{1}{2}\pi(\lambda+\nu)]}. \tag{D9}$$

Equation (D8) becomes

$$S(k,\nu) = e^{i\pi(\lambda-\nu)} \frac{1 + e^{i\pi\nu(\frac{B_2}{B_1})}}{1 + e^{-i\pi\nu(\frac{B_2}{B_1})}}, \tag{D10}$$

where B_2/B_1 is unknown function related to the logarithmic derivative $L(k,\nu)$ of the interior solution of (D2) at $r = r_0$ as shown

$$L(k,\nu)|_{r_0} = r_0 \frac{\phi'(k,\lambda,r_0)}{\phi(k,\lambda,r_0)} = \frac{1}{2} + (kr_0)\frac{J'_\nu(kr_0) + (\frac{B_2}{B_1})J'_{-\nu}(kr_0)}{J_\nu(kr_0) + (\frac{B_2}{B_1})J_{-\nu}(kr_0)}, \tag{D11}$$

we get

$$\frac{B_2}{B_1} = -\frac{[\nu + \frac{1}{2} - r_0 L(k,\nu)]J_\nu(kr_0) - kr_0 J_{\nu+1}(kr_0)}{[\nu + \frac{1}{2} - r_0 L(k,\nu)]J_{-\nu}(kr_0) + kr_0 J_{-(\nu+1)}(kr_0)}. \tag{D12}$$

Therefore, (D10) becomes

$$S(k,\nu) = -e^{i\pi(\lambda-\nu)} \frac{[\nu + \frac{1}{2} - r_0 L(k,\nu)]H^{(2)}_\nu(kr_0) - kr_0 H^{(2)}_{\nu+1}(kr_0)}{[\nu + \frac{1}{2} - r_0 L(k,\nu)]H^{(1)}_\nu(kr_0) - kr_0 H^{(1)}_{\nu+1}(kr_0)}, \tag{D13}$$

where

$$H^{(1)}_\nu(z) = \frac{i}{\sin\pi\nu}[e^{-i\pi\nu}J_\nu(z) - J_{-\nu}(z)],$$

$$H^{(2)}_\nu(z) = \frac{-i}{\sin\pi\nu}[e^{i\pi\nu}J_\nu(z) - J_{-\nu}(z)].$$

If the logarithmic derivative $L(k,v)$ is a real analytic function of both arguments, the S-matrix is unitary.

D.2 CONTINUOUS SOLUBLE POTENTIALS

Recall the radial Schrödinger eqauation with $k \in C$ again (in units such that $\bar{h}^2 = 2m + 1$),

$$(\frac{d^2}{dr^2} + k^2 - \frac{\lambda^2 - \frac{1}{4}}{r^2} - V(r))\phi(k, \lambda, r) = 0.$$

With the continuous potentials

$$V(r) = \begin{cases} -V_0[1 + \epsilon - (1 + \epsilon\rho - \rho)(\frac{r}{r_0})^2 - \rho(\frac{r}{r_0})^2], & r < r_0 \\ -V_0\epsilon(1 - \rho)(\frac{r}{r_0})^2, & r > r_0 \end{cases} \tag{D14}$$

where V_0 and r_0 determine the strength and the range of the potential, ϵ and ρ characterize its shape. The potential is continuous for all values of ϵ and ρ.

The interior solution of the Schrödinger equation is

$$\phi = (\frac{r}{r_0})^{c-\frac{1}{2}} e^{\frac{1}{2}z(\frac{r}{r_0})^2} \Phi(a, c; z(\frac{r}{r_0})^2),$$

where $\phi(a, c; z)$ is the confluent hypergeometric function defined by the series

$$\phi(a, c; z) = 1 + \sum_{n=1}^{\infty} \frac{\Gamma(a + n)\Gamma(c)z^n}{\Gamma(a)\Gamma(c + n)n!},$$

and $a, c, and\ z$ are given by

$$z = [V(1 + \epsilon\rho - \rho)]^{\frac{1}{2}},$$

$$c = 1 + (\lambda^2 - \rho V)^{\frac{1}{2}},$$

$$\alpha = \frac{1}{2}\left[c - \frac{x^2 + V(1 + \epsilon)}{2\epsilon}\right], \quad x = kr_0.$$

Recalling that the S-matrix expression from (D13), for this case we have

$$S(k, \nu) = -e^{i\pi(\lambda - \nu)} \frac{[\nu + \frac{1}{2} - r_0 L(k, \nu)]H_\nu^{(2)}(kr_0) - kr_0 H_{\nu+1}^{(2)}(kr_0)}{[\nu + \frac{1}{2} - r_0 L(k, \nu)]H_\nu^{(1)}(kr_0) - kr_0 H_{(\nu+1)}^{(1)}(kr_0)},$$

where

$$v = [\lambda^2 - \epsilon(1 - \rho)V]^{\frac{1}{2}} \quad V = r_0^2 V_0 \quad \lambda = l + \frac{1}{2},$$

and the logarithmic derivative function obtained from the interior solution is

$$r_0 L(k, \lambda) = c - \frac{1}{2} - z + 2z\frac{\Phi'(a, c; z)}{\Phi(a, c; z)}.$$

VITA

Umaporn Nuntaplook
Department of Mathematics and Statistics
Old Dominion University
Norfolk, VA 23529

Education

- Ph.D. in Computational and Applied Mathematics, Old Dominion University, Norfolk, VA (August 2013).
- M.S. in Computational and Applied Mathematics, Old Dominion University, Norfolk, VA (December 2008).
- B.Sc. in Applied Mathematics, Mahidol University, Bangkok, Thailand (July 2004).

Experience and Awards

- John A. Adam and Umaporn Nuntaplook, "Electromagnetic and Potential Scattering from a Radially Inhomogeneous Sphere", submitted to Applied Mathematics Letters.
- Adjunct Instructional Faculty, Department of Mathematics and Statistics, Old Dominion University, Norfolk, VA (Fall 2011 - Summer 2013).
- Vice president of the Math/Stat Club, Department of Mathematics and Statistics, Old Dominion University, Norfolk, VA (2008 - 2009).
- Full scholarship from the Commission on Higher Education Congress: University Staff Development Consortium of Thailand, (2006 - 2012).
- Full scholarship from the Development and Promotion of Science and Technology Talents Project of Thailand, (2001 - 2006).

Typeset using LaTeX.